Earth and Planetary Sciences ETDs   Electronic Theses and Dissertations

Summer 7-15-2020

Fluvial Geomorphic and Hydrologic Evolution and Climate Change Resilience in Young Volcanic Landscapes: Rhyolite Plateau and Lamar Valley, Yellowstone National Park

Benjamin Newell Burnett
University of New Mexico

Follow this and additional works at: https://digitalrepository.unm.edu/eps_etds

Part of the Geology Commons, Geomorphology Commons, and the Hydrology Commons

Benjamin Newell Burnett

Candidate

Earth and Planetary Sciences

Department

This dissertation is approved, and it is acceptable in quality and form for publication:

Approved by the Dissertation Committee:

Dr. Grant Meyer   , Chairperson

Dr. Peter Fawcett

Dr. Leslie McFadden

Dr. Julia Coonrod

**FLUVIAL GEOMORPHIC AND HYDROLOGIC EVOLUTION
AND CLIMATE CHANGE RESILIENCE IN YOUNG
VOLCANIC LANDSCAPES: RHYOLITE PLATEAU AND
LAMAR VALLEY, YELLOWSTONE NATIONAL PARK.**

by

BENJAMIN NEWELL BURNETT

BS, Earth and Environmental Sciences, Lehigh University, 2001
BA, Anthropology, Lehigh University, 2001
MS, Earth and Planetary Sciences, University of New Mexico, 2004

DISSERTATION

Submitted in Partial Fulfillment of the
Requirements for the Degree of

**Doctor of Philosophy
Earth and Planetary Sciences**

The University of New Mexico
Albuquerque, New Mexico

July, 2020

ACKNOWLEDGEMENTS

Fluvial Geomorphic and Hydrologic Evolution and Climate Change Resilience in Young Volcanic Landscapes:

Rhyolite Plateau and Lamar Valley, Yellowstone National Park

By

Benjamin Newell Burnett

BS, Earth and Environmental Sciences, Lehigh University, 2001

BA, Anthropology, Lehigh University, 2001

MS, Earth and Planetary Sciences, University of New Mexico, 2004

PhD, Earth and Planetary Sciences, University of New Mexico, 2020

ABSTRACT

Quaternary volcanism associated with the last caldera cycle in Yellowstone included emplacement of ash-flow tuffs, massive rhyolite flows ranging from 79 to 484 ka, and valley-filling basalts. This study examines (1) the evolution of spring hydrology with flow age on the Rhyolite Plateau, (2) initial development and evolution of stream networks on the rhyolite flows, and (3) the impact of the 630 ka caldera formation and volcanic flow emplacement on Lamar Valley incision rates.

Integrated stream networks formed within 79 kyr on the Rhyolite Plateau. Incision is focused on steep flow margins and knickpoints and is dependent on local stream power. Plugging of fractures causes hydraulic conductivity of the flows to decline over time. Snowmelt infiltrates rapidly into younger flows, leaving ephemeral surface streams, but many flow-margin springs experience a delayed snowmelt response and enhanced

discharge during late-summer periods of water stress, providing important refugia for

aquatic organisms threatened by climate change.

Incision rates over the past 630 kyr in the Lamar Valley are greatest (≤ 0.55 mm/yr)

where the greatest thickness of Quaternary volcanic material was emplaced, where they are

higher than most rivers in the region. Incision rates are lowest (≤ 0.15 mm/yr) above a

knickpoint caused by erosion resistant crystalline bedrock, and in the upper reaches of two

tributaries, where I infer that faulting associated with caldera formation led to stream

capture of portions of the headwater areas.

Table of Contents

PREFACE

The three chapters in this dissertation are independent papers that will be submitted for publication. Dr. Grant A. Meyer will be listed as second author on all these papers, due to his vital role in helping to develop the projects, interpreting results and editing manuscripts. However, I created and analyzed all the data sets presented and wrote all drafts of each paper.

Chapters 1 and 2 are closely related and include data regarding the hydrology and geomorphology of the Rhyolite Plateau in Yellowstone National Park. Both papers utilize the space-for-time substitution method to infer the stages of evolution of the stream networks and groundwater systems on young rhyolite flows ranging from 79 to 484 ka.

Chapter 3 focuses on the Lamar River drainage basin, which is northeast of the Rhyolite Plateau and experienced valley floor disruption due to the emplacement of volcanic material, as well as inferred stream capture due to the formation of the Yellowstone caldera.

All three papers emphasize the role that stream network evolution and incision into Quaternary volcanic units plays in defining the geomorphic and hydrologic systems of Yellowstone National Park.

Chapter 1

Control of Rhyolite Flow Age on Summer Season Hydrology and Resilience of Freshwater Streams and Springs to Climate Variability on the Rhyolite Plateau, Yellowstone National Park.

1. Abstract:

The snowy volcanic highlands of Yellowstone National Park (YNP) house one of the greatest ecological preserves in the USA and serve as major headwaters for the Snake, Missouri and Yellowstone Rivers. After spring snowmelt, many small freshwater streams, springs and wetlands dry out; prior research has shown that the number of perennial bodies of water in YNP has declined during recent droughts. It is thus critical to identify physical factors that influence late summer streamflow and evaluate the resilience of springs to climate change.

The Rhyolite Plateau of central and southwestern YNP consists of large young rhyolite flows with irregular low-relief surfaces and steep margins. I hypothesize that this flow morphology promotes rapid and deep infiltration of snowmelt and that fracture networks act as seasonal reservoirs and conduits, releasing the snowmelt during summer and fall at springs located around the margins of the flows. In 2016 and 2017, I collected repeat discharge data on and around the Rhyolite Plateau in late June and early August. In 2017, six flumes were installed to measure spring discharge from late June to early October. Discharge measurements show that streams on the upper plateau surfaces of the younger

rhyolites (< 200 ka) tend to be ephemeral, whereas those on the oldest flow (484 ka) tend to be perennial. About 50% of springs around the margins of the younger flows displayed an increase in discharge from June to August, which I interpret as a delayed snowmelt pulse. In contrast, springs around the margin of the oldest flow predominantly experienced flow recession through the summer. The timing of peak discharge from springs varies from late June to October, indicating that snowmelt pulses require 1-4 months to reach the rhyolite flow margins. Hydraulic conductivity calculated using the lag times for delayed snowmelt pulses on the flows is 10^{-3} to 10^{-2} m/s, consistent with flow through highly permeable fracture zones within the rhyolite flows and rubble layers near their surface and base. Weathering, sedimentation, hydrothermal alteration and precipitation of minerals within the rhyolites progressively reduces permeability, promoting greater surface runoff and a dominantly shallower groundwater system on older flows that is more like the hydrology of other older rocks in the area.

The delayed snowmelt pulses provide surface water during late summer and early fall, a time of water stress for humans and ecosystems. I infer that springs receiving delayed snowmelt pulses and those that maintained similar August discharge in both the wet 2017 and dry 2016 water years have greater potential to maintain perennial flow during warmer and drier summers in coming decades. These streams have more potential resilience to climate change and drought, and may become a critical refuge for aquatic organisms, as well as an increasingly important resource for local wildlife and downstream consumers. Nonetheless, these springs are still vulnerable to reductions in snowpack, as

discharge and delayed snowmelt pulses were significantly lower during 2016, when maximum snowpack was ~35% lower than 2017.

2. Introduction and Study Area:

The snowy volcanic highlands of Yellowstone National Park and the Greater Yellowstone Region (GYR) serve as a critical headwaters region for several large rivers (Snake, Madison, Shoshone and Yellowstone Rivers) and as an important wildlife refuge. Over the last several decades, freshwater resources in YNP have been significantly impacted by rising temperatures and decreasing annual precipitation. Many small ponds and streams have become ephemeral, which has resulted in a loss of habitat for moose, beaver, amphibians and other aquatic organisms (McMenamin et al., 2008; Persico and Meyer, 2013; Oates, 2016). Increasing water stress for natural systems and urban and rural water users has spurred a massive effort to understand and predict the potential impacts that climate change and climate variability will have on water resources in upcoming decades. The bulk of this research has focused on modeling global atmospheric dynamics and temperature feedbacks to predict potential changes in precipitation patterns and evapotranspiration. However, the effects that changing temperature and precipitation have on local and regional water resources are strongly influenced by many factors, including the timing and spatial distribution of groundwater recharge and discharge, and the hydrologic properties of soil, surficial deposits, and bedrock (Jefferson et al., 2008; Tague and Grant, 2009). Understanding the role that drainage basin properties have on local water resources requires detailed, field-based studies of the bedrock and surficial materials and direct measurement of the response of discharge to climate variability. In

order to better understand the potential impacts of climate change and drought on freshwater resources in Yellowstone National Park, I have measured the spatial and temporal variations in summer discharge of springs and low-order streams draining the Rhyolite Plateau in Yellowstone National Park (Fig. 1).

2.1 Climatic and geologic controls on summer discharge

Precipitation in the GYR is strongly seasonal, with ~70 % of annual precipitation falling as snow during the winter. The snowpack serves as a natural reservoir, storing water until the spring melt season, which begins in April in lower elevation areas outside the park and reaches its peak in May and June, with only the highest elevations preserving snow through August. Runoff and shallow throughflow derived from snowmelt drive a seasonal discharge peak in rivers in the GYR and across the Rocky Mountain region, limited to spring and early summer on undammed watercourses. By August, however, discharge in most rivers drops by one to two orders of magnitude (Fig. 2) and many small streams, springs and ponds dry up. While summer thunderstorms are common, their effects are generally short-lived and have only minor impacts on the seasonal hydrographs of local rivers, and flow recession continues until winter storms bring snow to the high country.
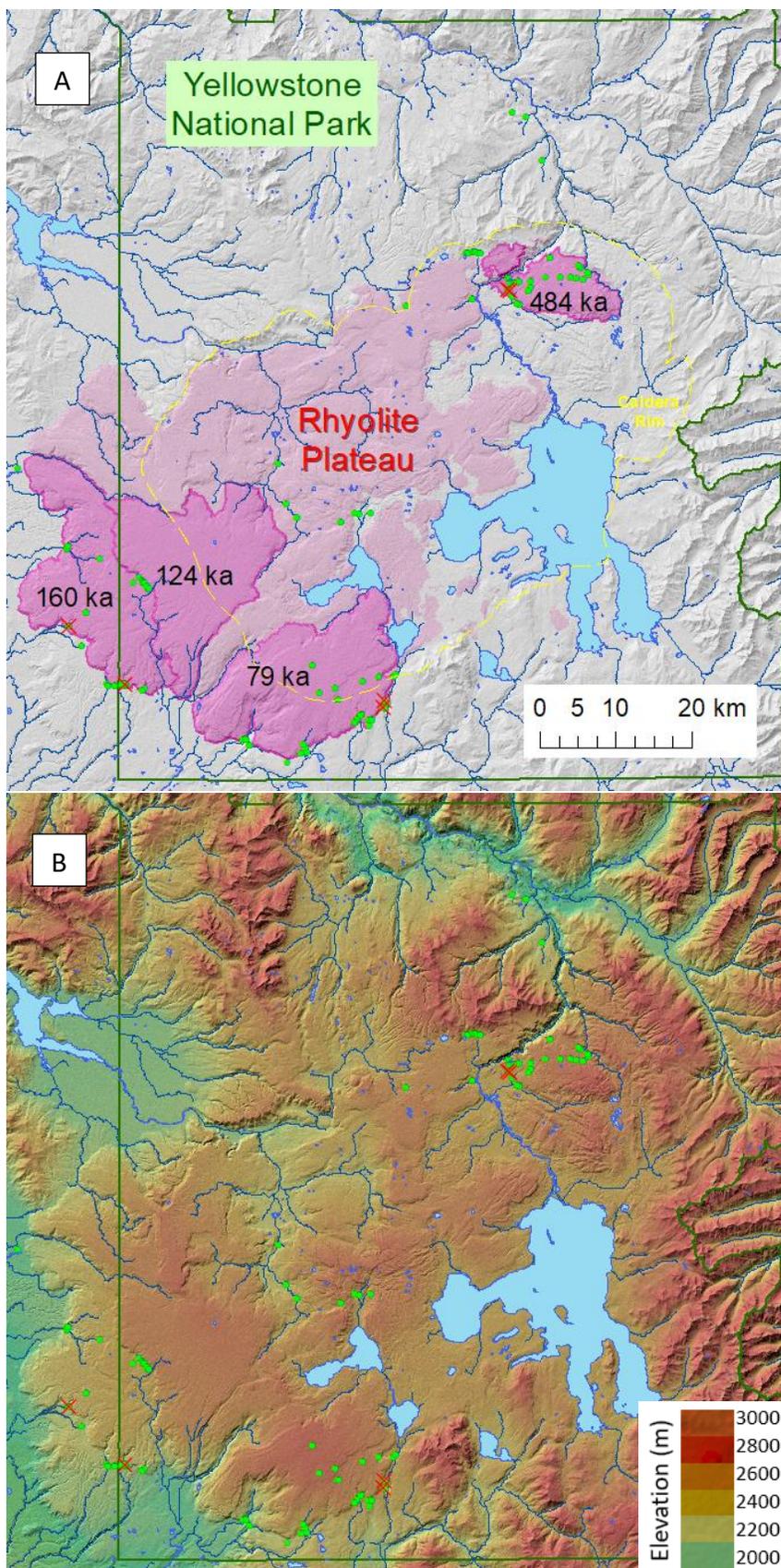
Figure 1. Shaded relief maps of the Rhyolite Plateau at the same scale with spring discharge locations (green) and flume locations (red) marked. A: Rhyolite Plateau in pink with four of the largest flows highlighted and labeled by age. YNP boundary (green line) and caldera rim (yellow line) are shown. B: Elevation of the study area shown using color.
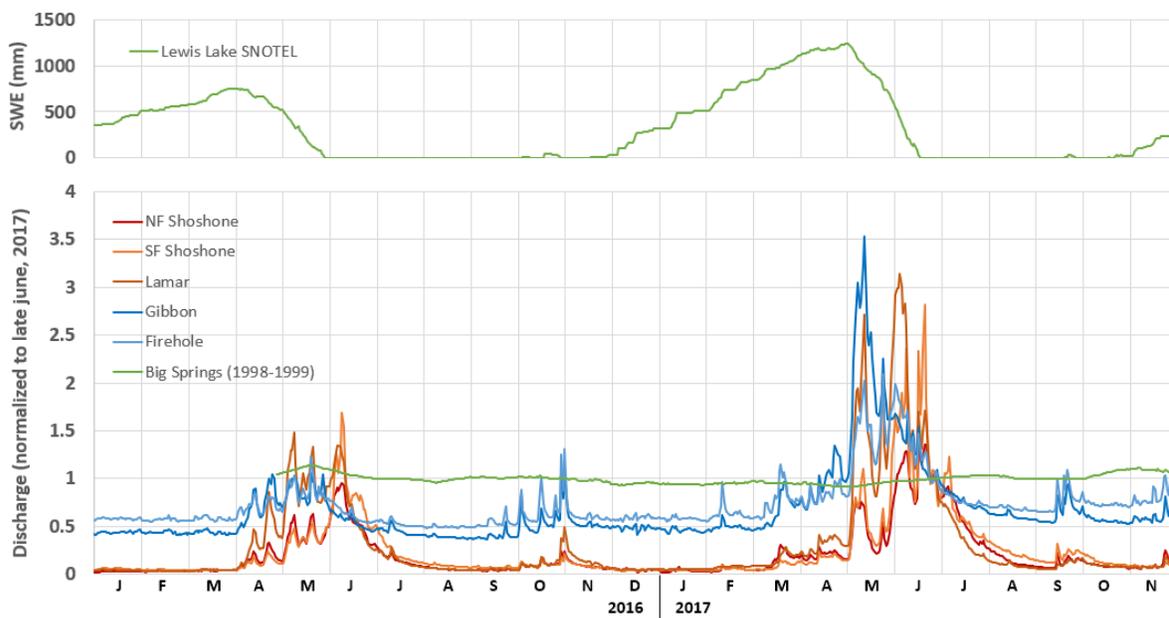
Figure 2. Snowpack measured as snow water equivalent (SWE) at the Lewis Lake SNOTEL station near Pitchstone Plateau, the depth of water that would result from melting the snowpack, during 2016 and 2017. Discharge hydrographs are of major rivers in the GYR, including the Gibbon and Firehole rivers that drain the Rhyolite Plateau, and 3 others with drainage basins largely in Eocene volcaniclastic rocks. Big Springs is a large Rhyolite Plateau margin spring gaged by the USGS in 1998-1999. Discharge for each river and Big Springs is normalized to the late June value to illustrate relative degrees of flow recession in the summer of 2017.

In recent decades, snowpack in the northern and central Rocky Mountains has declined significantly (Pederson et al., 2011) and attribution studies suggest that the majority of this decline is likely the result of warming from anthropogenic increases in greenhouse gases (Barnett et al., 2008; Tercek et al., 2015). Increased winter and spring temperatures in recent years have led to more precipitation falling as rain rather than snow, higher snowlines, overall decreased snowpack and earlier melt of that snow. Earlier snowmelt and warmer summer temperatures in turn lead to a longer recession period (Stewart et al., 2005), greater evapotranspiration and higher water stress during the dry

season (McMenamin et al., 2008; Gardner et al., 2010). Climate models predict that spring and summer temperatures will increase by an additional 4.5-5.5 °C by the end of this century in the Greater Yellowstone Region (Westerling et al., 2011; IPCC, 2014; Chang and Hansen, 2015). These rates are higher than the global average and the warming will likely be even greater at higher elevation (Fyfe and Flato, 1999; Minder et al., 2018). This predicted warming poses a direct threat to water resources and ecosystems dependent on seasonal and perennial water sources (Pederson et al., 2010). The next step in understanding how these changes will impact the GYR is to examine how physical factors of local drainage basins influence the hydrologic response to climate change.

Geology is one of the most important physical controls on surface and subsurface hydrology. Much of Yellowstone National Park is underlain by young (2.4-0.07 ma) volcanic rocks that are highly heterogenous in composition and morphology (Christiansen, 2001). Young volcanic flows (< 10 Ma) have been shown to exert major controls on infiltration, runoff and groundwater hydrology (Wells et al., 1985; Gardner et al., 2010; Jefferson et al., 2010). Infiltration dominates fresh lava flows because water can readily enter bedrock fractures formed during eruption and cooling. Rapid percolation and highly connected pore spaces promote the formation of large springs around young lava flows and other highly porous media such as karst and talus deposits (Flerchinger et al., 1992; Manga, 1999; White, 2002; Jefferson et al., 2010; Kurylyk and Hayashi, 2017). Springs fed by these aquifers exhibit lag times between peak recharge and peak spring discharge of hours to months depending on aquifer length, hydraulic gradient and permeability. Studies on basaltic flows in the Mojave Desert indicate that surface runoff and drainage network development only

occur after the bedrock is buried by sediments that clog the fracture network and eventually develop low permeability soil horizons (Wells et al., 1985, Dohrenwend et al., 1987; 1989). Fine sediment derived from aeolian sources is transported into the fracture network with infiltrating water where it produces a progressive reduction in porosity and permeability of the lava flow. In the wetter climates of the western Oregon Cascades, subsurface weathering plays a key role in reducing the transmissivity of Quaternary volcanic rocks. Analysis of hydrographs from rivers in the basaltic to andesitic Cascade Range shows that drainage basins with younger volcanic bedrock (< 700 ka) are dominated by groundwater springs with very steady discharge, whereas streams in basins with older average bedrock ages exhibit a more flashy discharge behavior driven by runoff and shallow subsurface stormflow (Jefferson et al., 2008; 2010). This change in stream behavior is attributed to the progressive reduction in permeability of the volcanic bedrock leading to a shallower hydrologic system. On the Rhyolite Plateau, in addition to sedimentation and weathering, hydrothermal alteration and precipitation of minerals within the fracture network also likely reduce bedrock porosity and permeability. Fenner (1936) observed significant weathering, alteration and precipitation of minerals in core samples taken from hydrothermal areas on the Rhyolite Plateau. Dobson et al. (2003) measured porosity and permeability within the cores and concluded that silicification is responsible for significantly reducing permeability in some portions of the cores.

Gardner et al. (2010) compared hydrographs from rivers draining the Yellowstone volcanic field to those of other nearby rivers and modeled baseflow recession during the summer and fall. This analysis revealed that cool groundwater discharge from Yellowstone

volcanics has a significant positive effect on summer streamflow. As compared to other nearby rivers, rivers that drain the Yellowstone Quaternary volcanic field exhibit a greater proportion of groundwater baseflow to surface runoff, slower baseflow recession through the summer season, and smaller declines in discharge from the late spring peak runoff to fall minimum discharge. These observations, combined with environmental age tracers in cool springs, indicate that large, shallow, rapidly circulating groundwater aquifers exist in the young Yellowstone volcanic rocks, which exert a major control on late summer stream discharge in gaged rivers (generally > 100 km^2 basin areas; Gardner et al., 2010).

The Yellowstone volcanic field is complex and bimodal in composition, and includes basalt flows, thick rhyolite flows and extensive rhyolitic ash-flow tuffs of varying ages interlayered with surficial sediments. Hydraulic properties vary between these different rock types (Dobson et al., 2003), and even between flows of similar composition and morphology, because hydrology evolves through time in volcanic rocks (Jefferson et al., 2010). Wildlife may be subject to water variability at a quite local scale, as exemplified by amphibians that have limited ability to move between isolated ponds and wetlands (McMenamin et al., 2008) or beavers that are restricted to perennial streams with limited peak discharges and gradients (Persico and Meyer, 2013). It is therefore critical to evaluate hydrologic variability at smaller spatial scales in order to identify specific processes and factors such as bedrock lithology and flow age that control late season discharge. Here I examine discharge from cool groundwater springs and low-order streams with recharge and drainage areas entirely on individual rhyolite lava flows. By doing so, I can relate patterns of water availability over the summer season directly to the age, composition, morphology

and sediment cover of the flows. Additionally, in order to compare stream behavior on the Rhyolite Plateau to that in older rocks, I have measured discharge in small streams draining Eocene volcanics adjacent to the Rhyolite Plateau.

2.2 Geology of the Yellowstone volcanic field

Volcanism in the GYR is the result of a mantle plume hot spot, which has uplifted the GYR, creating a zone of anomalously high elevation (Lowry et al., 2000; Pierce and Morgan, 2009), relatively high precipitation, and a radial drainage pattern that makes Yellowstone an important source region for the hydrologic system of the northwestern United States. Geophysical imaging including seismic tomography has revealed a plume of warm mantle material extending from at least 500 km depth to the base of the Lithosphere under Yellowstone (Pierce and Morgan, 2009) and a large, dominantly felsic body of partial melt within the crust below the modern Yellowstone caldera (Farrell et al., 2014). The Quaternary volcanism in Yellowstone is divided into 3 cycles, each of which culminated in a caldera-forming supereruption that produced ash-flow tuff units estimated to be at least 2450 km^3, 280 km^3 and 1000 km^3, respectively for the three events. Rhyolitic flows, and to a lesser extent basalt flows, were erupted before and after each caldera-forming eruption. The most recent supereruption occurred at ~630 ka, forming the modern Yellowstone Caldera and the Lava Creek ash-flow tuff. The Rhyolite Plateau is comprised of >25 rhyolitic flows extruded after the formation of the modern caldera (79-484 ka) that extend across ~3000 km^2 and comprise 30% of the park area. Many of the flows originated from vents located on or near the caldera ring fracture system, and while much of the plateau lies within the caldera, several of the largest flows have spilled over its southwestern rim.

Individual flows may be as small as 0.5 km^2, but I restricted this study to flows that are large enough (100-350 km^2) to contain independent drainage basins and groundwater reservoirs. The flows are composed of vesicular, perlitized obsidian, vitrophyre, and flow-banded rhyolite. Although lithologic variation occurs at scales of 1-1000 meters within individual flows, the overall lithologic and geochemical composition of the large plateau-forming flows is broadly similar (Christiansen, 2001).

Unlike basalt flows and ash-flow tuff units that fill valleys or blanket low- to moderate-relief surfaces, the rhyolite flows used in this study create very broad plateau-like forms with volcanic vents near the summits. Typical flow morphology consists of a gently sloping upper plateau surface (< 10% gradient) marked by an extensive network of concentric pressure ridges that run sub-parallel to steep flow margins (10-50% gradient). Constructional features such as flow lobes and pressure ridges give the upper surfaces an undulating topography (Fig. 3). Maximum relief on the large flows ranges from 400-700 m, with about 100-300 m of local relief near flow margins. Bedrock is well exposed along pressure ridges and in areas incised by drainages near the flow margins. Flow banding, other compositional banding, and fractures are common within the rhyolites, and these structures predominantly have strike values sub-parallel to pressure ridge traces and dips angled towards the flow margins. Dip angles on and near pressure ridges are commonly within 30° of vertical, and dip values away from pressure ridges tend to be either similar to those on nearby ridges or sub-parallel to the surface slope (< 20°, Fig. 3).
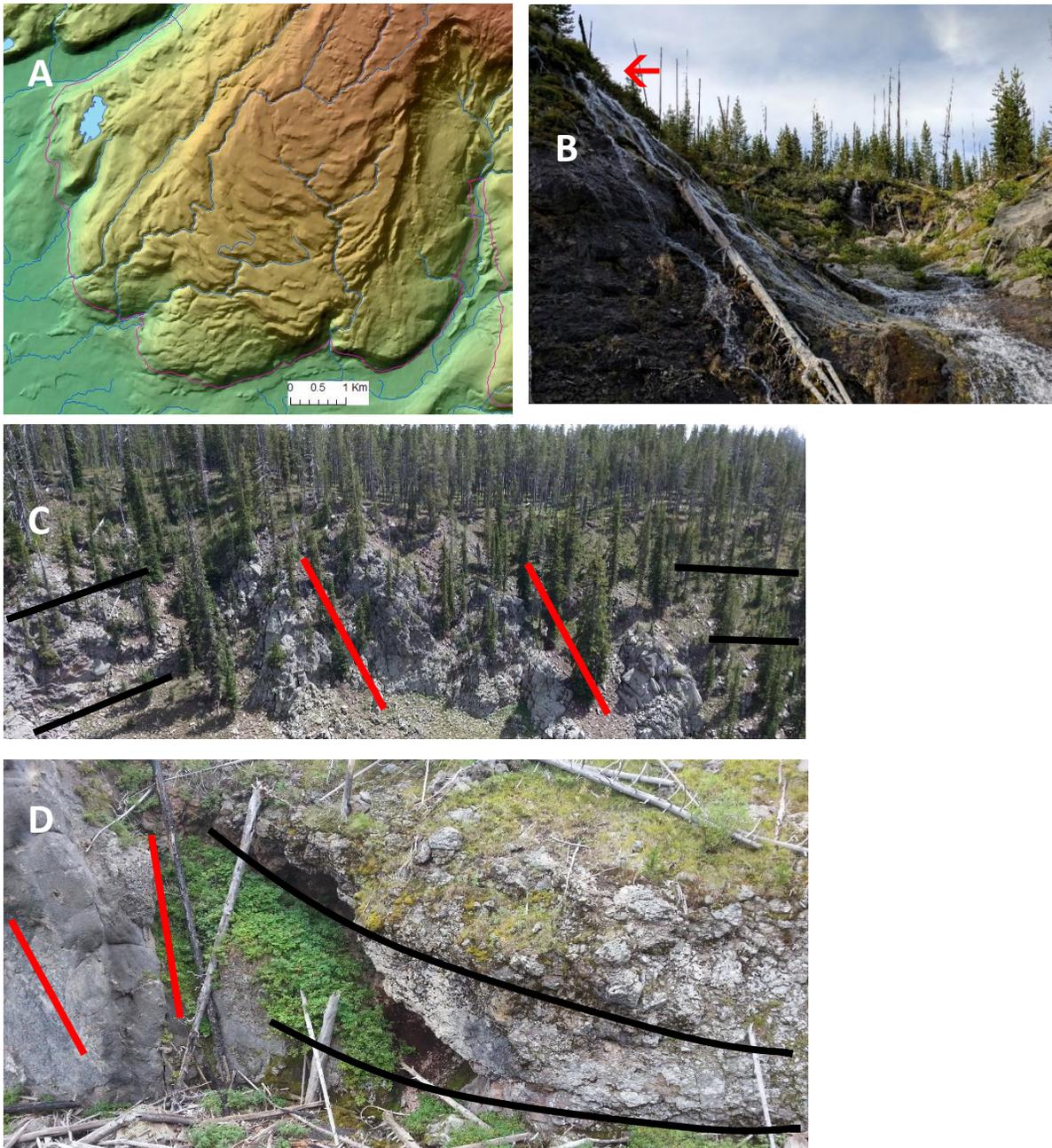
Figure 3. A: Shaded relief map produced from a 10-m DEM shows pressure ridge morphology and its impact on stream networks on a flow lobe of Pitchstone Plateau (79 ka). The flow margin is marked in pink. B: Spring emanating from the base of the surface rubble layer just above a bedrock pressure ridge. C: The internal structure of rhyolite flows exposed in a small canyon. Orientation of compositional banding and sub-parallel fractures within pressure ridges are marked in red and structures in other portions of the flow are marked in black. D: Seepage occurs along fractures at the edge of a pressure ridge creating small pools and verdant vegetation in an otherwise ephemeral stream channel. Same structures marked as in C.

Large ice caps formed in the GYR during peak glacial periods of the Pleistocene, and

almost all of the Rhyolite Plateau was glaciated during the end of the last glacial maximum

at ~13-16 ka (late Pinedale glaciation), the penultimate glaciation ~150 ka (Bull Lake

glaciation), or both (Pierce, 2003, Licciardi and Pierce, 2008, 2018). All of the flows used in

this study were glaciated, and bedrock is partially buried by till and thin glacial rubble

deposits, and eolian, lacustrine and fluvial deposits.   Surficial sediments in low-relief

portions of the flows typically consist of bouldery volcanic rubble directly overlying bedrock,

buried by up to 2 m of fine eolian and lacustrine silt or glacial till. Steeper slopes and

pressure ridges are mantled with colluvial sediments which have likely integrated till and

eolian silt. The perlitized obsidian readily disintegrates into pea gravel and very coarse

sand, which dominate stream channel deposits. Where perennial water is present, organic

mats up to 2 m thick exist. The mats consist primarily of grass roots, silt, and to a lesser

extent large woody debris. Fine sedimentary cover may be thicker in unincised closed

basins, especially those containing lakes. Steeper slopes are often mantled by boulder talus

or colluvium.

2.3   Characteristics of streams and springs on the Rhyolite Plateau

Stream position and gradient are largely controlled by structural features of the

rhyolite flow. Streams run through broad flat basins between pressure ridges and then cut

steeply across the ridges at structural low points. In areas with closely spaces ridges,

stream networks have a rectangular pattern, running between and then across ridges (Fig.

3). Longitudinal profiles tend to be stair-stepped, with knickpoints at each ridge and where

they cross over the flow-lobe margins. Fluvial incision has occurred in knickpoint zones and

has created canyons that range from 10-50 m deep depending on the local relief, age of the flow, and size of the drainage basin (Burnett et al., 2020 [Ch. 2])). While stream networks have extended across most of the plateau, areas between pressure ridges tend to be unincised, and many contain closed basins.

Streams on the upper plateau surface tend to be intermittent, running only when fed directly by snowmelt, or more rarely, briefly during summer thunderstorms. Perennial groundwater-fed stream reaches are only common where incision into bedrock has occurred, usually near the plateau margins where steep gradients have promoted the formation of deep canyons. Perennial stream segments tend to be more consistent in channel and sediment size, but bedrock knickpoints and waterfalls are common since these segments tend to be in steeper reaches. By July, the snow has melted and the majority of water in streams draining the plateau comes from springs located around the flow margins. The majority of these springs are perennial, however some run dry by late summer or fall. Most of these springs originate at the basal contact of the rhyolite flow, which is commonly along a broad slope or the side of a valley.

3. Methods

Repeat discharge measurements of springs and low-order streams were made during the summers of 2016 and 2017 to quantify spatial differences in discharge across the Rhyolite Plateau. Data were collected during 2-week periods in late June and in August of both years. Measurements were made in June, shortly after snowmelt runoff was no longer directly contributing to discharge. Discharge was measured again in the same locations in

August. Discharge on the smallest streams (generally < 0.01 m^3/s) was measured using direct capture, where water was collected for a set time period in a flexible bucket as it flowed over a short drop. At least 6 measurements were taken at each location, and the highest and lowest values were removed before averaging the remaining measurements. For larger streams, discharge was obtained using cross-section and velocity measurements. Straight, smooth-bedded stream reaches were selected for cross-section measurements to reduce error from bedforms, turbulence and eddies.

Repeat discharge measurements were made at over 50 locations in 2016, and over 100 locations in 2017 (Fig. 1). Each location is classified as surface, margin, or mixed, depending whether the water originates from springs on the upper plateau surface, around the plateau margin, or both, respectively. In 2017, snow persisted on the upper surfaces of many flows into July, which limited the number of upper surface and mixed locations that could be sampled independently of snowmelt runoff.   Instead, 11 streams in drainage basins containing mostly pre-Yellowstone Eocene volcanics were sampled. The bedrock in most of these basins consists of andesite flows and volcanic vent facies associated with the Mount Washburn eruptive center; two of these drainage basins contain Eocene epiclastic volcanic breccia, conglomerate and sandstone, and the 630 ka Lava Creek ash-flow tuff (Prostka et al., 1975). These streams were selected with the intent of measuring small stream behavior outside the Rhyolite Plateau, and the elevation ranges and relief of these basins are similar to those of the Rhyolite Plateau. The original constructional landscape on the Eocene volcanic rocks has been highly modified by erosion, and these much older rocks are likely less permeable than the Quaternary Yellowstone volcanics. Eocene volcanic rocks

and associated volcaniclastic sedimentary rocks comprise a large portion of the Absaroka

Range on the eastern flank of the GYR, and drainages in these rocks exhibit flashy discharge

patterns and are heavily influenced by large floods, in part due to very steep, high-relief

topography (Meyer, 2001).

Repeat discharge data were used to calculate the net (%) change in discharge of

springs through July using Equation 1.

(Eq. 1) $Change\ in\ discharge\ through\ July = \frac{(Q_{Aug}-Q_{Jun})*31}{Q_{max}*\#days} * 100\%$

The number of days (#days) between the June measurement (Q_{Jun}) and the August

measurement (Q_{Aug}) varied between locations, with an average time between

measurements of 51 +/- 9 days. Longer delays between measurements would, for most

hydrologic systems, produce larger changes in discharge, so this variation was reduced by

normalizing the change in discharge to a one-month (31 day) period approximately

representing the change in discharge through July. The average midpoint between

measurements was July 18 (+/- 7 days). Spring discharges range over 5 orders of

magnitude, so the discharge change values were normalized by the higher discharge value

(Q_{max}) to keep values within a range of +100% to -100%. Two-sample t-tests were used to

assess whether there were significant differences in the mean values of discharge change

through July between three age-based groups of margin springs (79-103 ka, 124-164 ka, and

484 ka). Two-sample F-tests were used to assess whether variance was significantly

different between the same groups of margin springs.

Multiple repeat discharge data points were collected along Surface Creek, a perennial stream located on top of the oldest (Canyon) rhyolite flow, in order to evaluate the impact of flow-structures and surficial sedimentary cover on discharge. The stream crosses a large basin and a pressure ridge. Discharge was measured above, within and below the pressure ridge in 2016 and 2017 and in and above the basin in 2017. Discharge was also measured near the spring source and near the edge of the plateau surface both years.

Six small PVC-pipe flumes installed below flow-margin springs collected continuous discharge data from late June to early October 2017. These open-channel flumes were constructed and calibrated following the circular design of Samani (2017), which forces the water into critical flow around a well inserted into the flume. A pressure sensor in the well was used to measure stage in the flumes, and variations in atmospheric pressure were accounted for by subtracting measurements taken at a centrally located meteorology station within Yellowstone National Park. The individual sensors had slightly different sensitivities to pressure change and responded slightly to fluctuations in temperature. These subtle variations were significant given the low stage values (< 15 cm) of small streams, so stage at each sensor was individually calibrated using temperature (measured by the sensor), air pressure measured at a nearby meteorology station, and measured stage. These sensitivity studies were done both in the field and in the lab to evaluate the accuracy of the calibrations. Sensor drift over the summer was minor (< 5 %) and was corrected for with at least three direct stage measurements taken during the season. Drift was assumed to be linear between measurements. Discharge was calculated from stage

using principles of critical flow (Samani, 2017) and compared to discharge values measured

manually while the flumes were installed.

Many of the flows in the Rhyolite Plateau are overlapping, with surface drainage and

groundwater recharge originating from multiple flows. Nearly all discharge measurements

were taken on or adjacent to four of the largest, most topographically distinct flows,

Pitchstone Plateau (79 ka), Summit Lake (124 ka), Buffalo Lake (160 ka) and Canyon (484

ka). These flows span the full age range of the Rhyolite Plateau and have distinct summit

areas from which stream networks originate. Each of the selected flows has completely

independent surface drainage except for the Buffalo Lake flow, which is partially buried by

the Summit Lake flow. Discharge measurements associated with the Buffalo Lake flow were

taken only in areas with independent surface drainage, located over a topographic divide

from the portions of the flow that are overlain by the younger flow. Discharge

measurements taken around flows other than the four above are from areas where there is

little or no overlap between different flows.

Hydraulic properties of rhyolite aquifers and aquifers in other young volcanic rocks

and porous sediments were approximated using a modification of the D'Arcy equation

solved for average linear velocity within the aquifer (Eq. 2).

(Eq. 2) $$v = \frac{K}{n_e} * \frac{h}{l}$$

where v is average linear velocity of water through the aquifer, l (length) is the distance

from the recharge area to a gaged spring, h is the change in height of the water table along

the aquifer length, K is hydraulic conductivity, n_e is effective porosity (after Fetter, 2018).

For small basins with high permeability and dynamic water tables, residence time is short

and delayed discharge pulses likely represents direct flow of water through the system

(Flerchinger et al., 1992; White, 2002). With this assumption, I can use the substitution in

Eq. 3 to solve Eq. 1 for hydraulic conductivity (Eq. 4):

(Eq. 3) $$v = \frac{l}{t_{lag}}$$

where t_{lag} is the lag time between peak snowmelt and a peak in spring discharge inferred to

be a delayed snowmelt response.

(Eq. 4) $$K = \frac{l^2\, n_e}{h\, t_{lag}}$$

Hydraulic conductivity was estimated for aquifers feeding springs around the

Rhyolite Plateau using lag times between the peak snowmelt date from the nearest SNOTEL

SWE record, and delayed snowmelt responses identified in flume records. Aquifer length

and change in water table height were estimated from topographic maps where it was

assumed that large, relatively flat areas with limited drainage networks serve as the

recharge areas, and the water table is assumed to be close to the surface. I calculated K

values representing flow through either large fracture networks and boulder rubble layers,

or the bulk bedrock. A porosity of 0.3 was used for fractured bedrock and rubble zones

based on porosity measurements made in volcaniclastic sediment layers from Rhyolite

Plateau drill cores (Dobson et al., 2003). A porosity of 0.1 was used for flow through bulk

rhyolite bedrock based on measurements of perlitized lava samples from these same cores.

Estimates of n_e, distance to recharge areas, and lag times restrict the precision of this

method to a single significant digit. However, since hydraulic conductivity values for Earth

materials range over 12 orders of magnitude (Fetter, 2018), this calculation provides a reasonable estimate for the aquifers studied. Hydraulic conductivity was also calculated for aquifers in Quaternary basalts in the Cascades using lag times measured by Manga (1999), and in an alpine talus deposit studied by Muir et al. (2011) and Kurylyk and Hayashi (2017). I used a porosity of 0.1 for calculating flow through basalt (Manga, 1999), and a porosity of 0.5 for the talus slope (Pierson, 1982; Davinroy, 2000; Muir et al., 2011). I evaluate our method by comparing our K values to those calculated using tracer experiments (Muir et al., 2011) and hydrogeologic modeling (Kurylyk and Hayashi, 2017) in the talus deposit, and the K value determined for one of the Cascade basalts by Manga (1999).

Discharge data from USGS gaging stations on undammed rivers draining the GYR (waterdata.usgs.gov) and snowpack and precipitation data from SNOTEL locations in the GYR (www.wcc.nrcs.usda.gov/snow) were acquired and used to identify differences in precipitation, snowpack and river discharge between the 2016 and 2017 on the Rhyolite Plateau and surrounding areas. Snowpack was recorded as (1) snow-water equivalency (SWE) for April 1 (Bohr and Aguado, 2001) and (2) recorded on the date of maximum snowpack for the water year (starting October 1 of the previous year).

Basic soil descriptions were made at 55 locations across the Rhyolite Plateau. Soils were described in basin areas of the upper plateau and on slopes of pressure ridges and flow margins. Most soil description locations were on the same four flows emphasized for discharge data collection. In most locations, only the thickness of master horizons was measured. At 10 locations, full soil descriptions following methods of Buol et al. (2011) were made that include information regarding soil texture, structure, color, and the

presence of roots, rocks, carbonates and translocated clays, and whether the modern

vegetation was dominated by grass or conifer trees.

Topographic depressions were identified on the upper rhyolite flow surfaces using

USGS 7.5-minute topographic quads and aerial photography. Depressions were identified

where closed depression contours had been mapped and where seasonal and ephemeral

lakes and ponds exist. Depressions were classified as either larger or smaller than 0.1 km^2,

and depressions associated with hydrothermal activity were also noted.   A 1-km UTM grid

was placed over the maps and photos, and 50 1-km^2 areas were selected on each of the

four principal flows in this study. The areas were selected primarily along transects that had

been traversed in the field and extend from near the margin to the flow summit. The use of

these transects allowed for confirmation of depression locations based on field notes and

observations.

4. Results

While all major undammed rivers in the region experienced flow recession through

the 2016 and 2017 summer seasons, many small springs around the margins of the younger

(< 200 ka) rhyolite flows experienced an increase in discharge from late June to August (Figs.

4, 5 & 6), especially in 2017. In contrast, springs on the upper plateau surfaces of the

younger rhyolites tended to be ephemeral or experience significant declines in discharge

through July. Almost all streams on and around the oldest rhyolite flow experienced flow

recession both years, with springs near the margin experiencing more flow recession than

those on the upper surface. Streams in basins dominated by Eocene andesite flows and
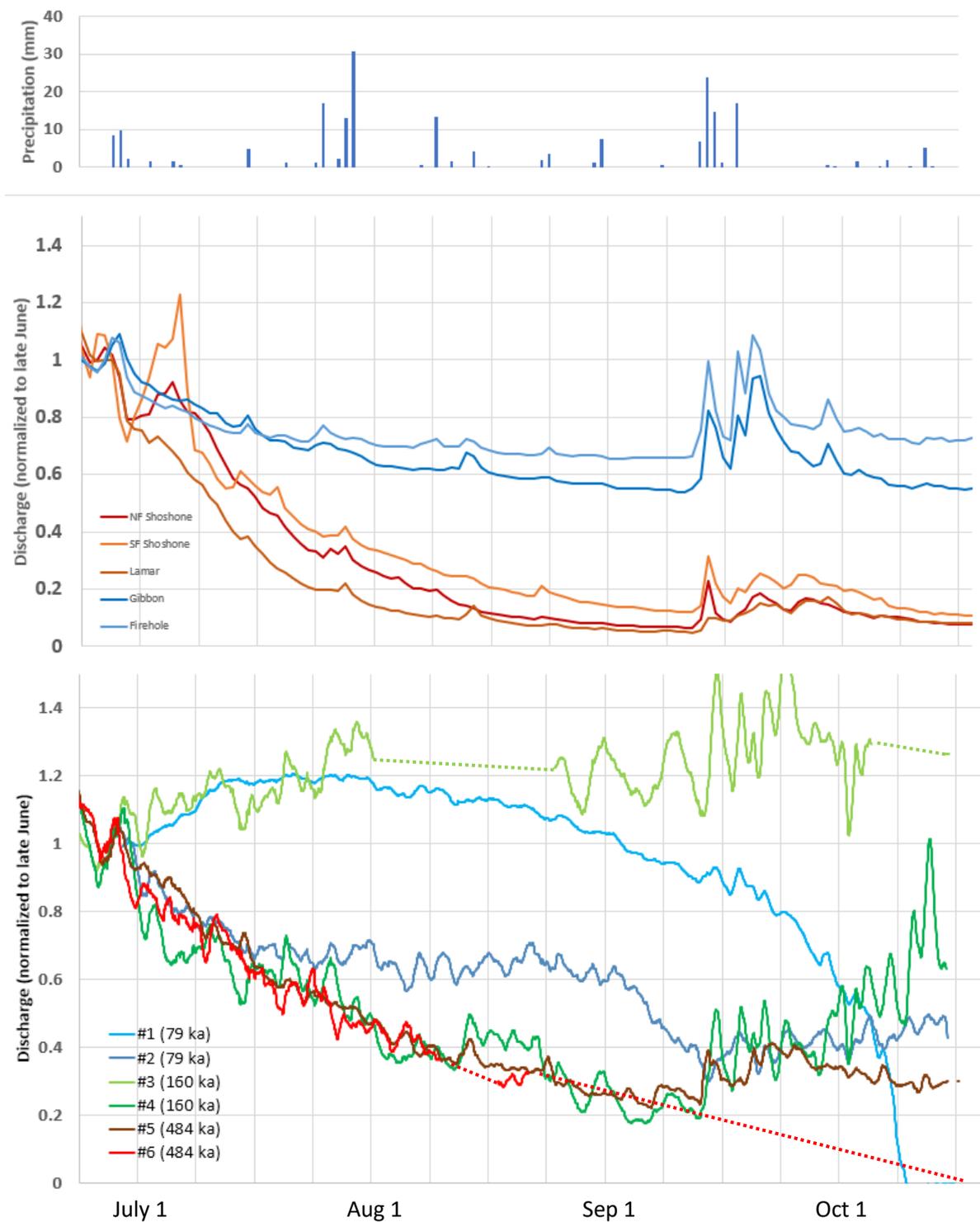
Figure 4. Daily precipitation measured in the park and discharge (normalized to late June) for the summer of 2017 from 5 GYR rivers and from flumes on 6 rhyolite flow margin springs numbered 1-6 and labeled by age of adjacent flow. Dashed lines indicate interpolation between known points.
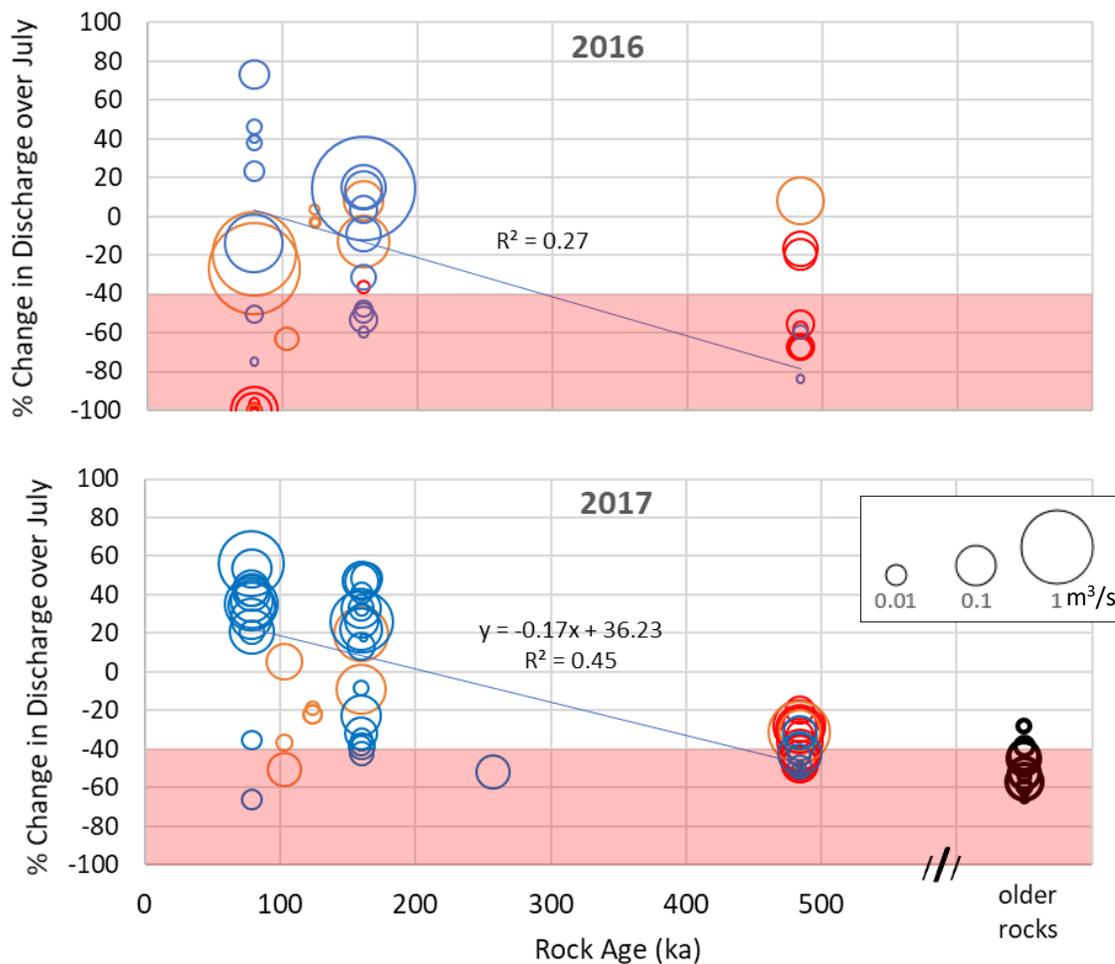
Figure 5. Change in discharge from late June to early August in springs and streams on and around the Rhyolite Plateau. Data are plotted against the age of the associated rhyolite flow. Bubble size indicates average discharge. Color indicates water source: flow-margin springs (blue), flow-surface springs (red), contribution from both surface and margin springs (orange), and older (Eocene) volcanic rocks (black). Regression lines are for flow-margin springs only ($p < 0.05$). Positive values indicate increase in discharge over July; negative values indicate flow recession. Field observations indicate that small springs in the pink shaded area commonly run dry before winter.
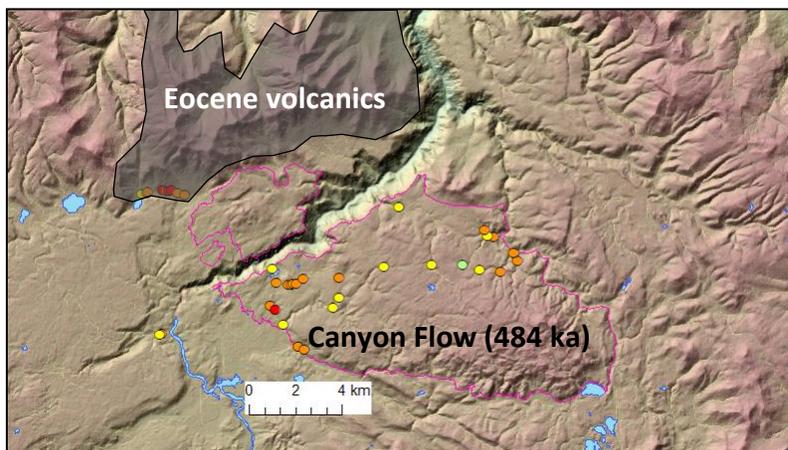
Figure 6. Repeat discharge data locations colored by percent change in discharge (Q) over July 2017 (or 2016 if not collected in 2017). Four large flows are labeled, and their margins are marked in pink. Some of the Eocene volcanics are shaded gray.
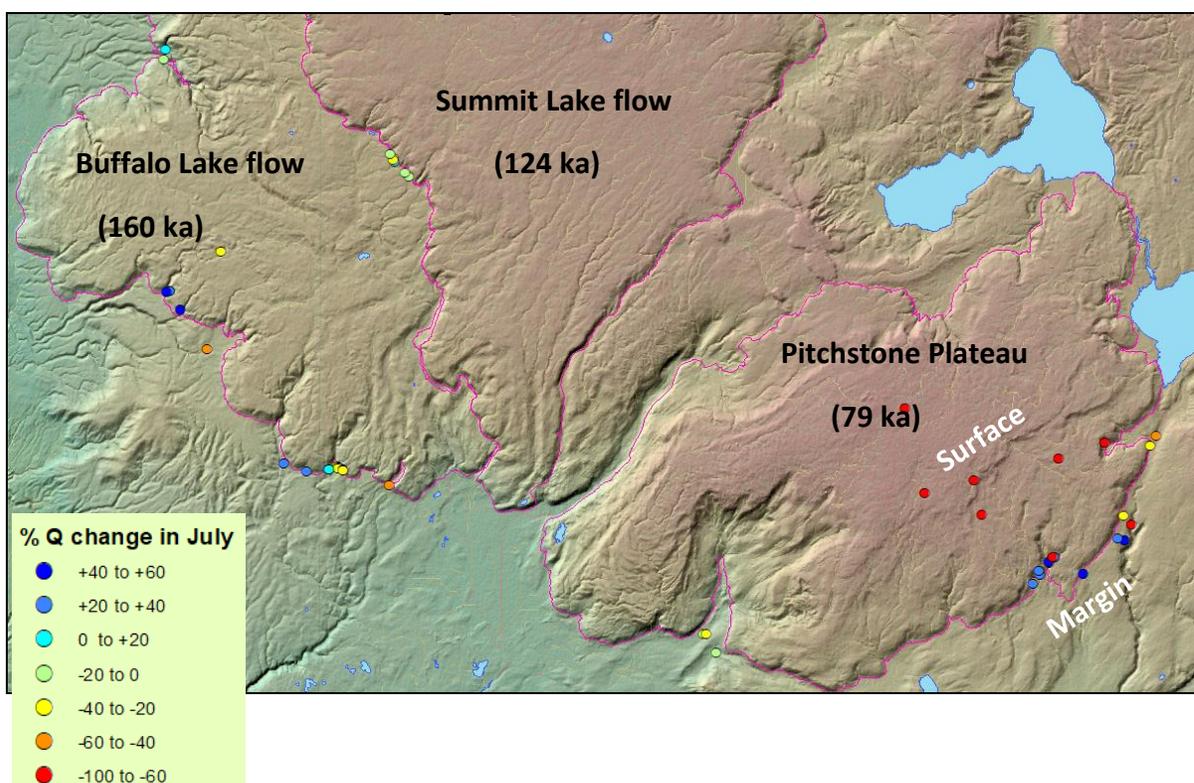
volcaniclastic and sedimentary rocks experienced more flow recession than those draining rhyolite flows (Fig. 5).

Repeat discharge data collected along Surface Creek show that the creek is generally a gaining stream, except where it crosses the pressure ridge, and in the headwaters reach during August 2016 (Fig. 7). The greatest increase in discharge occurs near the base of the

pressure ridge. Discharge was greater in both 2017 measurements at every point along the stream than at either time in 2016.
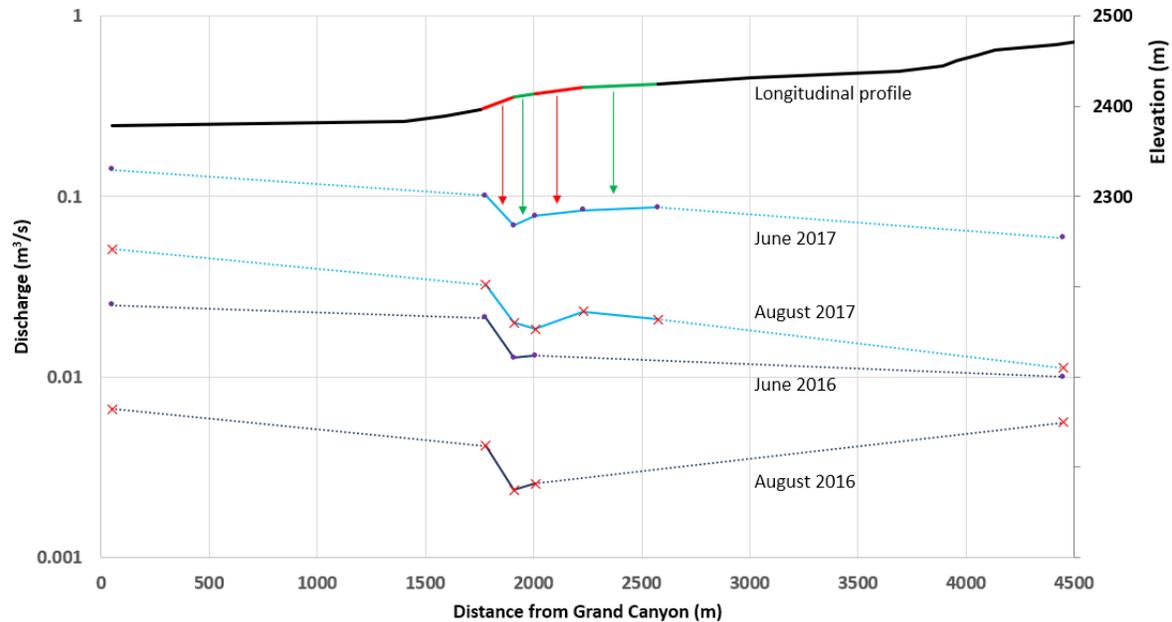
Figure 7. Longitudinal profile and discharge of Surface Creek along the upper surface of the Canyon Flow (484 ka) from its headwaters to where it flows over the rim of the Grand Canyon of the Yellowstone. Green sections of the profile indicate alluvial channel reaches through shallow sedimentary basins and red sections are bedrock confined reaches. Discharge is plotted using direct measurements at each point. Dashed lines indicate linear extrapolation to the headwaters and Grand Canyon rim measurements.

Discharge measured in flumes in 2017 (Figs. 1, 4) confirms that springs around the margin of the oldest (Canyon) flow, like nearby rivers, experience continuous flow recession except for a modest response to rainfall. All gaged springs showed little response to summer thunderstorms except during a week in mid-September, when 63 mm of rain fell in the park. Two springs on younger flows showed an increase in discharge through July, and two springs experienced recession through July, but then stabilized or increased in discharge during August and October. These periods of increasing or stable discharge are

interpreted as delayed snowmelt pulses (Table 1). Delayed snowmelt pulses are evident in

all flumes around the younger rhyolites, but only one potential delayed snowmelt response

was identified on the oldest flow; flume 5 experienced very slow recession following the

September precipitation, possibly reflecting a small contribution from spring snowmelt at

the end of the record.

Table 1. Timing of delayed snowmelt pulses in flow margin springs, 2017.

Flume (flow age)	Timing of delayed snowmelt pulses
#1 (79 ka)	7/1 – 9/25
#2 (79 ka)	8/1 – 9/3 and 9/25 – 10/15
#3 (160 ka)	7/1 – 10/15 (entire summer season)
#4 (160 ka)	9/28 – 10/15
#5 (484 ka)	None, or possibly 10/1 – 10/15
#6 (484 ka)	None

Each delayed snowmelt pulse was used to calculate the hydraulic conductivity (K) of the

associated aquifer using Eq. 4. Tables 2 and 3 present K values derived from delayed

snowmelt responses for each gaged spring on the Rhyolite Plateau, Cascade basalts studied

by Manga (1999) and the talus slope studied by Kurylyk and Hayashi (2017). Two to four

likely recharge areas were identified for each spring using topographic and geologic maps,

and K values in Tables 2 and 3 are averages of the results obtained using the different

recharge areas. Values for the Canyon flow are considered maximum values because the

peak response may have been later than the period of record. T-tests assuming unequal

variance for difference in mean K values indicate that the Canyon flow has significantly

lower K than the other flows and talus ($p < 0.05$), but the other groups are not statistically

different from each other. It is possible that the snowmelt pulses that arrived at the margin of the Buffalo Lake flow have recharge areas on the partially overlapping Summit Lake flow, but much higher K values (2-3 x 10^{-2} m/s) would be required to transmit pulses that far (~20 km).

Table 2. Hydraulic conductivity calculated using snowmelt responses and porosity of 0.3 (fractures or rubble layers)

Rhyolite Plateau flow	Pitchstone (79 ka)			Buffalo Lake (160)				Canyon (484)
Flume #, peak response month	#1 July	#2 Aug	#2 Oct	#3 July	#3 Sept	#4 Aug	#4 Oct	#5 Oct?
Average K for response (m/s)	1×10^{-2}	6×10^{-3}	6×10^{-3}	8×10^{-3}	8×10^{-3}	6×10^{-3}	5×10^{-3}	$\leq 2\times10^{-3}$
Average K for flow (m/s)	7×10^{-3}			6×10^{-3}				$\leq 2\times10^{-3}$

Aquifer material	Cascade Basalt[1]				Talus[2]
Spring location	Big Sp., CA		Cultus R, OR	Browns Cr, OR	Babylon Creek, BC
Average K for response (m/s)	3×10^{-2}		1×10^{-2}	6×10^{-3}	1×10^{-2}
Average K for material (m/s)	2×10^{-2}				1×10^{-2}

[1]Cascade basalt lag times from Manga (1999)
[2]Porosity of 0.5 used for talus

Table 3. Hydraulic conductivity calculated from delayed snowmelt responses using bulk rock porosity (0.1)

Rhyolite Plateau flow	Pitchstone (79 ka)			Buffalo Lake (160)				Canyon (484)
Flume #, peak response month	#1 July	#2 Aug	#2 Oct	#3 July	#3 Sept	#4 Aug	#4 Oct	#5 Oct?
Average K for response (m/s)	3×10^{-3}	2×10^{-3}	2×10^{-3}	3×10^{-3}	3×10^{-3}	2×10^{-3}	2×10^{-3}	$\leq 6\times10^{-4}$
Average K for flow (m/s)	2×10^{-3}			2×10^{-3}				$\leq 6\times10^{-4}$

Aquifer material	Cascade Basalt[1]			
Spring location	Big Springs, CA		Cultus River, OR	Browns Creek, OR
Average K for response (m/s)	9×10^{-3}		3×10^{-3}	2×10^{-3}
Average K for material (m/s)	5×10^{-3}			

[1]Cascade basalt lag times from Manga (1999)

Soil and sediment cover on the plateau are variable, with bedrock exposed intermittently on pressure ridges, steep flow margins and in incised stream channels and small canyons. In the basins between pressure ridges, there is commonly a coarse volcanic rubble layer consisting of locally derived gravel- to boulder-sized sediment. Thickness of this rubble layer is poorly constrained because basins are rarely incised through to bedrock, but exposures in roadcuts and gullies suggest that this layer is 0.5-2 m thick and grades into

fractured bedrock. Above the rubble layer or directly on bedrock is a layer of silt-dominated eolian and lacustrine deposits and stony glacial till with abundant silty matrix. These sediments are modified by fairly weak soil development. Soils can be broadly grouped into 3 distinct categories: (1) Soils on pressure ridges and forested slopes and basins typically contain a 5-30 cm dark brown A horizon and a slightly reddened B horizon of similar thickness. Tree throw and other bioturbation disturbs any original stratification of the sediments and soil horizons, and mixes coarse material from the rubble layer into the overlying silt-loam soil. These soils tend to be loose or blocky in structure, are well aerated, and have a moderately high infiltration rates as indicated by little evidence for runoff generation in forested areas. (2) Dry basins or basins with only ephemeral streams are dominated by grasses growing in silt to silt-loam soils with thin gray A horizons (0-20 cm) and weakly reddened B horizons. Soil structure ranges from blocky to prismatic. The underlying sediment commonly contains layers of compacted silt with very hard dry consistence and relatively low permeability that produces surface ponding and many small rivulets during precipitation events. (3) In basins with perennial water sources, dark brown to black organic-rich soils have developed. These soils consist largely of root masses, decaying biomass and fine sediment up to pea gravel in size. These peat-like mats form over the rubble layer and create overhanging banks where streams cut through to the gravelly substrate.

On average, rhyolite flows contain between 0.5 and 1.2 closed depressions per km^2, or about 1 small (< 0.1 km^2) closed depression per 1.5 km^2, and 1 larger depression (up to 1 km^2) per 7 km^2. Depressions are more common on younger flows (Fig. 8) with significant (p

< 0.05) differences between (1) the Buffalo Lake flow (160 ka) and the Pitchstone Plateau flow (79 ka), and (2) the Canyon flow (484 ka) and the Summit Lake (124 ka) and Pitchstone Plateau flows. The Canyon flow has a significantly higher density of closed basins associated with hydrothermal features or alteration as compared to the younger flows, which are not significantly different from each other.
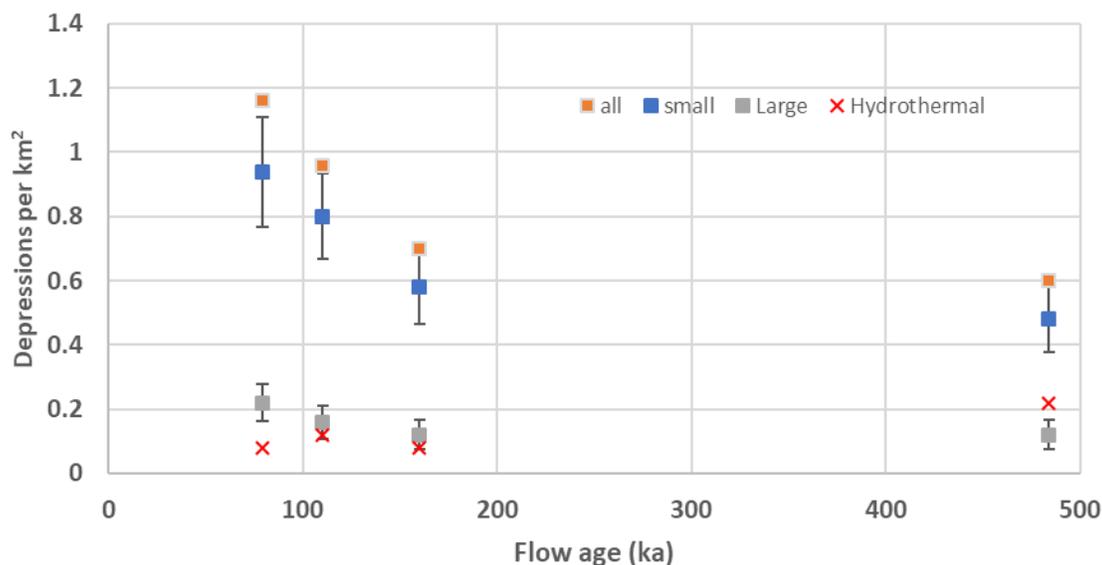
Figure 8. Mean density of closed depressions on individual rhyolite flows. Standard error bars shown for large and small basins are derived from bootstrap resampling; error bars generated with the jackknife method lie within the point symbols.

5.   Discussion

While all major rivers in the GYR experience flow recession through the summer, many springs around the younger flows of the Rhyolite Plateau experience a net increase in discharge (Fig. 5). These springs help maintain high baseflow conditions in rivers draining the plateau, and create wetlands that persist through the hot, dry summer months. The springs therefore produce stability in both local water resources required for wildlife habitat

and regional water resources used by municipalities and agricultural centers in semiarid

regions downstream. Stable discharge throughout the summer season and from one year

to the next are also indicators that many of these springs will have a high resilience to

climate change and may become increasingly important in coming decades. However,

spring behavior on the Rhyolite Plateau varies greatly over short spatial and temporal

scales. Springs on the surfaces of younger flows tend to run dry by August, when many

springs around the flow margins are running high. Although many springs gained discharge

through July, there is high variance in discharge behavior for these springs, even between

those that are < 1 km apart (Fig. 4 springs #1 and #2, Fig. 6 Pitchstone Plateau margin).

Conversely, springs on the oldest flow behave more like water sources found outside of the

Rhyolite Plateau, which indicates that the hydrology of these rhyolite flows evolves over

time. Understanding these spatial and temporal variations in spring discharge requires

detailed assessment of the connectivity between surface waters and the aquifers of the

Rhyolite Plateau.

5.1 Aquifer characteristics and connectivity to surface waters

Snowmelt provides the majority of surface water and groundwater recharge for high

altitude streams in the GYR (Gardner et al., 2010, Tercek et al., 2015), but it is the bedrock

and surficial geology that determines where and when that water flows from springs.

Spring locations indicate that the rhyolite flows have two primary types of aquifers: perched

aquifers in the surface rubble layer, and deeper bedrock fracture aquifers with a high

permeability zone near the basal contact of the rhyolite flow.

The surface rubble-layer aquifers are in many places capped by thin, low-permeability silt-rich deposits. Many first-order streams begin on top of the silty deposits where concave basin areas concentrate and channelize snowmelt and rain runoff.   As low-order streams conjoin, they incise through the silty layer and access the highly permeable rubble layer, where water drains into the perched aquifer, creating losing reaches near the lower ends of the broad grassy basins. Upper rhyolite flow surface structures create many closed depressions (Fig. 8). Water pools in these depressions and behind snow dams during the snowmelt season, favoring infiltration and recharge of the shallow aquifers. At least locally, the silty sediment cap acts as a confining unit for the shallow aquifer; below one snow dam, positive head in the aquifer lifted the soil off of the underlying rubble, creating a floating surface. Flowing "wells" were generated by drilling through the elevated upper deposit with a sharp metal pole. This confining action reduces loss of water to the surface and likely encourages deeper percolation. Rubble-layer aquifers are discontinuous and bounded by bedrock pressure ridges, and a single stream may access many individual perched aquifers as it traverses the flow surface. Where major drainages have incised small canyons (< 30 m deep) into the rhyolite flows, seepage occurs along the canyon slopes at the base of the rubble layer. Locally, water is funneled to a single point by underlying bedrock, producing a gushing spring that cascades down to the main channel (Fig. 3B). Individual springs from the shallow aquifers have discharges less than 0.01 m^3/s, but combined along a stream length, they produce streams with discharge up to 2 m^3/s.

The larger and more productive aquifers are contained within and below the heavily fractured rhyolite. The discharge values of individual springs are typically < 1 m^3/s, but

range up to 6 m^3/s. These springs almost always occur near the basal contact of the rhyolite, which is typically buried by talus, colluvium or till. In one exposure, the contact consists of a rubble layer over a contact-metamorphosed welded tuff. Whether this porous rubble layer is pervasive or not, the basal contact appears to be a zone of high transmissivity. Springs emerge near the contact even when the valley bottom is incised well below the base of the rhyolite flow, indicating that there is a major permeability contrast between the rhyolite flow and the older volcanic units it sits on.

The deeper aquifers are recharged by surface waters that infiltrate through bedrock fracture zones. Three pieces of evidence suggest that these recharge zones are commonly associated with pressure ridges: (1) Major steeply dipping fracture networks are observed underlying and adjacent to pressure ridges where bedrock has been exposed in canyons. Seepage occurs at these fractures where the water table is higher than the canyon floor (Fig. 3D). (2) On younger rhyolite flows, early summer flow in ephemeral streams extends across basins but declines and disappears when crossing a pressure ridge. (3) Repeat discharge data collected on Surface Creek above, within, and below a pressure ridge show significant changes in discharge in bedrock reaches as the stream crosses the pressure ridge (Fig. 7).

Patterns of streamflow along Surface Creek on the Canyon flow provide indicators of the interconnectedness of the stream to the upper rubble aquifers as well as the bedrock aquifer. Above a major pressure ridge, Surface Creek crosses a broad grassy basin with a ~0.5 m thick silty organic mat overlying a coarse boulder gravel of unknown thickness. The stream then passes through a steep reach where it is incised ~5 m into bedrock, followed by

a small basin and another longer reach incised up to 10 m in bedrock (Fig. 7). The shallow

rubble aquifers located in both basins act like reservoirs, storing snowmelt for later in the

season. In June 2017, both basin reaches of Surface Creek were losing reaches, whereas in

August both were gaining reaches. In the early season, water drains out of the stream and

recharges the shallow rubble aquifer and likely also the bedrock aquifer below. Later in the

season, when stream discharge is lower, water drains back into the channel from the

shallow aquifer. In 2016, stream flow was lower than in 2017, and very little water was

transferred out of the channel into the lower basin aquifer in June. In August, discharge

continued to decrease through that reach, indicating that during this low snow year, the

shallow aquifer never filled, or was drained by August. The upper and lower bedrock-

incised reaches exhibited opposite behavior, with the upper reach losing water at all

measurement times (2017 only), and the lower bedrock reach gaining water during all 4

measurement periods. Bedrock exposures in the creek bed and on the adjacent hillslopes

rule out the perched rubble aquifers as drivers of this fluctuation in discharge and indicate a

high degree of connectivity between bedrock and the stream. The upper bedrock-confined

reach is near the top of the profile convexity, where the water table is lower due to the

steep slope below, thus surface water is probably lost to the bedrock aquifer at all times of

the year. The lower reach is at the base of the convex profile segment where the

topography drops abruptly, and the stream is incised into the bedrock and to the water

table.

5.2 Delayed snowmelt pulses

Many springs around the margins of the younger rhyolite flows experienced an increase or maintenance of discharge through the summer season that is not associated with precipitation events. I infer that these deviations from typical flow recession are delayed snowmelt pulses released from the deep bedrock aquifer (Table 1). The continuous spring measurements also show that the snowmelt pulses occur at different times during the summer and fall. Along with qualitative observations of stream and spring levels made in October 2017, these records suggest that snowmelt pulses tend to arrive earlier in the summer at the margins of the youngest flow, later towards the fall on the intermediate-age (160 ka) flow, and are rare around the oldest rhyolite flow (484 ka).

 Delayed snowmelt pulses are also evident in the repeat discharge records (Fig. 5), where many springs experienced a net increase in discharge through July. Some streams with relatively little recession (0 to -20% change) may also be influenced by a delayed snowmelt pulse, but without continuous discharge records, it is difficult to differentiate minor delayed snowmelt pulses (e.g., spring #2; Fig. 4) from very slow recession, as experienced by the Firehole and Gibbon rivers in July of 2016 (Fig. 2). Baseflow recession in local rivers is greatest in July (Gardner et al., 2010), which makes late June to August an optimal time frame for identifying springs and streams that deviate from the typical recession behavior and experience delayed snowmelt pulses. August is also an ecologically important time for water availability. It is a critical part of the growing season for plants and the reproductive season for many amphibians and other aquatic life (McMenamin et

al., 2008). July and August are also the warmest months of the year in the GYR, which

makes it a time of high water stress and increases demand for water by organisms.

Although the repeat measurements only document discharge at two times over the

summer, they provide a much larger sample size and distribution, which is valuable given

the spatial heterogeneity of spring behavior. Most springs around the margin of Pitchstone

Plateau (79 ka) gained discharge over July (Fig. 5), but some within 1 km of other gaining

springs showed strong recession (Fig. 4 springs #1 and #2, Fig. 6). Much of this local

variation in spring behavior is likely driven by (1) heterogeneity of the deep aquifer and the

basal contact of the rhyolite flow, (2) differences in the size of the recharge areas and (3)

the flow length and hydraulic gradient between recharge areas and springs. The rhyolites

flowed out over complex eroded landscapes containing a wide variety of surficial deposits,

with relief of up to 100 m or more. Subsequent erosion and deposition have yielded

differing degrees of exposure or burial of the basal contact along the flow margin, which

influences where the aquifer and surface intersect. Internal structures such as fracture

networks and pressure ridges likely produce an anisotropic flow regime in the deep aquifer.

Together, these factors produce clusters of springs along the flow margins and variations in

spring behavior within and between those clusters. High local variation in spring location

and behavior through time highlights the importance of data covering a range of spatial and

temporal scales.

Using Eq. 4 to calculate the hydraulic conductivity of young volcanic rocks and coarse

sediments is supported by a comparison of our values to those calculated by other

methods. Using parameters derived from hydrogeological modeling, environmental tracers,

and a porosity value of 0.1, Manga (1999) calculated K ≈ 2x10^{-3} m/s for the Cascade Range

basalt flow that feeds Rising River, but was unable to measure a snowmelt response lag

time due to the presence of a dam on Rising River. Using the same porosity, I used Eq. 4 to

calculate K values for three other flows in the Manga (1999) study (Table 3). This produced

the same K value for Browns Creek, and somewhat larger values that are within an order of

magnitude for the other 2 springs. Hydraulic conductivity calculated by Eq. 4 (Table 2)

matches the value of 1 x 10^{-2} m/s calculated for a talus slope by Kurylyk and Hayashi (2017)

using a homogeneous single-layer hydrogeological model, and falls between the values of K

= 2 x 10^{-2} and 2 x 10^{-3} m/s derived for a two-layer aquifer model. The Eq. 4 talus slope K also

closely matches an estimate for talus slopes in Colorado (Clow et al., 2003). Flerchinger et

al. (1992) used an equivalent form of Eq. 4 to show that snowmelt response lag time in an

unconfined aquifer roughly matched K values based on slug tests by Winkelmaier (1987).

These results indicate that using snowmelt travel times to estimate K is appropriate for

highly permeable aquifers. Our method is limited in that only aquifers with short flow paths

or high hydraulic conductivities produce delayed snowmelt pulses, because groundwater

response to a recharge pulse is damped over time (Kurylyk and Hayashi, 2017). This

method is also limited to largely unconfined aquifers, as confined aquifers may respond

faster to changes in water table elevation due to the transmission of a pressure pulse

(Flerchinger et al., 1992). Water ages at springs were not measured in this study, and the

delayed snowmelt pulses might consist of older water forced out at the margin by changes

in piezometric head that move through the aquifer faster than water flow. Water flowing in

a basal rubble layer could potentially be confined by overlying rock, so the values presented here represent values at the high end of the range of possible K values.

5.3 Evolution of hydrology on the Rhyolite Plateau

One of the most important variables controlling spring behavior on the Rhyolite Plateau is flow age. Significant (p < 0.05) correlations exist between the net change in discharge through July and rhyolite flow age for margin springs (Fig. 5). Variance in discharge change through July decreases significantly (p ≤ 0.05) between each of 3 flow groups (79-103 ka, 124-164 ka and 484 ka), and hydraulic conductivity of the oldest flow is significantly lower than that of the younger flows. These trends are likely caused by the evolution of both the shallow and deep aquifers over thousands of years. Coarse surface rubble layers and deep fracture networks are evident on very young (< 10 ka) lava flows around the world, and precipitation rapidly infiltrates into the flow where it either percolates into deeper aquifers or is discharged at a flow edge (Welhan and Reed, 1997; Jefferson et al., 2010). Lava flows contain no initial surface drainage network, and most network development occurs after soil development reduces infiltration (Wells et al., 1985; Dohrenwend et al., 1987, 1989) and fractures are clogged by fine surficial sediments and weathering products, which are commonly clays (Buol et al., 2011; Yokoyama and Banfield, 2002). Mineral precipitation and hydrothermal alteration are commonly observed in bedrock on the Rhyolite Plateau and reduce the permeability of the flows by filling voids (Fenner, 1936; Dobson et al., 2003). Secondary minerals fill macropores (vugs and cracks in perlitized obsidian) in outcrops of flows of all ages, but large (> 5 cm) opal nodules were only observed on the oldest flow, which also has significantly more depressions with clear evidence for past or present

hydrothermal alteration (Fig. 8). These processes are episodic but progressive in nature, and are likely responsible for the changes in spring hydrology observed on flows of different ages in the Rhyolite Plateau. A few rhyolite flows (e.g. the Elephant Back flow in the central caldera) contain major fault systems which could increase permeability, but I avoided these flows to minimize tectonic fracturing as an influence on aquifers.

Springs on young flows (79-164 ka) exhibit a wide range of behaviors through the summer season, with a strong contrast between surface and margin springs. Almost all surface waters dry up or are limited to non-discharging pools and lakes by August, whereas over half of margin springs increase in discharge from June to August (Pitchstone Plateau flow, Figs. 5, 6). These behaviors indicate that water rapidly percolates out of the shallow aquifers and into the deep aquifer, raising the water table of the deep aquifer under the upper plateau surfaces. The elevated water table promotes faster groundwater flow, which is expressed at the flow margins as delayed snowmelt pulses in the summer and fall. This interpretation is supported by a comparison of the hydrographs and repeat discharge measurements taken in 2016 and 2017, where 2017 had ~59% greater peak snowpack than 2016 and a later melt-out date, with streams running much higher in late June than at the same time the year before. The hydrographs of rivers draining the Rhyolite Plateau experienced significant recession in July 2017 as direct meltwater and shallow throughflow drained out of the system, but were almost flat throughout July 2016, indicating that they had already reached baseflow conditions by the end of June. In contrast, the average change in discharge through July for margin springs around young (< 164 ka) flows was significantly greater ($p < 0.05$) in 2017 (+9% change) than in 2016 (-12% change). Greater

snowpack in 2017 resulted in elevated river levels in the early season, but higher rhyolite

spring discharge later in August, indicating that these springs experienced a delayed

response to snowmelt as water flowed through highly transmissive aquifers.

Estimates of hydraulic conductivity for the young rhyolite flows based on lag times for

delayed snowmelt pulses (2 to 7 x10^{-3} m/s, Tables 2 and 3) are extremely high as compared

to most Earth materials (10^{-2} to 10^{-13} m/s), but comparable to values calculated for

Quaternary basalts in the Cascade Mountains (Manga, 1999), contact and rubble zones in

basalts of the Snake River Plain (Anderson et al., 1999), karst aquifers (Domenico and

Schwartz, 1990), unconsolidated gravel (Fetter, 2018), and alpine talus deposits (Kurylyk

and Hayashi 2017). Dobson et al. (2003) measured the permeability of perlitized lava from

core samples, which were mostly equivalent to K < 10^{-9} m/s. This value is 6 orders of

magnitude lower than the K values for the young Pitchstone Plateau and Buffalo Lake flows

calculated using delayed snowmelt lag times and a bulk rock porosity of 0.1 (Table 3). This

mismatch indicates that largely unfractured rhyolite is too impermeable to deliver

recognizable snowmelt pulses to the margin springs, and likely has a negligible influence on

seasonal variation in spring discharge. Values of K calculated with a porosity of 0.3 (Table 2)

represent flow through fracture zones and rubble layers (6 to 7 x10^{-3} m/s) and match well

with K values for aquifers that exhibit delayed snowmelt responses (Manga, 1999; Kurylyk

and Hayashi 2017). This indicates that fracture zones like those found near pressure ridges

and rubble layers at the bases and surfaces of the rhyolite flows are likely responsible for

generating the delayed snowmelt pulses and most rapid water transmission. High

transmissivity is also indicated by the large variance in margin spring behavior noted on

younger flows. A highly transmissive aquifer has the potential to fill and drain quickly, and high variance in measurements would be expected in repeat discharge data collected from springs associated with a dynamic aquifer, since these data capture just a snapshot of that behavior. Flume #1 (Fig. 4) near the 79 ka Pitchstone Plateau flow illustrates this point well, as it rose quickly in July and fell precipitously in late September, indicating rapid changes in the water table.

The Canyon flow (484 ka) is by far the oldest large (> 100 km^2) Yellowstone rhyolite flow that hasn't been buried by younger sediments or volcanics. Springs and streams on the Canyon flow have seasonal hydrographs more like nearby large rivers than those on the younger flows (Fig. 4), and changes in discharge are more like springs located in Eocene volcanics (Fig. 5). While some small ponds, first-order streams and springs on the Canyon flow dry up by August, almost all moderate-sized drainage basins (>1 km^2) contain perennial streams, even on the upper surface of the flow. Perennial streams on the surface tend to show less flow recession than springs around the margin (Fig. 6 Canyon). Delayed snowmelt pulses were rarely observed in springs around the Canyon flow margin and variance in spring behavior over July was very limited in 2017. These data indicate that the deep aquifer has undergone significant evolution as compared to the younger flows. Direct quantitative evaluation of the fracture network and rubble layer aquifers is impractical, but field and aerial photo observations indicate much greater hydrothermal alteration than the younger flows. The Canyon flow contains twice the density of large and small hydrothermal basins than the younger flows (Fig. 7), and bedrock exposed in many canyons is visibly altered with visible deposits of white silica, yellow sulfur and red iron oxides. A

mineralogical analysis of a hydrothermally altered portion of the Canyon flow found

abundant opal, kaolinite, alunite, dickite and illite of hydrothermal origin, and that feldspars

were commonly altered to pseudomorphic replacements by clay (Larsen et al., 2009). Large

deposits of secondary minerals were only rarely observed on younger flows.

Precipitation of secondary minerals and progressive weathering reduce porosity and

transmissivity of an aquifer, but because no spring or stream on the Canyon flow shows

clear evidence of a delayed snowmelt pulse, it is impossible to confidently estimate

hydraulic conductivity of its bedrock aquifer. Assuming that there is a minor snowmelt

signal at the end of the Spring #5 record (Fig. 4), a maximum hydraulic conductivity estimate

of 2×10^{-3} m/s results for flow through fractures and rubble in the Canyon flow (Table 3).

This is a maximum value, since if a snowmelt pulse exists, its peak may be later than the

period of record, and a porosity of 0.3 assumes no reduction in porosity relative to the

younger rhyolites. I infer that the deep aquifer in the Canyon flow has undergone

significant reduction in permeability, as the mean of the maximum K values calculated for

multiple potential source areas on the Canyon flow is significantly lower than mean values

for the other rhyolite flows and other porous materials. Delayed snowmelt responses are

not commonly observed in aquifers with more typical hydraulic conductivity values of $< 10^{-5}$

m/s and aquifer lengths of > 1000 m, because signal dampening increases as hydraulic

conductivity decreases (Kurylyk and Hayashi, 2017). Since most streams sourced from the

Canyon flow do not show delayed snowmelt pulses, the calculation of $\leq 6 \times 10^{-4}$ m/s based

on a porosity of 0.1 may be a better estimate of its K value.

Unlike the younger rhyolite flows, where very high permeability appears to allow water to drain away from the surface during the summer, reductions in porosity and permeability within the Canyon Flow have led to a shallower water table within the bedrock aquifer. Surface Creek discharge increased by > 50% as it flowed through the lower bedrock-confined reach in August of both years, indicating that the water table of the bedrock aquifer remains near the surface through the summer. Although water drains out of the channel and into the sedimentary and bedrock aquifers as it crosses the pressure ridge, the discharge of Surface Creek is higher below the pressure ridge than above it, indicating that water is not being lost to the deep aquifer. Total snowpack and precipitation are lower on the Canyon flow than on the younger flows, indicating that the relatively high water table is controlled by subsurface factors and not climatology. Low variance in spring and stream behavior through the summer of 2017 indicates slow and steady draining of aquifers and a highly damped response to the large snowmelt signal, which is consistent with a low-transmissivity deep bedrock aquifer. In 2016, variance in the repeat discharge data was greater and not significantly different from that on younger flows. Some of this variance can be explained by lower overall discharge values, since smaller changes in absolute discharge yield a larger percent change in discharge. High variance in 2016 also suggests that after multiple years of below average precipitation, some streams may become disconnected from the water table and become ephemeral, or more significantly impacted by surface runoff than baseflow. The one stream on the Canyon flow that showed an increase in discharge over July (Fig. 5) is a stream with a large drainage basin (15 km^2), and that increase may have been due to runoff from a recent precipitation event.

Hydrologic evolution will likely continue on the Canyon flow, but at a much slower rate. Infilling of fractures by weathering, hydrothermal processes and sedimentation is dependent on the porosity of the bedrock, and since the porosity and permeability of the Canyon Flow have been reduced, the rates of these processes will likely decrease as well. Springs around the Canyon Flow experienced only slightly less recession during July than those draining nearby Eocene volcanic rocks, indicating that the deep aquifer of the Canyon flow has almost reached the hydraulic conductivity of the surrounding Eocene volcanic rocks. Assuming that the Eocene volcanics are a representative end member of hydrologic evolution in volcanic materials, then deep aquifers on the Rhyolite Plateau may reach a state indistinguishable from other older volcanics roughly 700 kyr after emplacement. This rate is similar to or slightly faster than that of volcanic landscapes in the Western Cascades (Jefferson et al., 2010) and faster than that of basaltic terrains in drier climates (Wells et al., 1985). Water and sedimentation are two key driving factors in volcanic landscape evolution, so it is likely that higher precipitation and Quaternary glaciation in Yellowstone and the Cascades has accelerated hydrologic evolution relative to desert environments. Rhyolite aquifers also likely evolve faster because they lack the lava tubes common in basaltic flows that provide initial void spaces up to 10s of meters in diameter and kilometers long.

5.4 Resilience

Climate change has already had a significant negative impact on water resources and wildlife habitats of the GYR and will continue to do so for the foreseeable future (Chang and Hansen, 2015; Romme and Turner, 2015; Thoma et al., 2015). An important step in

understanding these impacts is to identify the potential resilience of freshwater springs and streams. Water demand is highest during the late summer growing season when water availability declines, so I propose two indicators of stream resilience that are tied strongly to August discharge values: (1) an increase in or relatively stable discharge through July, and (2) relatively consistent interannual discharge values as measured in August. Stable or increasing discharge through July may either indicate the presence of a delayed snowmelt pulse or a very stable water table that produces springs, like Big Springs, that have fairly consistent discharge throughout the year (Fig. 2). A relatively stable water table also produces springs and streams that maintain more consistent flow from year to year. Low interannual variability is indicated by a low ratio between August 2017 and August 2016 discharge values. Springs and streams with stable water tables may respond more slowly to drought conditions and be a refuge for wildlife in lean water years. These two measures of stability are plotted on Figure 9.
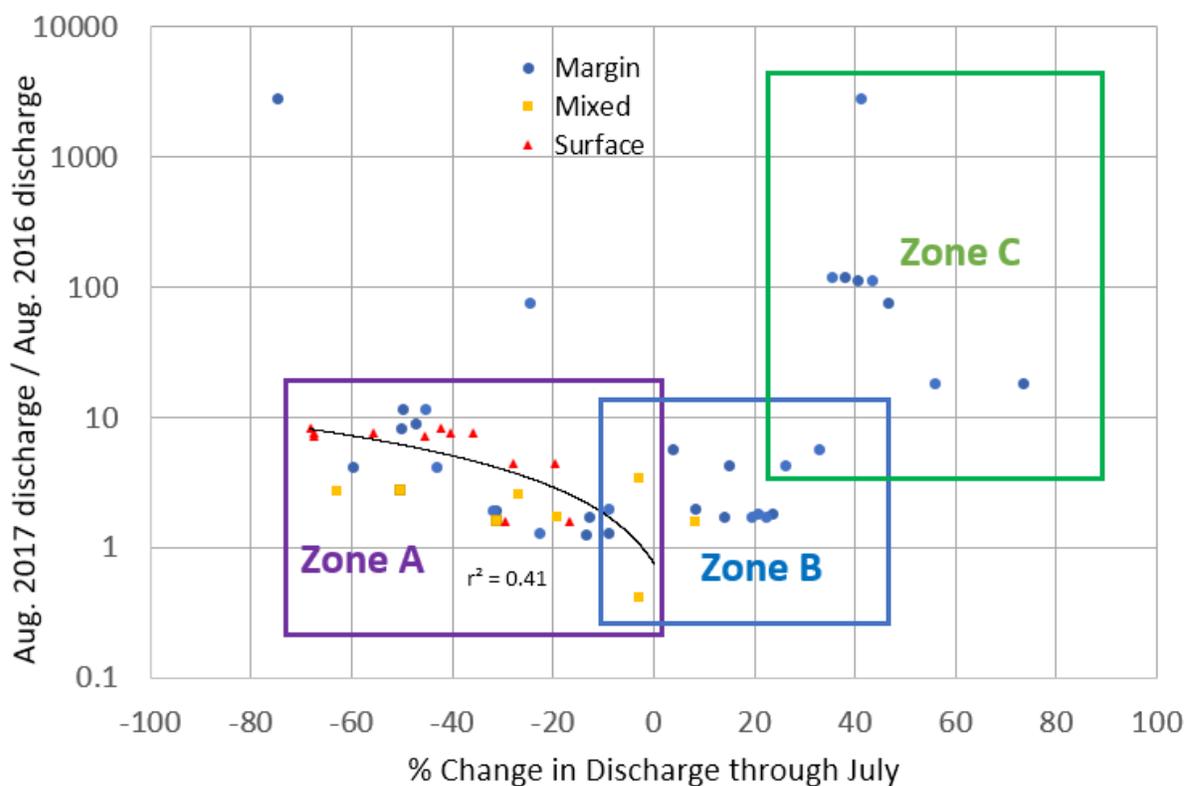
Figure 9. Ratio of August 2017 to August 2016 discharge of Rhyolite Plateau springs plotted against change in discharge over July for each year. Snowpack was ~59% higher in 2017 as compared to 2016, resulting in discharge ratios > 1. Data are broadly grouped into 3 zones which may indicate relative resilience to climate change. Springs with negative change in discharge through July and high August discharge ratios (Aug 2017/Aug 2016) are interpreted as having low resilience.

Springs around the Rhyolite Plateau broadly fall into 3 resilience-based zones (A, B, and

C on Fig. 9). Zone A contains all springs that experience recession through July. There is a

wide range of resilience in this group, with those on the left side of the group exhibiting

lower resilience in both measures. A significant linear relationship exists in group A

between the two resilience measures, which suggests that streams with more stable

discharge through the summer are also more stable from year to year. Zone B includes

springs with modest delayed snowmelt pulses, and low to moderate interannual variability.

Springs in Zone B are likely highly resilient to climate change and drought and may serve as

important wildlife hotspots if neighboring water sources become ephemeral. Zone C includes springs with large delayed snowmelt pulses and extreme interannual variability. While these springs may maintain aquatic habitat late in the season in a high snowpack year, their discharge may be dramatically lower in a dry year. Many Zone C springs will be strongly impacted by climate change, since total snowpack is predicted to decline over this century and snowmelt is likely to occur earlier in the season. Overall, we have the least confidence in assigning resilience to the springs in Zone C.

Stream resilience varies with flow age and topographic position, since almost all margin springs with delayed snowmelt pulses were on the younger flows (< 164 ka), with the youngest flow having the most such springs. However, water on the upper plateau surfaces of younger flows is already largely ephemeral, and the remaining perennial springs and non-discharging pools are likely at significant risk from continued climate change and drought. These water sources are poorly represented in Fig. 9 because snow conditions prevented adequate sampling of these areas in June 2017. Older rhyolite flows have an opposite but less pronounced pattern of resilience, with surface streams faring slightly better than margin springs, which seem to do poorly under drought conditions. Flow morphology and age therefore create a complex patchwork of adjacent zones with high and low stream resilience to climate change and variability.

6. Conclusions

The Rhyolite Plateau is an important headwaters region that is threatened by reduced snowpack, earlier snowmelt dates and higher water stress resulting from climate change

(Tercek et al., 2015; Thoma et al., 2015). The flows contain shallow rubble-layer aquifers perched over a deeper fractured bedrock aquifer. On young (< 164 ka) flows, water drains into the deep aquifer and away from the surface in July, leaving most surface streams and springs dry. Springs commonly occur around the margins of these flows where the basal contact is exposed. These springs often experience delayed snowmelt pulses in summer and fall, as water infiltrates readily across the broad upper surfaces and flows quickly through the bedrock aquifer, including through a highly conductive layer near the base of the flow. Lag times for delayed snowmelt pulses indicate that water is flowing through fracture zones and or rubble layers with hydraulic conductivities of 10^{-3} to 10^{-2} m/s. These K values represent flow through the most permeable components of a spatially heterogenous and likely anisotropic aquifer, which produces clusters of springs around the flow margins. Delayed snowmelt pulses arrive at margin springs at different times as a result of variable K values and distances between springs and recharge zones. When integrated across large (> 3×10^3 km^2) drainage basins, the delayed snowmelt signals are damped out, and rivers draining the Rhyolite Plateau have relatively high, stable baseflow through the summer and fall. These rivers therefore provide reliable water for downstream wildlife and human uses during periods of high water stress. As the rhyolite flows age, the deep aquifer becomes less permeable as a result of weathering, sedimentation, and precipitation of minerals by hydrothermal processes. The oldest flow exhibits nearly a reversal of the pattern observed in the youngest flow, with most of the snowmelt being stored in surficial sediments and a shallow bedrock aquifer. Runoff in surface streams is common on this flow, because deep percolation is limited. While margin springs still exist on the oldest flow, they rarely

experience delayed snowmelt pulses, and their hydrographs more closely resemble those of water sources outside the Rhyolite Plateau.

The ability of a stream to maintain perennial flow despite seasonal droughts or increased summer temperatures – i.e. its resilience to climate change – was assessed by two measures. Streams with delayed snowmelt pulses in August will likely maintain aquatic habitat into the water-stressed late summer and act as refuges for aquatic life that requires perennial water sources. Streams with very stable water tables show relatively little annual and interannual variation in August discharge and are likely best able to provide flow through drought years. Streams with the highest resilience are found around the margins of the younger rhyolite flows, where many springs exhibit either delayed snowmelt pulses or stable groundwater flow from the base of the rhyolite, creating sustained discharge over the summer and year to year. However, variance in margin spring behavior around the young flows is high, with some margin springs exhibiting dramatic fluctuations in discharge over the summer season and from year to year. Detailed mapping of stream resilience is necessary to further predict future spatial and temporal patterns of water availability. The water sources that are most threatened by climate change are those on the upper plateau surfaces of the same young flows, since high permeability leads to rapid draining of water table from the upper flow surfaces during the summer. Springs and streams on the oldest flow exhibit a summer flow recession pattern more like that of most streams in the GYR, but recession values tend to be less extreme than for those draining older rocks outside the Rhyolite Plateau. Thus, water on and around the oldest flow is likely still more resilient to climate change than in watersheds on older rocks. Understanding these patterns in stream

resilience is an important first step in identifying where climate change impacts will be

greatest, and in producing management plans that best protect a vital and dwindling

habitat. Aquifers associated with the Rhyolite Plateau act as seasonal reservoirs, but no

pattern of storage and release of water can compensate for reductions in snowpack and

increases in evapotranspiration associated with long-term warming or prolonged droughts.

These results highlight the need for immediate action to reduce the emissions driving global

climate change if we are to limit impacts to greater Yellowstone, one of the most intact

ecosystems in the temperate zone.

7. References

Anderson, S. R., Kuntz, M. A., & Davis, L. C. (1999). *Geologic controls of hydraulic conductivity in the Snake River Plain aquifer at and near the Idaho National Engineering and Environmental Laboratory, Idaho* (Vol. 99, No. 4033). US Department of the Interior, US Geological Survey.

Barnett, T. P., Pierce, D. W., Hidalgo, H. G., Bonfils, C., Santer, B. D., Das, T., ... & Cayan, D. R. (2008). Human-induced changes in the hydrology of the western United States. *science*, *319*(5866), 1080-1083.

Bohr, G. S., & Aguado, E. (2001). Use of April 1 SWE measurements as estimates of peak seasonal snowpack and total cold-season precipitation. *Water Resources Research*, *37*(1), 51-60.

Buol, S. W., Southard, R. J., Graham, R. C., & McDaniel, P. A. (2011). *Soil genesis and classification*. John Wiley & Sons.

Chang, T., & Hansen, A. (2015). Historic and projected climate change in the Greater Yellowstone Ecosystem. *Yellowstone Science*, *23*(1), 14-19.

Christiansen, R. L. (2001). *The Quaternary and Pliocene Yellowstone Plateau volcanic field of Wyoming, Idaho, and Montana* (No. 729-G).

Clow, D. W., Schrott, L., Webb, R., Campbell, D. H., Torizzo, A., & Dornblaser, M. (2003). Ground water occurrence and contributions to streamflow in an alpine catchment, Colorado Front Range. *Groundwater*, *41*(7), 937-950.

Davinroy, T. C. (2000). *Hydrological and biogeochemical characteristics of alpine talus, Colorado Front Range* (Doctoral dissertation, University of Colorado).

Dobson, P. F., Kneafsey, T. J., Hulen, J., & Simmons, A. (2003). Porosity, permeability, and fluid flow in the Yellowstone geothermal system, Wyoming. *Journal of Volcanology and Geothermal Research*, *123*(3-4), 313-324.

Dohrenwend, J. C., Abrahams, A. D., & Turrin, B. D. (1987). Drainage development on basaltic lava flows, Cima volcanic field, southeast California, and Lunar Crater volcanic field, south-central Nevada. *Geological Society of America Bulletin*, *99*(3), 405-413.

Dohrenwend, J. C., Abrahams, A. D., & Turrin, B. D. (1989). Drainage development on basaltic lava flows, Cima volcanic field, southeast California, and Lunar Crater volcanic field, south-central Nevada: Reply. *Geological Society of America Bulletin*, *101*(7), 982-986.

Domenico, P. A., & Schwartz, F. W. (1990). Physical and chemical hydrogeology, John Wiley and Sons. *Inc., New York, New York*.

Farrell, J., Smith, R. B., Husen, S., & Diehl, T. (2014). Tomography from 26 years of seismicity revealing that the spatial extent of the Yellowstone crustal magma reservoir extends well beyond the Yellowstone caldera. *Geophysical Research Letters*, *41*(9), 3068-3073.

Fenner, C. N. (1936). Bore-hole investigations in Yellowstone Park. *The Journal of Geology*, *44*(2, Part 2), 225-315.

Fetter, C. W. (2018). *Applied hydrogeology*. Waveland Press.

Flerchinger, G. N., Cooley, K. R., & Ralston, D. R. (1992). Groundwater response to snowmelt in a mountainous watershed. *Journal of Hydrology*, *133*(3-4), 293-311.

Fyfe, J. C., & Flato, G. M. (1999). Enhanced climate change and its detection over the Rocky Mountains. *Journal of Climate*, *12*(1), 230-243.

Gardner, W. P., Susong, D. D., Solomon, D. K., & Heasler, H. (2010). Snowmelt hydrograph interpretation: Revealing watershed scale hydrologic characteristics of the Yellowstone volcanic plateau. *Journal of hydrology*, *383*(3-4), 209-222.

IPCC (2014). Synthesis Report. Contribution of working groups I. *ii and iii to the fifth assessment report of the intergovernmental panel on climate change*, *138*.

Jefferson, A., Grant, G. E., Lewis, S. L., & Lancaster, S. T. (2010). Coevolution of hydrology and topography on a basalt landscape in the Oregon Cascade Range, USA. *Earth*

Surface Processes and Landforms: The Journal of the British Geomorphological Research Group, *35*(7), 803-816.

Jefferson, A., Nolin, A., Lewis, S., & Tague, C. (2008). Hydrogeologic controls on streamflow sensitivity to climate variation. *Hydrological Processes: An International Journal*, *22*(22), 4371-4385.

Kurylyk, B. L., & Hayashi, M. (2017). Inferring hydraulic properties of alpine aquifers from the propagation of diurnal snowmelt signals. *Water Resources Research*, *53*(5), 4271-4285.

Larson, P. B., Phillips, A., John, D., Cosca, M., Pritchard, C., Andersen, A., & Manion, J. (2009). A preliminary study of older hot spring alteration in Sevenmile Hole, Grand Canyon of the Yellowstone River, Yellowstone Caldera, Wyoming. *Journal of volcanology and geothermal research*, *188*(1-3), 225-236.

Lowry, A. R., Ribe, N. M., & Smith, R. B. (2000). Dynamic elevation of the Cordillera, western United States. *Journal of Geophysical Research: Solid Earth*, *105*(B10), 23371-23390.

Manga, M. (1999). On the timescales characterizing groundwater discharge at springs. *Journal of Hydrology*, *219*(1-2), 56-69.

McMenamin, S. K., Hadly, E. A., & Wright, C. K. (2008). Climatic change and wetland desiccation cause amphibian decline in Yellowstone National Park. *Proceedings of the national Academy of Sciences*, *105*(44), 16988-16993.

Meyer, G. A. (2001). Recent large-magnitude floods and their impact on valley-floor environments of northeastern Yellowstone. *Geomorphology*, *40*(3-4), 271-290.

Minder, J. R., Letcher, T. W., & Liu, C. (2018). The character and causes of elevation-dependent warming in high-resolution simulations of Rocky Mountain climate change. *Journal of Climate*, *31*(6), 2093-2113.

Muir, D. L., Hayashi, M., & McClymont, A. F. (2011). Hydrological storage and transmission characteristics of an alpine talus. *Hydrological Processes*, *25*(19), 2954-2966.

Oates, B. A. (2016). *Effects of predators and resource limitation on demography and behavior of moose in the Greater Yellowstone Ecosystem*. University of Wyoming.

Pederson, G. T., Gray, S. T., Woodhouse, C. A., Betancourt, J. L., Fagre, D. B., Littell, J. S., ... & Graumlich, L. J. (2011). The unusual nature of recent snowpack declines in the North American Cordillera. *science*, *333*(6040), 332-335.

Pederson, G. T., Betancourt, J. L., & McCabe, G. J. (2013). Regional patterns and proximal causes of the recent snowpack decline in the Rocky Mountains, US. *Geophysical Research Letters*, *40*(9), 1811-1816.

Pederson, G. T., Graumlich, L. J., Fagre, D. B., Kipfer, T., & Muhlfeld, C. C. (2010). A century of climate and ecosystem change in Western Montana: what do temperature trends portend? *Climatic change*, *98*(1-2), 133-154.

Persico, L., & Meyer, G. (2013). Natural and historical variability in fluvial processes, beaver activity, and climate in the Greater Yellowstone Ecosystem. *Earth Surface Processes and Landforms*, *38*(7), 728-750.

Pierce, K. L. (2003). Pleistocene glaciations of the Rocky Mountains. *Developments in Quaternary Sciences*, *1*, 63-76.

Pierce, K. L., & Morgan, L. A. (2009). Is the track of the Yellowstone hotspot driven by a deep mantle plume? — Review of volcanism, faulting, and uplift in light of new data. *Journal of Volcanology and Geothermal Research*, *188*(1-3), 1-25.

Pierson, T. C. (1982). Classification and hydrological characteristics of scree slope deposits in the northern Craigieburn Range, New Zealand. *Journal of Hydrology (New Zealand)*, 34-60.

Prostka, H. J., Blank, H. R. Jr., Christiansen, R. L., & Ruppel, E. T. (1975). *Geologic map of the Tower Junction Quadrangle, Yellowstone National Park, Wyoming and Montana*. US Geological Survey.

Romme, W. H., & Turner, M. G. (2015). Ecological implications of climate change in Yellowstone: Moving into uncharted territory. *Yellowstone Science*, *23*(1), 6-12.

Samani, Z. (2017). Three simple flumes for flow measurement in open channels. *Journal of Irrigation and Drainage Engineering*, *143*(6), 04017010.

Stewart, I. T., Cayan, D. R., & Dettinger, M. D. (2005). Changes toward earlier streamflow timing across western North America. *Journal of climate*, *18*(8), 1136-1155.

Tague, C., & Grant, G. E. (2009). Groundwater dynamics mediate low-flow response to global warming in snow-dominated alpine regions. *Water resources research*, *45*(7).

Tercek, M., Rodman, A., & Thoma, D. (2015). Trends in Yellowstone snowpack. *Yellowstone Science*, *23*(1), 20-27.

Thoma, D., Rodman, A., Tercek, M. (2015). Water in the Balance: Interpreting Climate Change Impacts Using a Water Balance Model. *Yellowstone Science*, *23*(1), 29-35.

Welhan, J. A., & Reed, M. F. (1997). Geostatistical analysis of regional hydraulic conductivity variations in the Snake River Plain aquifer, eastern Idaho. *Geological Society of America Bulletin*, *109*(7), 855-868.

Wells, S. G., Dohrenwend, J. C., McFadden, L. D., Turrin, B. D., & Mahrer, K. D. (1985). Late Cenozoic landscape evolution on lava flow surfaces of the Cima volcanic field, Mojave Desert, California. *Geological Society of America Bulletin*, *96*(12), 1518-1529.

Westerling, A. L., Turner, M. G., Smithwick, E. A., Romme, W. H., & Ryan, M. G. (2011). Continued warming could transform Greater Yellowstone fire regimes by mid-21st century. *Proceedings of the National Academy of Sciences*, *108*(32), 13165-13170.

White, W. B. (2002). Karst hydrology: recent developments and open questions. *Engineering geology*, *65*(2-3), 85-105.

Winkelmaier, J. R. (1987). *Ground water flow characteristics in fractured basalt in a zero order basin* (Doctoral dissertation, University of Idaho).

Yokoyama, T., & Banfield, J. F. (2002). Direct determinations of the rates of rhyolite dissolution and clay formation over 52,000 years and comparison with laboratory measurements. *Geochimica et Cosmochimica Acta*, *66*(15), 2665-2681.

Chapter 2

Initial Development and Evolution of Stream Networks and Longitudinal Profiles on Young Rhyolite Flows, Yellowstone National Park, and the Importance of Volcanic Bedrock Structures

1. Abstract

Much of what we know about the initial development and evolution of fluvial systems comes from computer models, and small-scale natural laboratories and experiments, which require considerable extrapolation for relevance to large-scale (> 1 km^2) natural watersheds incised into bedrock. Large natural landscapes with young (< 1 Ma) surfaces containing independently formed stream networks are rare and provide important insights into the initial development of fluvial systems (Wells et al., 1985; Jefferson et al., 2010). The Rhyolite Plateau in Yellowstone National Park contains several young (79-484 ka), large (100-350 km^2) rhyolite flows with many independent drainage basins, which makes them exceptional surfaces for use in a space-for-time substitution study. Using digital elevation data and aerial imagery supported by field observations, I evaluate a wide range of drainage basin, stream network and channel incision parameters on Rhyolite Plateau surfaces of different ages to determine patterns in initial development and evolution. The stream networks and incision patterns are strongly controlled by volcanic pressure ridges and the initial convex plateau morphology. Incision and reduction in convexity occur at nearly linear rates when accounting for differences in slope and drainage area (a proxy for stream power). Significant incision on the youngest flows is limited to small knickpoints, but on the oldest flow, stream incision has cut deeply into the steep flow

margin and has propagated several kilometers headward. Stream junctions on all flows

correlate well with predictions for minimum power loss (Howard, 1971), which suggests

that efficient junctions are a characteristic of initial stream networks or evolve rapidly (< 79

ka). However, where streams of very different magnitude join, the junction angles are more

rectangular (80°-90°) due to stream alignment with pressure ridge morphology. These

results highlight the roles that bedrock structure and topography play in modulating initial

drainage development and the expression of the quantified geomorphic processes used in

landscape evolution studies.

2. Introduction

Understanding stream network patterns and channel gradient is critical for studies

of stream geomorphology. Fluvial processes commonly control rates of hillslope erosion

and are fundamentally important for river ecology, water resources management, flooding

and hazard assessment (Pallard et al., 2009; Brierley and Fryirs, 2013).   However, the initial

development of stream networks and concave-up longitudinal profiles is still poorly

understood and is likely influenced by initial conditions (Pelletier, 2003). Direct observation

of the development of integrated stream networks and incision of the typical concave-up

profile into bedrock for large (>1 km^2) drainage basins is not possible because they require

timescales of 10^4-10^7 years (Knighton, 2014; Phillips and Lutz, 2008). Therefore, most of our

knowledge of initial stream development comes from computer models, small-scale

physical models and experiments, and natural laboratory settings with soft sediments

(Pazzaglia, 2003). Each of these methods has significant limitations. Computer models rely

on assumptions to quantify processes and cannot fully simulate the full diversity of earth

materials, structures, surficial processes and environmental conditions that exist in a real drainage basin over long periods of time. Small-scale experiments and natural laboratory studies range in size from < 1 m^2 to ~10^4 m^2 and typically utilize unconsolidated sediments. These studies require considerable extrapolation for comparison to large natural stream basins (> 1 km^2) incised into bedrock.

To investigate landscape evolution, space-for-time substitution studies compare natural, large-scale geomorphic features of different ages, but which are similar to each other with regards to climate, biological activity, topography, and geology. The advantage of space-for-time studies is that by using natural landscapes, all relevant geologic and biologic factors are integrated into the geomorphic expression of the full-scale landscape. These studies have successfully demonstrated important changes in natural drainage systems over time, but processes and outcomes vary by location due to variations in climate, vegetation, relief and active surface processes (Wells et al., 1985; Jefferson et al., 2010). More field-based studies are needed that make use of large natural systems in different environments in order to better understand the initial development of stream networks and the channel incision that forms longitudinal profiles that are distinct from the original topography. Here, I use several young, well-dated lava flows on the Rhyolite Plateau of Yellowstone National Park (YNP) in a space-for-time substitution study to investigate evolution of drainage basins, stream networks, and bedrock incision (Fig. 1).
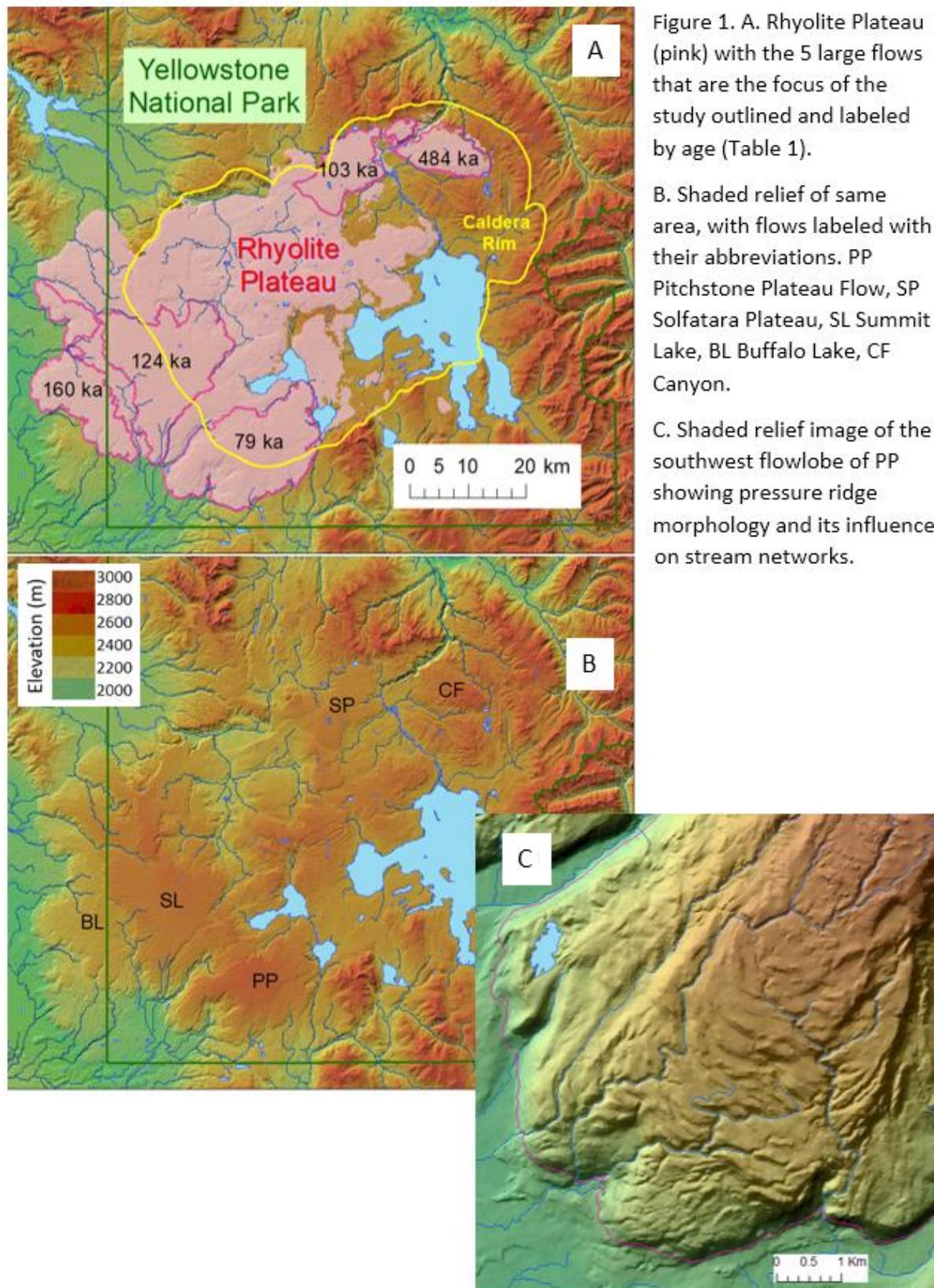
Figure 1. A. Rhyolite Plateau (pink) with the 5 large flows that are the focus of the study outlined and labeled by age (Table 1).

B. Shaded relief of same area, with flows labeled with their abbreviations. PP Pitchstone Plateau Flow, SP Solfatara Plateau, SL Summit Lake, BL Buffalo Lake, CF Canyon.

C. Shaded relief image of the southwest flowlobe of PP showing pressure ridge morphology and its influence on stream networks.

The principal research questions are: (1) Which measures of stream network morphology, stream incision and basin morphology evolve through time and what are their rates of change? (2) In what ways, and to what extent do rhyolite flow structures control the development of the fluvial system?

2.1 Study area

The Rhyolite Plateau is comprised of > 25 rhyolitic flows (0.5 to 300 km^2) extruded after the formation of the modern Yellowstone Caldera at 630 ka (Matthews et al., 2015), and which extend across ~3000 km^2, comprising 30% of the park area. Many of the flows originated from vents located on or near the caldera ring fracture system, and while much of the plateau lies within the caldera, several of the largest flows have spilled over its southwestern rim. The rhyolite flows have many characteristics that make them exceptional surfaces to work with in a space-for-time substitution study. First, radioisotopic age dates and local stratigraphy provide good estimates of the flow ages (Table 1; Christiansen, 2001; Christiansen et al., 2007) which range from 79 to 484 ka, appropriate for studying the development of stream networks and initial stream incision. Second, many of the flows are large enough (100-350 km^2) to encompass many large (> 1 km^2) drainage basins and stream networks for comparative analysis. Third, the flows are convex constructional surfaces with broad upland plateaus and steep margins, similar to generalized plateau or escarpment-style topography used in many models of landscape development (e.g. Pelletier, 2003; Braun, 2018). This original profile shape allows for the measurement of profile convexity development through time and produces independent headwaters areas, such that most drainage basins lie entirely on a single flow. Individual

flows may be as small as 0.5 km^2, but this study is primarily restricted to 5 flows (Fig. 1, Table 1) that are large enough (100-350 km^2) to contain many large drainage basins. The flows are composed of vesicular, perlitized obsidian, vitrophyre, and flow-banded rhyolite. Although lithologic variation occurs at scales of 1-1000 meters within individual flows, the overall lithologic and geochemical composition of the large plateau-forming flows is broadly similar (Christiansen, 2001). Unlike basalt flows and ash-flow tuff units that fill valleys or blanket low- to moderate-relief surfaces, the rhyolite flows typically create very broad dome-like forms with volcanic vents near the summits. Typical flow morphology consists of a gently sloping upper plateau surface (< 10% gradient) marked by an extensive network of concentric pressure ridges (Fig. 1C, 2) that run sub-parallel to steep flow margins (10-50% gradient). Maximum relief across the large flows ranges from 300-600 m, with about 100-200 m of local relief near flow margins. Constructional features such as flow lobes and pressure ridges commonly produce 5-50 m of relief on the upper surfaces, which produces an undulating topography (Fig. 1, 2).

Table 1. Characteristics of the 5 large rhyolite flows used in this study.

| Name	Abbreviation	Age (ka)			Area (km^2)
Pitchstone Plateau	PP	79	+/-	11	343
Solfatara Plateau	SP	103	+/-	8	118
Summit Lake	SL	124	+/-	10	331
Buffalo Lake	BL	160	+/-	3	222
Canyon	CF	484	+/-	15	106
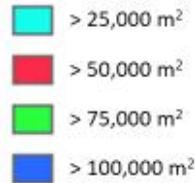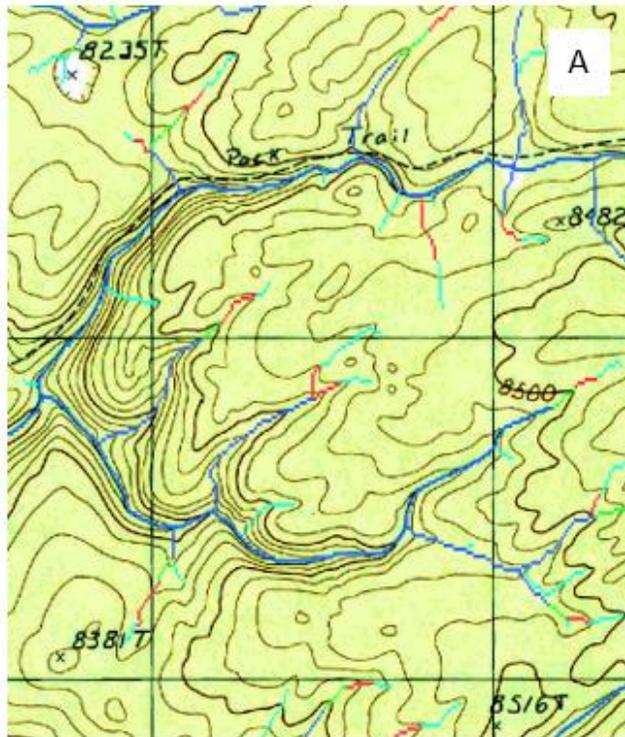
Figure 2 A: Contributing area thresholds shown on a part of the Canyon flow. 1 km UTM grid squares shown. Cyan lines commonly fill colluvial hollows and other non-channelized depressions. Ground truthing indicates that channels most commonly initiate in the red or green zones (50,000-100,000 m^2 drainage areas).

B: Drainage network produced using the 50,000 m^2 area threshold and colored by stream order on the Summit Lake Flow (124 ka). All streams are incised less than 20 ft.
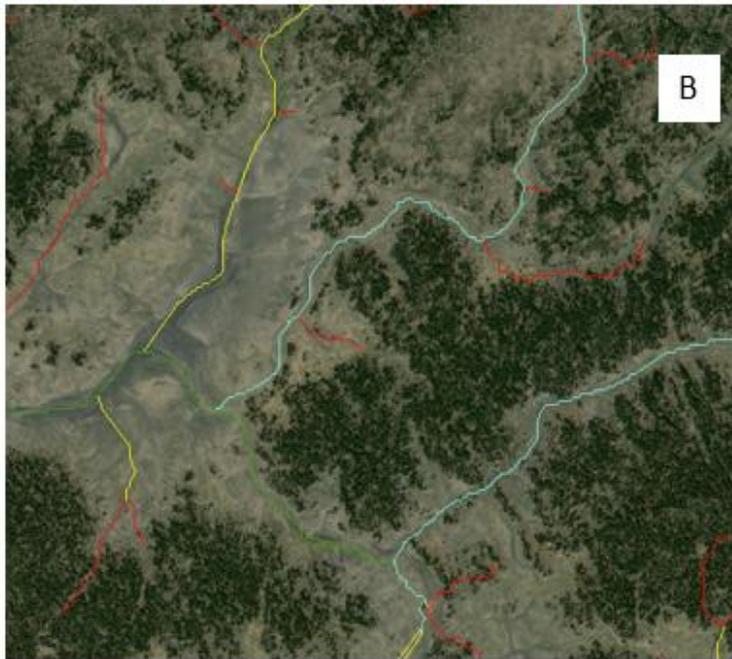
The rectangular stream network pattern on both flows is produced by pressure ridge morphology.

Stream order:

— 1
— 2
— 3
— 4
— 5
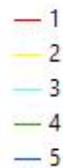
Soil and sediment cover on the plateau are variable, with bedrock exposed locally on pressure ridges, steep flow margins and in incised stream channels and small canyons. In the basins between pressure ridges, there is commonly a coarse volcanic rubble layer

consisting of locally derived gravel- to boulder-sized sediment. Thickness of this rubble

layer is poorly constrained because basins are rarely incised through to bedrock, but

exposures in roadcuts and gullies suggest that this layer is 0.5-2 m thick and grades into

fractured bedrock. Above the rubble layer or directly on bedrock is a layer of silt-dominated

eolian or local lacustrine deposits or stony glacial till with abundant silty matrix. These

shallow basins occasionally contain closed depressions, which account for about 3-9% of the

total area of the flows, with older flows containing less closed depression area (Burnett,

2020 [Ch. 1]). Seasonal ponds are common, and some form during snowmelt when

snowbanks dam the narrow stream gaps between pressure ridges, even in otherwise well-

drained areas. The perlitized obsidian bedrock readily disintegrates into pea gravel and very

coarse sand, which dominate stream channel deposits in these basins. Where channels cut

through pressure ridges, their beds are dominated by cobble- to boulder-sized sediment

and short bedrock channel reaches. Large ice caps formed in the greater Yellowstone

region during peak glacial periods of the Pleistocene, and almost all of the Rhyolite Plateau

was glaciated towards the end of the last glacial maximum at ~13-16 ka (late Pinedale

glaciation), the penultimate glaciation ~145-155 ka (Bull Lake glaciation), or both (Pierce,

2003; Licciardi and Pierce, 2018). Bedrock is locally buried by till and thin glacial rubble

deposits. Steep slopes and pressure ridges are mantled with colluvial sediments which have

likely incorporated till and eolian silt. Surficial deposits are modified by weak soil

development.

The initial surfaces of volcanic flows have no stream network and extremely high

infiltration and permeability (e.g. Wells et al., 1985). Fine sediments deposited on the flow

surfaces enhance runoff and stream networks have developed on all the rhyolites and now drain most of their surface area (Burnett, 2020 [Ch. 1]). Evidence for runoff and channel initiation is greatest in areas with substantial fine sediment cover and less forest cover, and uncommon where bedrock is exposed, shallowly buried or covered with highly permeable rubble or talus. Deep infiltration and fracture flow through the rhyolite are common, as indicated by the very limited number of perennial streams on the flows, even in basins with >10 km^2 of drainage area, and the presence of many perennial springs at the margins of the flows. The oldest flow (Canyon, 484 ka) contains the greatest density of perennial streams >1 km in length, which may be the result of weathering, surficial materials, soil development and hydrothermal alteration reducing infiltration and permeability over time (Burnett, 2020 [Ch. 1]), as is commonly observed on other volcanic flows (Wells et al., 1985; Lohse and Dietrich, 2005; Jefferson et al., 2010). The stream networks are strongly controlled by rhyolite flow structures; streams often run parallel to or between pressure ridges before or after crossing them or run parallel to the general surface gradient. First- and second-order stream channels are small (0.5-2 m wide by 0.25-0.5 m deep), but third-order and larger streams may reach widths of up to 50 m in broad basin areas. Channels on the upper surfaces are for the most part shallowly incised into basin fill, except where they cross pressure ridges. As larger (>1 km^2 drainage area) streams approach the steep flow boundary or other major knickpoints, the channel forms the bottom of a long, narrow canyon incised 2-10 m into bedrock. At the flow margin, these canyons deepen to 10-50 m and become 50-250 m wide. The canyon rims commonly display original constructional topography, making it possible to quantify the total fluvial incision that has occurred.

2.2 Measures of stream network morphology and incision

In this space-for-time substitution study, I examine flows of different ages to identify trends in parameters used to describe the stream networks, stream incision and profile concavity, and the morphometry of the associated drainage basins. Simple drainage basin shape parameters can provide information on the hydrologic behavior of a drainage basin and parameters used in hydrologic modeling (Bárdossy and Schmidt, 2002). I utilized 4 parameters derived from drainage basin size, shape and perimeter:

Eq. 1   Width to length ratio   W/L   where L is the longest dimension of the basin and W is the maximum width perpendicular to L;

Eq. 2   Shape factor (Rigon et al., 1996) $s = \dfrac{A}{W*L}$ where A is the basin area;

Eq. 3   Compactness (Gravelius, 1914) $C = \dfrac{P}{2\sqrt{\pi A}}$ where P, the basin perimeter, is divided by the perimeter of a circle with area equal to the basin area;

Eq. 4   Bounding box compactness $C_b = \dfrac{P}{2*W+2*L}$

W/L provides a measure of the elongation of the drainage basin, with lower W/L values representing longer, narrower basins. W/L has been observed to decrease with slope and basin size (Hack, 1957; Castelltort and Yamato, 2013), and increase with stream concavity (Shelef, 2018), but has been observed to be invariant after initial development of stream networks in many landscape evolution experiments and models (Bennett and Liu,

2016; Castelltort and Yamato, 2013). Regions of drainage basins are considered to be self-similar where s and W/L remain constant for basins of different sizes. Self-affinity exists where as basin size increases, shape-factor remains constant and W/L ratio decreases (Hack, 1957; Bennett and Liu, 2016). Compactness (C and C_b) provides a measure of sinuosity of the perimeter of the drainage basin and is low for round basins with smooth drainage divides, and has been shown to be higher where erosion in headwater reaches produces tortuous drainage divides (Bárdossy and Schmidt, 2002).

The hypsometric curve and slope-area curve can be extracted from Digital Elevation Models (DEMs) and represent the basin-wide distribution of elevation and slope (Cohen et al., 2008). The hypsometric curve of a drainage basin illustrates the generalized distribution of area at different elevations within the basin (Strahler, 1952), and these curves have been linked to the dominant geomorphic processes or a region (e.g. Tucker and Whipple, 2002; Brocklehurst and Whipple, 2004; Minasny and McBratney, 2001). The distribution of slope angles in stream channels and hillslopes has been noted to follow a power law relationship (Gilbert, 1909; Horton, 1945; Hack, 1957; Flint, 1974) such that:

Eq. 5 $\qquad$ $S = kA^u$

where S is the slope or gradient of a short stream reach or hillslope segment, A is the contributing drainage area for that reach, k is a slope-scaling coefficient and u is the slope-area exponent coefficient. The values of k and u vary by bedrock, soil and topographic parameters (e.g. Cohen et al., 2008), and u is a measure of slope or channel concavity used to identify the transition between hillslope and fluvial processes (Willgoose et al., 1991).

Development of the typical concave-up profile has been linked to a downstream increase in discharge and decrease in sediment size that result in a downstream reduction in channel gradient (Hack, 1957; Snow and Slingerland, 1987). These trends are explained by and modeled after stream power laws. Steeper slopes and greater discharge create stream reaches with higher stream power and a greater potential for erosion. Therefore, steeper channel gradients develop where discharge is low or sediment sizes is large. Research on longitudinal profile concavity has focused on streams that are presumed to be in, near, or developing towards steady-state (Tucker and Whipple, 2002) or perturbed from steady-state by tectonic, geologic or climatic factors (Wilson, 1985; Pazzaglia et al., 1998; Snyder et al., 2000; Radoane et al., 2002; Phillips and Lutz, 2008). The magnitude of profile concavity and the best fit function (logarithmic, exponential or linear) has been shown to vary by total relief (Wheeler, 1979), stream length (Leopold and Langbein, 1962), rate of downstream sediment size fining (Hack, 1957; Brush, 1961; Snow and Slingerland, 1987) and states of aggradation and degradation (Shepherd, 1985; Ohmori, 1991). However, streams in some areas do not exhibit a smooth concave-up profile or conform to the concavity trends found elsewhere and are not consistently well-modeled by mathematical functions (Phillips and Lutz, 2008). Instead, a concavity index (CI) is commonly used in areas with streams containing major convexities in longitudinal profiles (Langbein and Leopold, 1964; Larue, 2008; Phillips and Lutz, 2008). The CI measures the proportion of the profile that is above or below a straight-line profile; by convention concave profiles have a positive CI (Fig. 3).
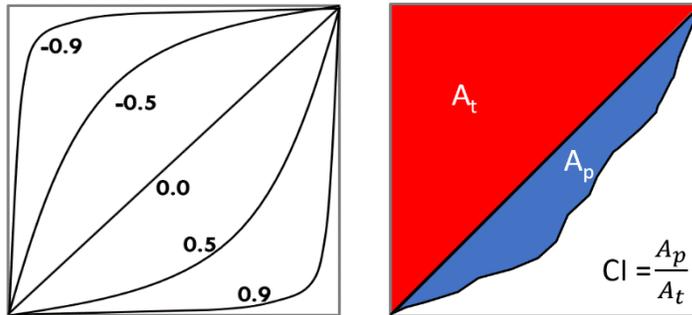
Figure 3. Concavity index (CI) illustrated. The CI is the area between a stream profile and a straight line connecting the endpoints of the profile (A_p) divided by the area of half of the total box (A_t). Concave-up profiles have positive CI and convex-up profiles have negative CI by convention.

Drainage density (D_d) and stream frequency (f_s) are important characteristics of stream networks proposed by Horton (1945), and are defined as:

Eq. 6 $\qquad D_d = \dfrac{L_{ts}}{A}$

where L_{ts} is the total stream length of all streams in a drainage basin with area of A, and

Eq. 7 $\qquad f_s = \dfrac{n_s}{A}$

where n_s is the number of stream segments in the drainage basin. D_d has been shown to vary with climate, lithology, and other basin parameters (Morgan, 1976; Rodriguez-Iturbe and Escobar, 1982) and play a critical role in flood statistics (Pallard et al., 2008). Changes in drainage density have also been observed in stream network development (e.g. Morisawa, 1956; Schnider et al., 2013). Using stream networks from a wide variety of environments as examples, Glock (1931) proposed a conceptual model for network development, where initial closed depressions link together into a stream network and over time. The young stream network undergoes a period of extension and elaboration marked by a dramatic increase in drainage density and stream frequency. Later, these parameters decline as the network undergoes a set of processes termed integration. During integration, the highest order streams incise and broaden their valleys at the expense of smaller tributaries. Stream

piracy and the development of more efficient flow paths may also contribute to the

decrease in drainage density and stream frequency during the integration phase. Glock's

model has been generally supported by experimental studies (Gomez and Mullen, 1992;

Hancock and Willgoose, 2003), numerical models (Leheny and Nagel, 1993; Leheny, 1995;

Giacometti et al., 1995) and field studies (Abrahams, 1972; Wells et al., 1985; Dohrenwend

et al., 1989; Ritter and Gardner, 1993; Keller et al., 1998; Schneider et al., 2013). While

Glock's stages can be observed in many different settings, the timescales for network

development vary with materials and climate (Knighton, 2014).

Junction angles are an important measure of the stream network and Horton (1932)

proposed a model based on the geometric relationship of tributary slopes to explain

variation in tributary junction angles. The convention used to define junction angles is

illustrated in figure 4. Junction angles have also been shown to vary with discharge and

drainage area, influence stream efficiency and power expenditure, and play an important

role in stream capture and network stability (Horton, 1945; Howard, 1971; and Hooshyar et

al., 2017). Howard (1971) modified Horton's original model to fix a geometric deficiency

and related the equation to minimum power loss, which was confirmed by Roy (1983). The

modified Horton equation (Eq 8) uses the slope-area exponent (u) and discharge of the

tributaries and can be used to either calculate optimal junction angles from a measured u

value, or to predict the u value of a basin from measured junction angles.

Eq. 8 $\qquad \cos(\beta_i) = (\frac{Q_1 + Q_2}{Q_i})^u$

where β is the angle between the tributary and the trunk stream and Q is discharge of the

tributary denoted as 1 (larger tributary), 2 (smaller tributary) or i (tributary being

measured); each junction has two β values, one for each tributary.
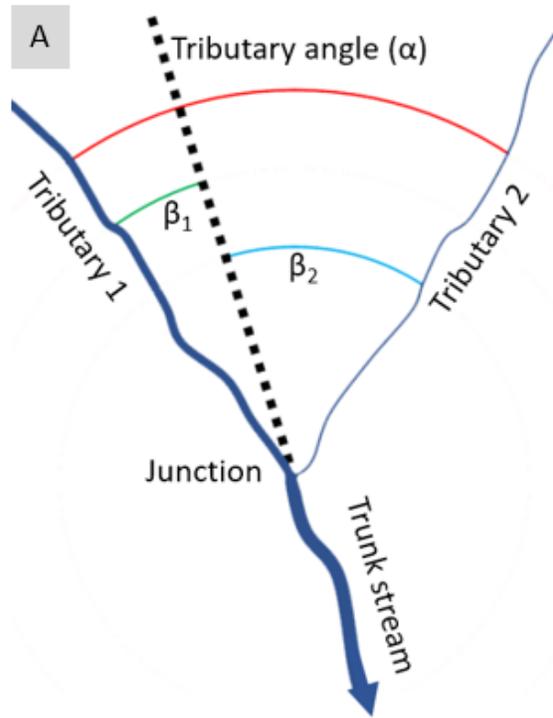
Figure 4. A: Convention for defining stream junction angles. Tributary 1 is defined as having a larger drainage basin than tributary 2. The tributary angle (α) is the sum of the two angles (β_1 and β_2) formed by a straight-line continuation of the trunk stream (dotted line) and tributary 1 and 2 respectively.

B: example of junction extracted from the DEM. Junction angles calculated based on stream intersections with a 30-m radius circle centered on the junction.
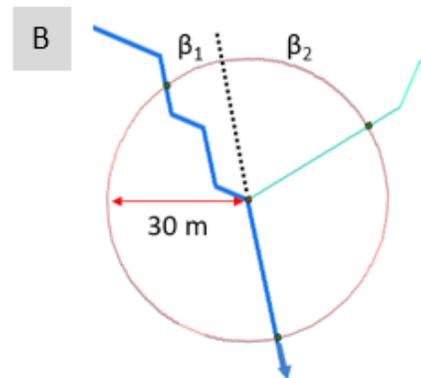
3. Methods and Results

3.1 Hypsometry

Hypsometric curves were derived from a 10-m DEM for basins on the 5 study-area

flows shown in Fig. 1. Basins with drainage areas < 1 km^2 were removed from analysis

because they generally did not extend far above the margin and were not representative of

the full plateau morphology or its drainage pattern. Five basins were excluded because the

margin was buried or obscured by sediments or other volcanic rocks, leaving 157 drainage

basins for analysis. Average hypsometric curves for the 5 large rhyolite flows are broadly

similar and indicate that the flows have similar morphology. Small, craggy cones and

uplifted blocks near the vents comprise the highest elevations, with the bulk of flow area

forming a broad, sloping plateau. The steep flow margin represents ~10% of the flow area,

but 30-50% of the relief (Fig. 5). The Canyon Flow is least like the other flows, although not

statistically different in hypsometry. It contains a relatively larger vent area with several

faulted and eroded peaks (Fig 6) which results in a relatively lower plateau surface;

additionally, the hypsometric curve is less steep near the margin than the other flows.
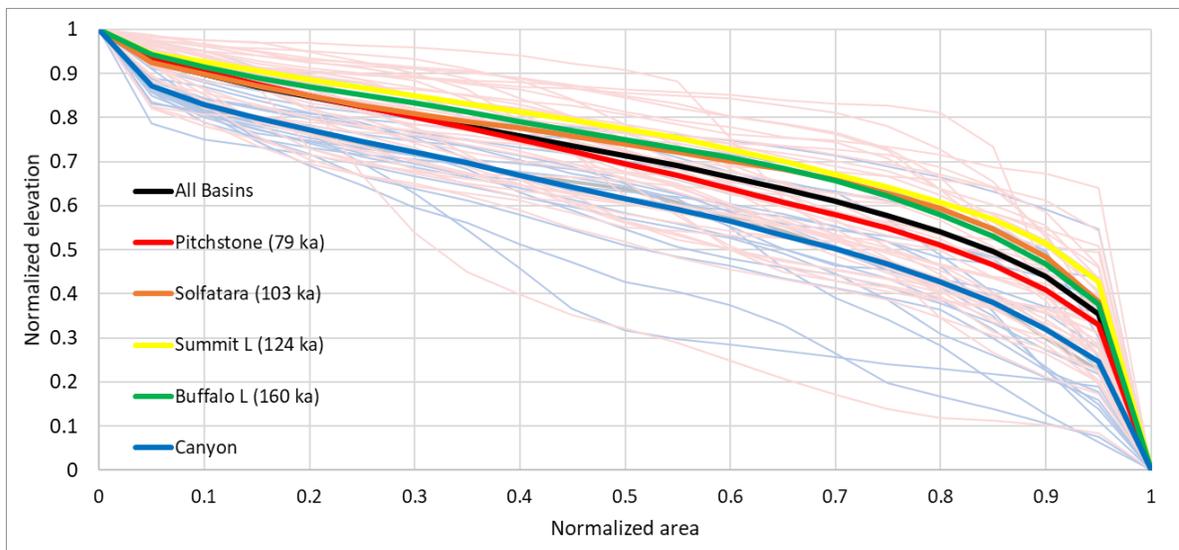
Figure 5. Hypsometric curves for the study area drainage basins; bold lines show averaged curves for each of the 5 study area rhyolite flows. Individual drainage basins on the Pitchstone Plateau (pink) and the Canyon Flow (light blue) provide an indication of variation within flows and overlap between flows.
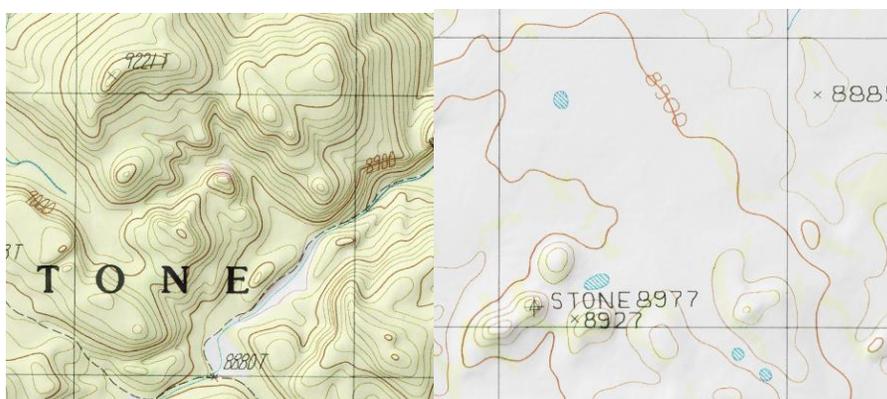
Figure 6. Vent areas of the Canyon Flow (left) and Pitchstone Plateau (right). Both maps are extracted from USGS 7.5' quads with shaded relief from caltopo.com, 20-ft contours and 1-km UTM grid.

3.2 Definition of drainage network

A drainage network was produced using a 10-m DEM and the National Hydrography Dataset (NHD) available from the USGS. Due to the undulating, irregular topography with low relief of many portions of the upper plateaus, the DEM contained many false closed basins. Evaluating every closed basin was impractical, especially in areas where field work had not been conducted, so the closed depressions in the DEM were filled. The NHD stream network defines high-order streams well, with only a few inaccurate flow paths identified on the Rhyolite Plateau. Field observations indicated that the NHD network generally does not include first-order and some second-order channels in the study area. Low-order streams were generated from the DEM with using a variety of methods including numerous drainage area thresholds, slope-area thresholds (Montgomery and Dietrich, 1992) and a morphometric method that incorporates curvature based on Luo and Stepinski's (2008) method. Each network was evaluated by comparing the generated network to streams observed and cataloged in the field. For 4 of the study area flows, twenty-five 1 km^2 UTM grid squares were selected where previous field research allowed

for accurate locating of first-order streams. Limited fieldwork on Solfatara Flow meant that only 10 grid squares could be selected. The grid squares were selected along paths that traverse the flows and represent the full range of the flow morphology from margin to summit. Each stream network was evaluated on its accuracy in representing the number of first-order tributaries present and the initiation points of those streams. Field records were supplemented by air photos (ESRI.com, Google Earth and USGS.gov) for accurately defining stream locations. The goodness of fit of each model could not be quantified, but the models were subjectively ranked from best to worst in each grid square and for each flow.

Slope-area thresholds and morphometric methods for determining stream initiation points have been shown to perform well in dissected landscapes (Montgomery and Dietrich, 1992; Luo and Stepinski, 2008), but they did poorly or no better than simple area threshold methods on the Rhyolite Plateau. Poor performance of these networks was due to three factors: (1) the slope angle and curvature of rhyolite flow surfaces is controlled by volcanic features instead of produced by erosional processes; (2) first-order streams often initiate in nearly flat basins filled with fine sediments with low-permeability; and (3) artifacts in the DEM resulting from the digitization of contour lines created small artificial changes in slope and curvature that are picked up by these methods. Relief on the upper surfaces is low in many areas and smoothing the DEM to remove curvature artifacts generated undesirable loss of topographic information, which was evaluated by overlaying the smoothed and unsmoothed DEMs on USGS topo maps. The low resolution of the DEM as compared to the size of first-order streams also makes stream delineation based on multiple derived measures (slope and curvature) less desirable. A higher resolution DEM produced by LIDAR

might improve the stream networks delineated by slope-area or morphometric methods, however factors 1 and 2 listed above suggest that the morphology of the Rhyolite Plateau may violate the process-based assumptions built into those methods.

The stream networks defined by area thresholds performed well at capturing the frequency and initiation of first-order streams. The 50,000 m^2 (0.05 km^2) threshold network provided the best results on all flows based on the ranking of methods in the UTM grid squares, with a 25,000 m^2 threshold ranking second for the younger flows and a 75,000 m^2 threshold ranking second for the oldest (Canyon) flow (Fig. 2). This indicates that the drainage network may be slightly underestimated on the younger flows and overestimated on the oldest one.

Since the NHD stream network more accurately defines higher-order streams than the DEM and includes meanders and accurate flow paths through flat basins, the DEM was trained to the NHD stream network using the ArcHydro tool set available for ESRI ArcMap. The toolset modifies the DEM to force flow paths along the predefined stream network and creates more realistic stream lengths and junctions. Training the DEM also eliminates some of the errors created by filling the DEM. The slope map rasters used in analysis were also trained to the resulting stream networks. For non-channel areas, the slope of each cell is calculated using the standard DEM-slope method which calculates the maximum slope across the cell as a percent gradient, using its eight neighbors. For channel reaches (cells with contributing area A > 50,000 m^2), using the standard slope method produces artificially elevated gradients in incised areas where steep sideslopes adjacent to the channel cells influence the slope calculation. When these stream gradients are multiplied by the length

of the canyon, the resulting apparent change in elevation can be 2-3 times that of the actual

relief. To accurately calculate stream gradients, only adjacent cells in the channel system

were used to define that cell's slope. This method eliminates steep hillsides from impacting

channel slopes. Stream gradients calculated by this method were similar to those extracted

from a topographic map, and stream relief values calculated along canyon reaches were

accurate to within a few meters.

3.3 Drainage basin delineation and shape factors

The stream network was used to define drainage basins that are fully contained

within the 5 study area rhyolite flows, with no overlap or run-on from other surfaces.

Streams within the basins were categorized using the Strahler (1957) stream order

classification scheme and sub-basins were created based on the Strahler ordered network.

Shape factor, W/L and compactness (Eq. 1 through 4) were calculated for each drainage

basin and for each stream order sub-basin. Comparison of the metrics between basins of

different stream orders provides a measure of how the metric scales with basin size (Fig. 7).

Shape factor and W/L are invariant across basin orders, but both compactness measures

changed significantly from the 1st- and 2nd-order basins to the 4th- and 5th-order basins. For

comparison between flows of different ages, the 4 metrics were normalized by basin area to

account for variation due to scaling (Bárdossy and Schmidt, 2002). Some planform measures

demonstrated significant trends with rhyolite flow age (Fig. 8), but due to high variability

between basins, relatively little of the total variance in these measures is explained by flow

age ($r^2 < 0.07$). However, when shape factor and compactness are averaged by flow age the

relationship to age becomes strong ($r^2 > 0.9$ and $p < 0.05$).
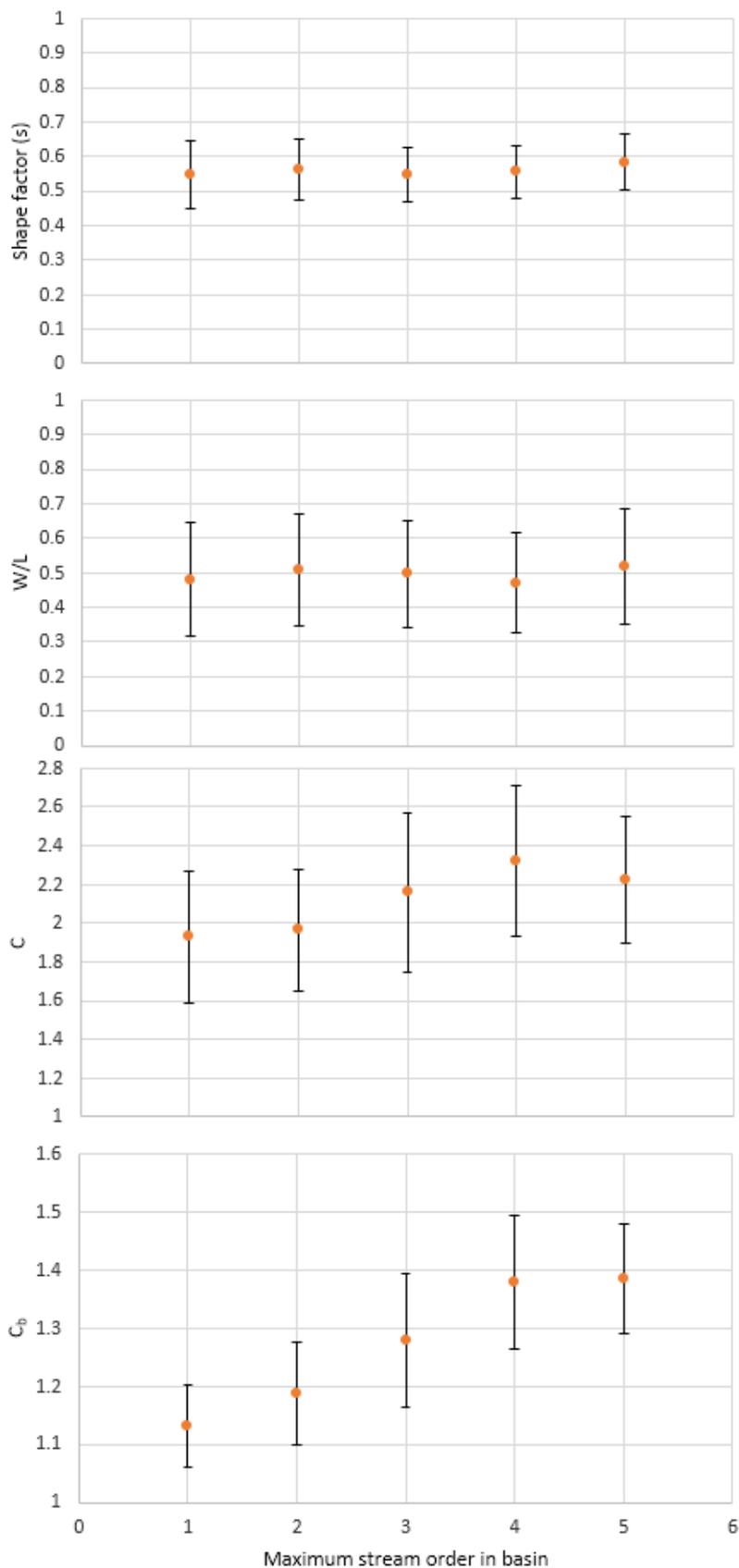
Figure 7. Average values for planform basin metrics plotted by maximum stream order in each sub-basin with standard deviation. Mean values are not significantly different except between high-order (4th and 5th) streams and low-order (1st and 2nd) streams for both compactness measures (C and C_b).
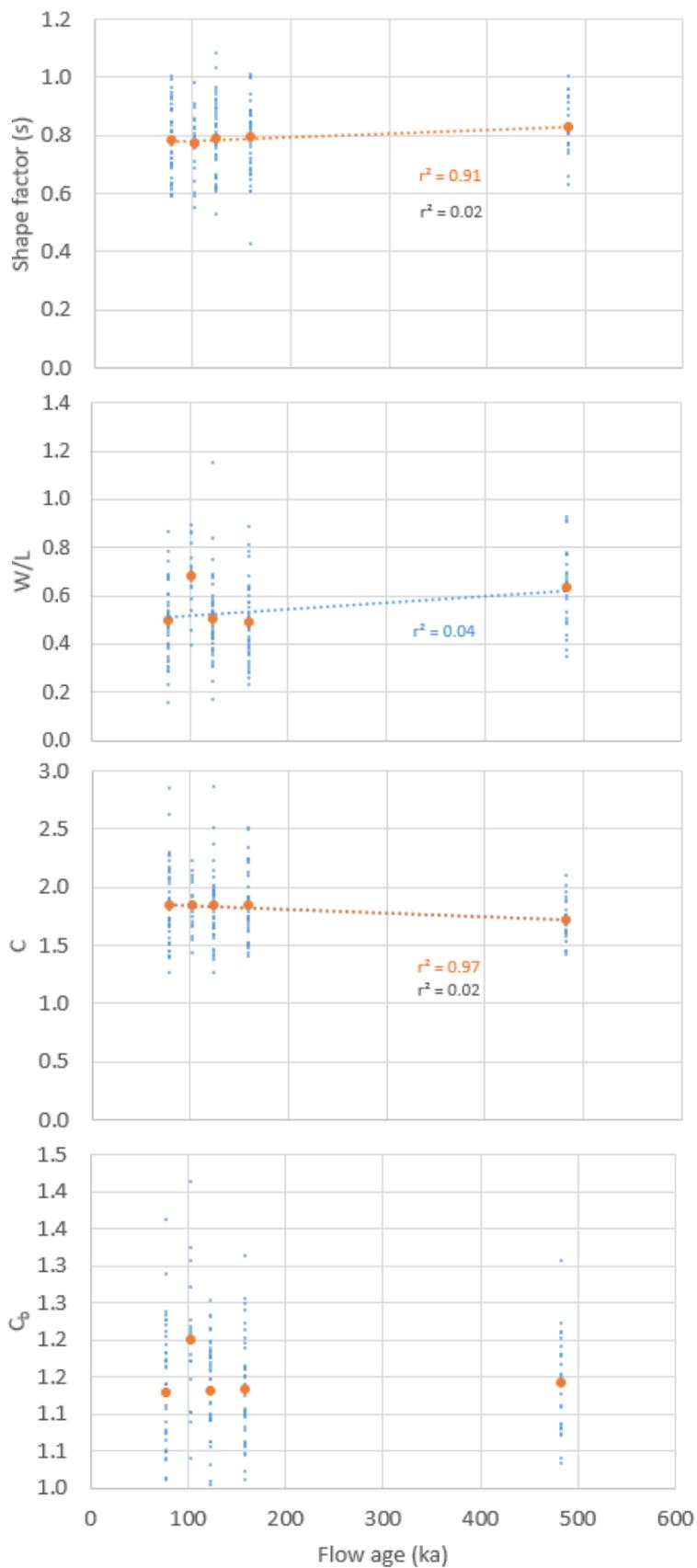
Figure 8. Planform metrics of the Rhyolite Plateau drainage basins plotted by flow age. Individual basins are blue and flow averages are orange. Goodness of fit (r^2) for significant regressions are color coded to the data set used in the regression; orange r^2 values are for the averages and black r^2 values are for the individual basins ($0.1 < p < 0.05$).

3.4 Drainage density and stream frequency

Some small basins, typically < 1.5 km^2, displayed irregular or unbranching stream networks and so all basins < 1.5 km^2 were removed from the drainage density analysis. D_d and f_s were calculated for 122 basins on the Rhyolite Plateau (Fig. 9). Drainage density is controlled to an extent by the area threshold used to define small tributaries, but values for individual basins range over about a factor of 2, from 2.5 to 4.3 km of stream length per km^2. There is not a trend of drainage density with basin size, but it decreases significantly with increasing rhyolite flow age (Fig. 9). Most of the change in drainage density occurs as a result of first order streams becoming shorter, as indicated by Fig. 9C, which shows that when drainage density is separated by stream order, only first-order drainage density decreases consistently with increasing flow age. Standard deviation of drainage density calculated for basins on the same flow also decreases significantly with flow age. Stream frequency data exhibited higher variance than drainage density and showed no significant trends with regard to basin area or flow age when using the full data set, flow averaged data, or variance in stream frequency.
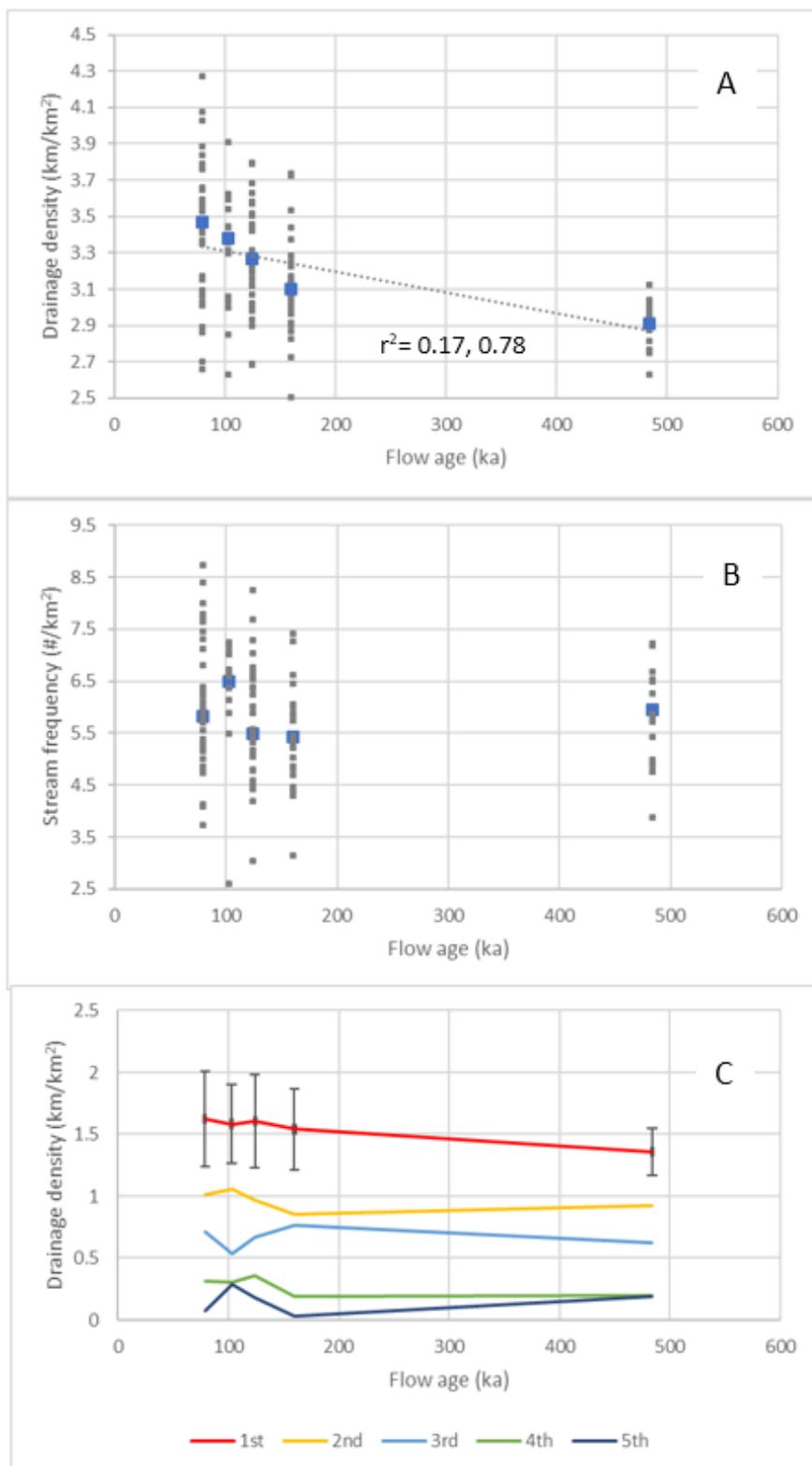
Figure 9. Drainage density (A) and stream frequency (B) plotted by flow age for individual drainage basins (gray) and averaged by flow (blue). Regression line is for both full data and flow averaged data with r^2 values of 0.17 and 0.78 respectively, both are significant ($p < 0.05$).

C: Drainage density of the entire flows split into contributing components by stream order. Only first-order basins vary significantly with flow age.

3.5 Tributary junction angles

Tributary junction angles were measured using the same stream network developed for drainage density analysis (50,000 m^2 drainage area threshold). Junction angles were defined using a standard convention (Fig. 4), after Howard (1971). Using high resolution DEMs, Hooshyar et al. (2017) found that tributary angles were best represented by stream segments extending from the junction out to distances of 10 to 30 meters from the junction. I calculated angles and gradients using 30-meter stream segments originating from the junction (Fig. 4). Given the relatively low resolution of the DEM used to define our stream networks (10-m), calculations made with stream lengths less than 30 meters long were dominated by artifacts generated by the DEM grid size. Complex junctions involving more than 2 tributaries were either excluded or were simplified to 2-tributary systems in cases where tertiary streams were more than an order of magnitude smaller than the largest two. First-order streams less than 30 meters long were also excluded. Sample sizes used in analyses range from about 400 tributary angles (α) on the smallest individual flow to nearly 6000 tributary-to-trunk stream angles (β) for the full data set.

Spatial trends in tributary junction angles discussed below tend to be subtle, with relatively low explanatory power ($r^2 < 0.3$) and high variance, but many trends are significant ($p < 0.05$) due to large sample sizes. Variables that produce only a slight trend (spanning less than a 20° range) in 100-point running average of median junction angles were considered unimportant and are not discussed.

The gradient of the tributary plays a role in defining the junction angle, with steeper tributaries intersecting the trunk stream at higher angles (Fig. 10). The gradient of the trunk

stream on its own had little impact on junction angles, but the difference in gradient

between the tributary and trunk stream had the largest impact on β angles of any gradient

measure (Fig. 10 B). Total tributary angle (α) was not highly impacted by tributary or trunk

stream gradients, with the difference between the gradient of the smallest tributary and

the trunk stream having the greatest range impact on median junction angles (Fig. 10 C).

Values of α were lowest where the tributary gradient was slightly higher than the trunk

stream gradient and α values were higher where the trunk stream was steeper than the

tributary (negative difference values) and where the tributary was more than 10° steeper

than the trunk stream. Trends between stream gradient and junction angles were similar

amongst the different ages of rhyolite flows.
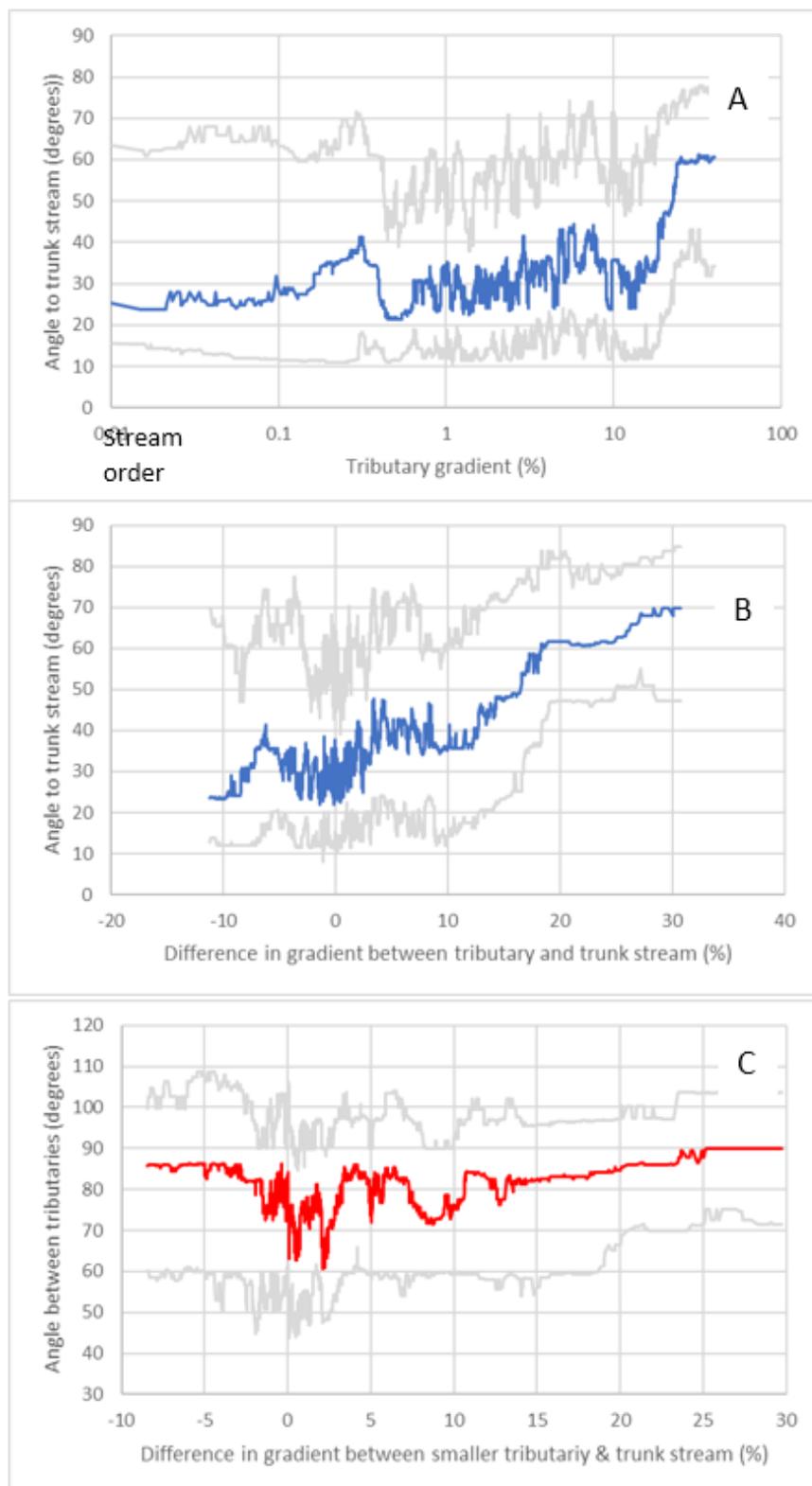
Figure 10. Plots of median, 75th percentile and 25th percentile of junction angles for all rhyolite flows.

A: angle between tributary and trunk stream (β) plotted against the gradient of the tributary.

B: Plot of β against the gradient of the tributary minus the gradient of the trunk stream.

C: The total tributary angle (α) plotted against the difference between the gradients of the smaller tributary and the trunk stream.

Drainage area of the tributary plays a major role in tributary angle, with larger tributaries maintaining a straighter path through the junction into the trunk stream (Fig. 11). The relative size of the two tributaries plays the largest role in controlling junction angles. Drainage area ratio (R) is used to compare the relative sizes of the streams and is defined by:

Eq. 9 $$R_i = \frac{A_i}{A_1 + A_2} = \frac{A_i}{A_T}$$

where A_i is the drainage area of the tributary being assessed, A_1 and A_2 are the drainage areas of tributaries 1 and 2 respectively, and A_T is the drainage area of the trunk stream at the junction.

For streams of roughly equal size (R ≈ 0.5) median β values are about 30°. For tributaries that are at least an order of magnitude larger than the other tributary (R > 0.9), β values are around 20°, whereas median β values for the smaller tributary (R < 0.1) are between 60° and 70° (Fig. 12). The trend between α and R is similar to that of β and R, since α = $β_1$ + $β_2$. For tributaries with very different drainage basin sizes, α approaches 90° following a rectangular drainage pattern (Fig. 13).

Junction angles do not vary much between flows and the only significant difference between flows is that total junction angles (α) on the Canyon Flow are greater than those of the other flows (determined with t-test, assuming unequal variances, Fig. 13).
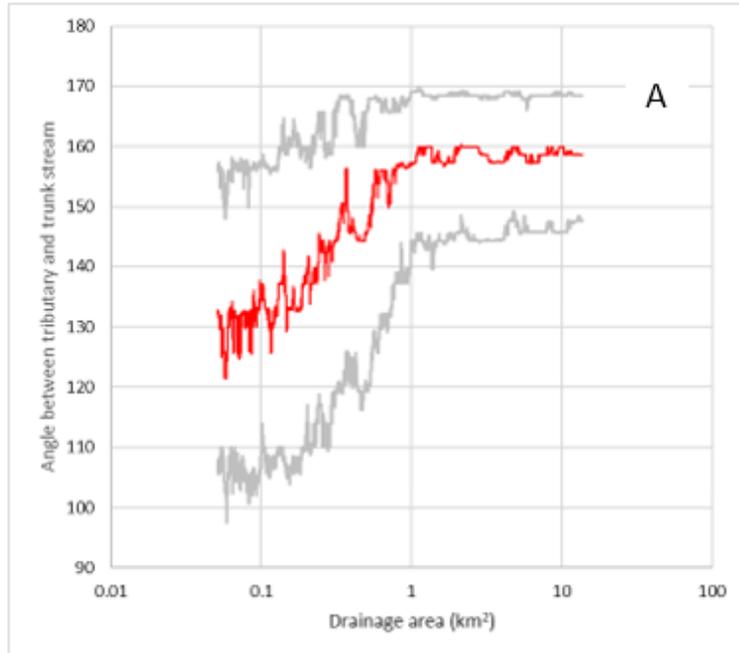
Figure 11. A: Median angle between tributary and trunk stream (β) plotted against the tributary drainage area.

B: Total junction angle (α) plotted against the tributary drainage area. The 25th and 75th percentiles are shown.
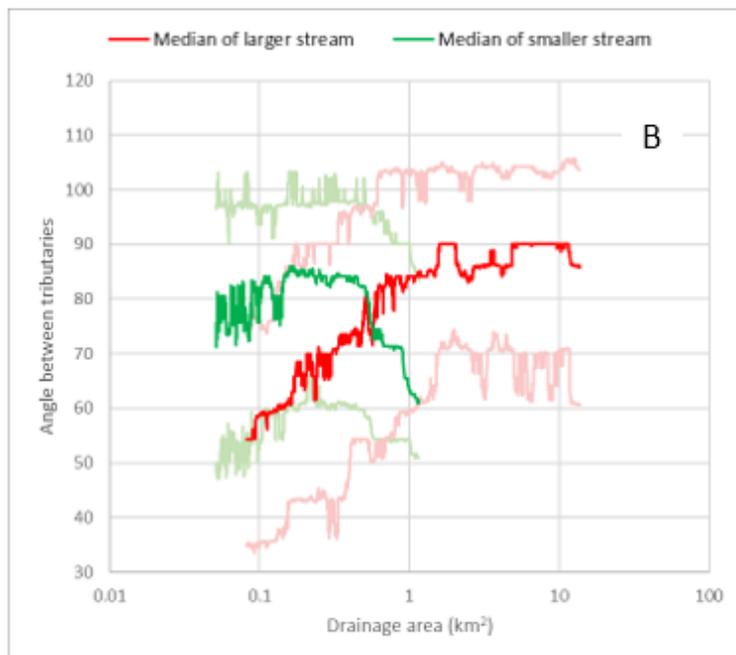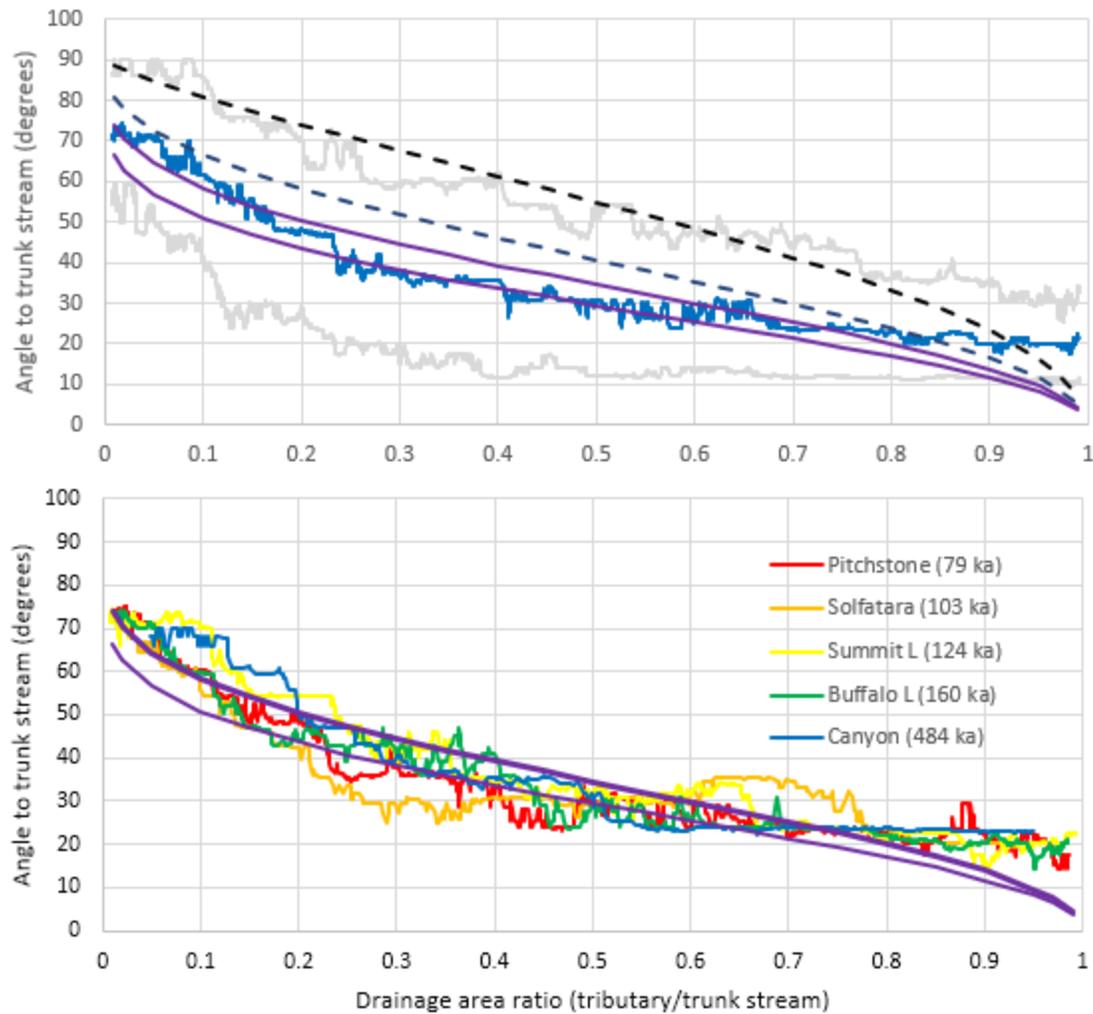
Figure 12. Angle between the tributary and the trunk stream (β) plotted against drainage area ratio.

A: Median for all rhyolite flows in blue, 75th and 25th percentile in gray. Purple lines are predicted angles of junction based on Eq. 8, a modification of Horton's (1932, 1945) model of junction angles and are similar to predictions made for minimum power expenditure (Howard, 1971). The modified Horton model includes the slope-area exponent (u) and the lines shown utilize u = -0.20 and u = -0.28, which are the minimum and maximum u values derived from region 2 of the slope-area curve on the Rhyolite Plateau. Black dashed lines are junction angles predicted by Eq. 8 using u = -0.4 and u = -0.8, which bracket common values for stream systems (Flint, 1974).

B: Median for each rhyolite flow plotted separately.
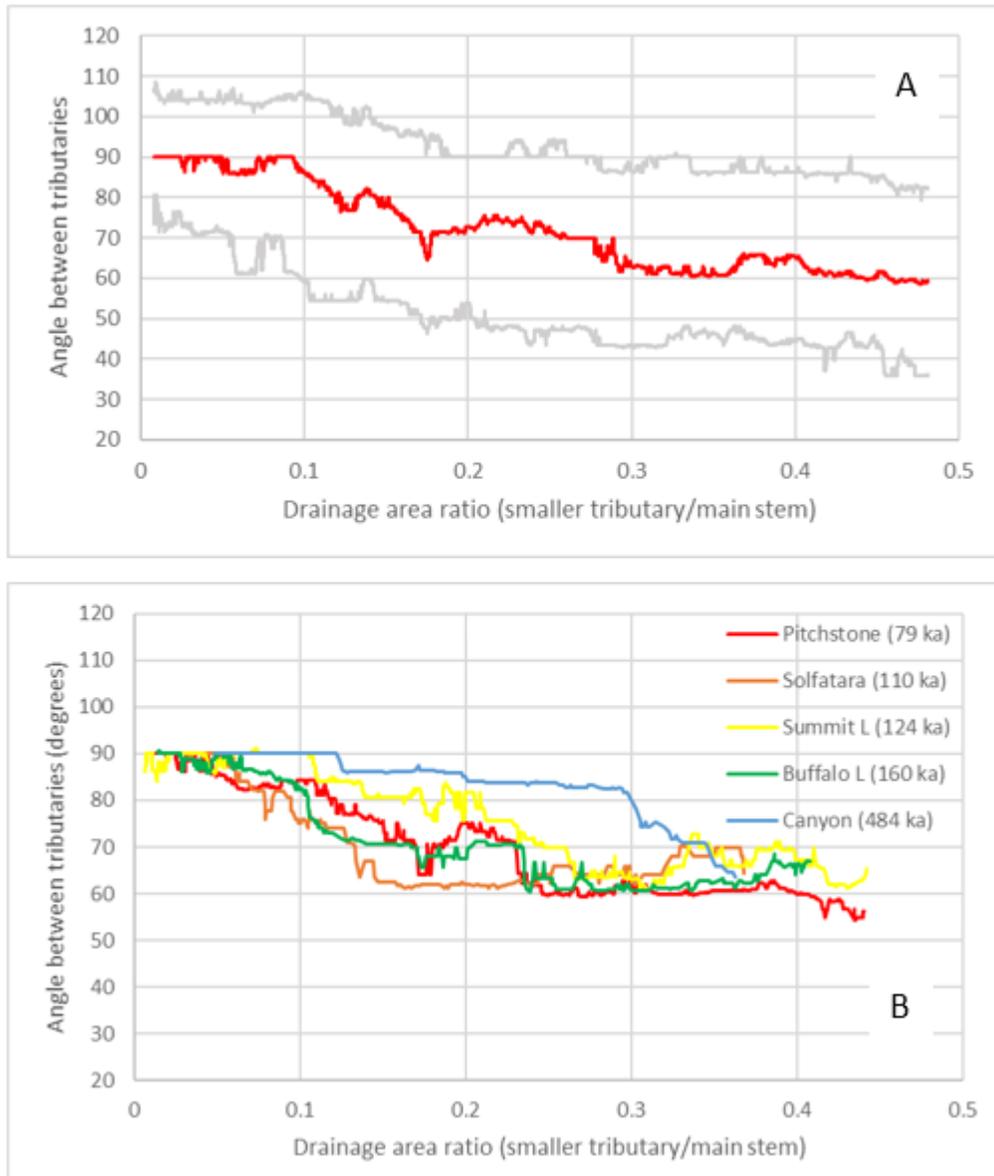
Figure 13. Angle between tributaries (α) plotted by the drainage area ratio of the smaller tributary (R_2).

A: Median for all flows in red, 25th and 75th percentiles in gray.

B: Medians for all rhyolite flows plotted separately.

3.6 Slope-Area relationship

The relationship between local slope at the DEM cell scale and contributing drainage area (Eq. B1) was plotted for all drainage basins in the study area. Three regions of the plot were identified for each basin (Fig. 14). Region 1 consists of convex upper slopes with little to no contributing area, which is commonly assumed to be the portion of the landscape dominated by diffusive sedimentation processes (Willgoose et al., 1991), but which in the Rhyolite Plateau also consists of convex volcanic features such as pressure ridges. Convex slopes have a positive slope-area exponent, but above A ≈ 700-1000 m^2, slopes straighten out and then become concave. Region 2 is the concave portion of the lower slope and first-order drainages, defined with an upper limit of A = 0.1 km^2. Region 2 represents portions of the slope influenced by fluvial processes and the transition to channelized networks. Region 3 consists of all cells with contributing drainage areas > 0.1 km^2 and represents predominantly 2nd- to 5th-order stream channels. The slope-area exponent (u) obtained from Regions 2 and 3 are summarized in Table 2 and shown in Fig. 15. Region 3 u values decrease with increasing flow age. Regression analysis completed using the flow averaged data indicated a strong relationship when the values are averaged over then entire flow surfaces (r^2 = .99, p << 0.05), however variance in u is high between individual basins on the younger flows and the when the regression is performed on the data set using individual basin values, the power and significance of the relationship decrease dramatically (r^2 = 0.03, p = 0.04). A t-test for difference of means and an F-test for difference in variance indicate that Region 3 u values and the variance in u values (from the individual basin data set) are significantly lower on the Canyon Flow (484 ka) than on the younger flows.
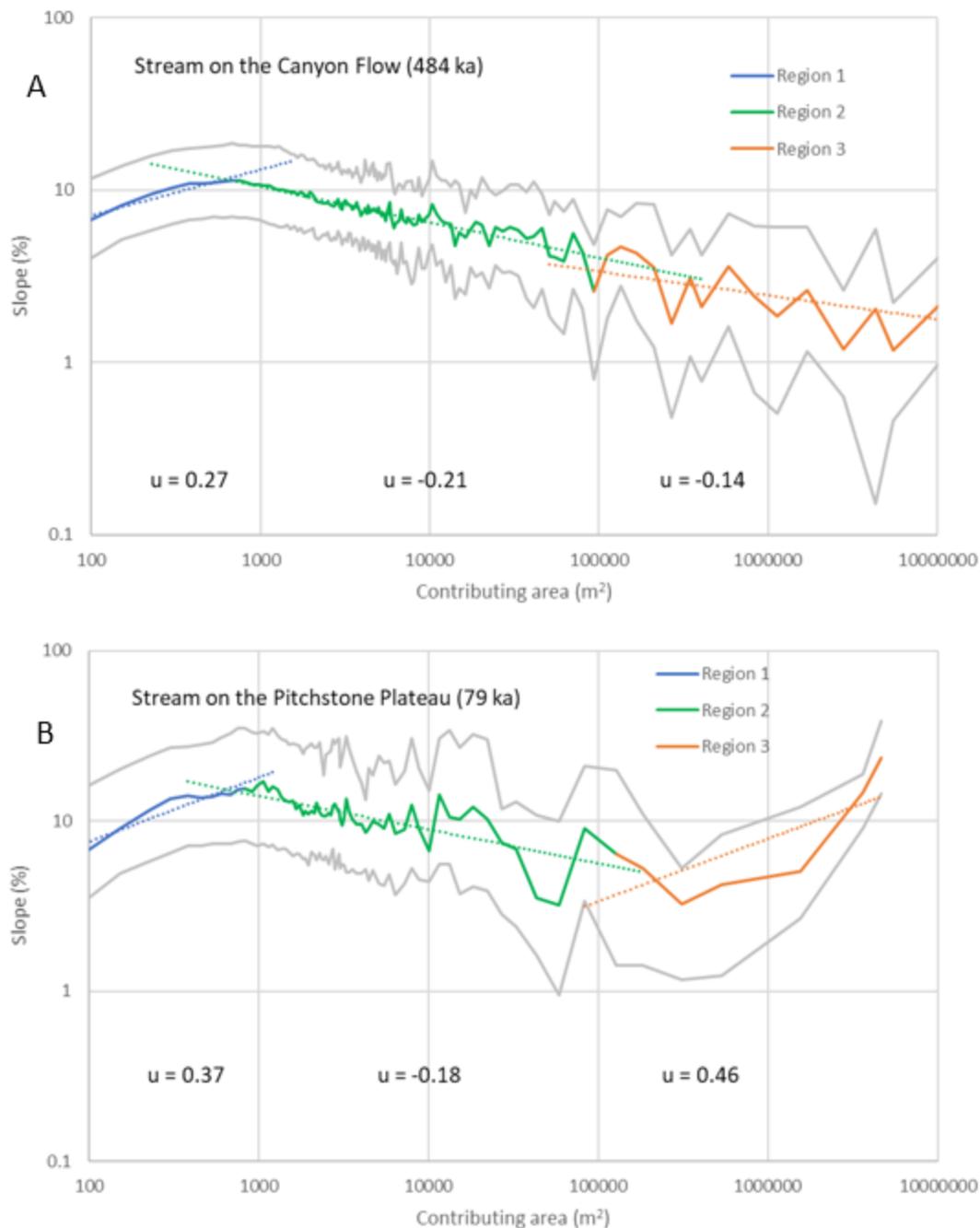
Figure 14. Slope-area plots for representative streams on the Canyon Flow and Pitchstone Plateau. Median values are color coded to region and 25th and 75th percentile lines shown in gray. Slope-area exponents (u) calculated from the power-law regression lines (dotted) are shown for each region.
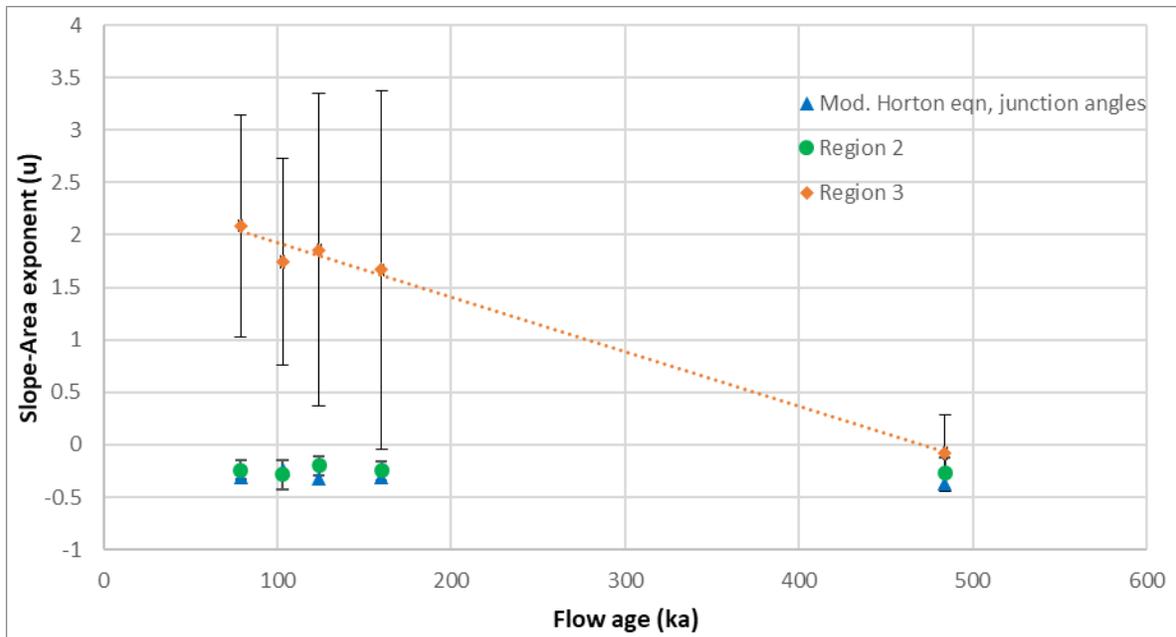
Figure 15. Average slope-area exponents for each rhyolite flow calculated using the modified Horton equation for stream junction angles, and regions 2 and 3 of the slope-area curve. Standard deviation shown for regions 2 and 3.

The modified Horton equation for stream junction angles (Howard, 1971) was also used to calculate the slope-area relationship exponent (u) from junction angles. Following common convention, I assumed that runoff is equal across the basin which allows for the substitution of drainage area for discharge (e.g. Flint, 1974) in the modified Horton equation (Eq. 8) to produce:

Eq. 10 $\qquad \cos(\beta_i) = \left(\dfrac{A_1 + A_2}{A_i}\right)^u = \left(\dfrac{1}{R_i}\right)^u$

Values of u derived from Eq. 10 are shown in Table 2 and Fig. 15. For each flow, a power-law regression was fitted to the median value of cos(β) plotted against R to solve the modified Horton equation for u. All regressions had high correlation coefficients and were highly significant (p << 0.05).

Table 2. Slope-area relationship exponent (u), from junction angles and slope area curves.

| Flow | Age (ka) | Modified Horton eqn. for junction angles | | Slope-area curve | | | |
| | | | | Region 2[*] | | Region 3[+] | |
Flow	Age (ka)	u	r^2	Average u	St. Dev.	Average u	St. Dev.
Pitchstone	79	-0.31	0.94	-0.24	0.09	2.09	0.86
Solfatara	103	-0.24	0.85	-0.28	0.14	1.75	1.16
Summit L	124	-0.32	0.91	-0.20	0.09	1.86	0.62
Buffalo L	160	-0.31	0.95	-0.25	0.09	1.67	0.63
Canyon	484	-0.37	0.91	-0.27	0.14	-0.08	0.10

[*] Region 2 contains concave hillslopes and 1st-order streams.

[+] Region 3 consists only of stream channels with contributing drainage areas > 0.1 km^2.

3.7 Stream incision and concavity

Streams on the Rhyolite Plateau have cut through knickpoints in pressure ridges and the steep flow margin. In order to place greater control on the factors that cause high variance in DEM-derived data, 18 streams were selected for more detailed analysis of incision and profile concavity. Streams were selected that (1) originate on the upper plateau area and cross the flow margin, (2) do not flow in interlobe regions, and (3) are contained within a single rhyolite flow. These criteria were designed to select representative streams with similar properties other than flow age. Two streams were selected on the Spring Creek Flow (257 ka) that met these criteria. The Spring Creek Flow is mostly buried by younger flows making it unsuitable for full analysis of the other metrics described above, but does contain two drainage basins suitable for the identification of knickpoints and fills in a gap in the range of flow ages. The largest tributary in each basin was digitized directly from USGS 7.5' topographic quads (Fig. 16) to allow for more accurate

measurement of gradients and curvature along the stream's length. Profiles were also

measured on either side of the stream along the relatively unincised plateau surface.
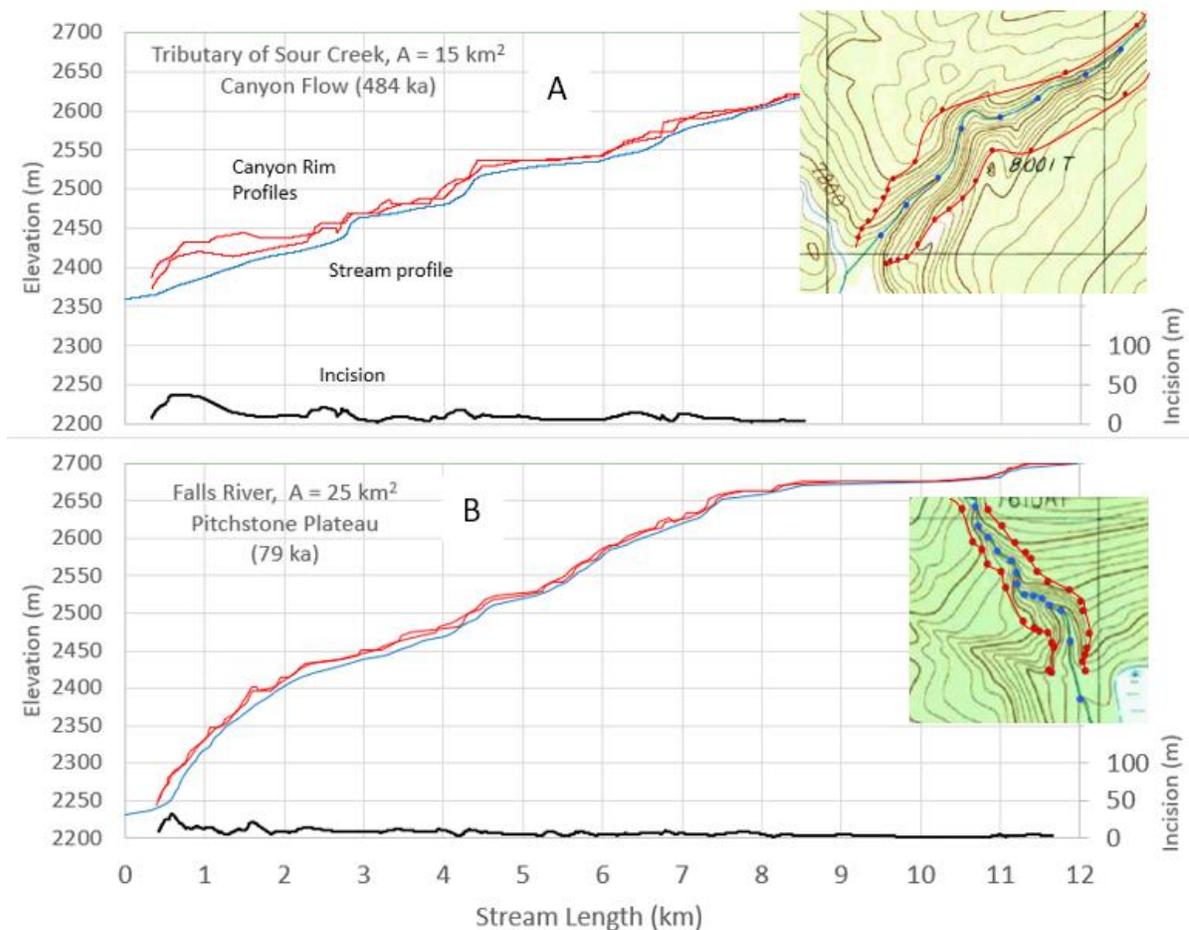
Figure 16. Stream profiles digitized from USGS 7.5' topographic maps (blue) with profiles of the rhyolite bedrock surface measured along the edge of the fluvial canyons (red). Incision between the stream and lower rim in black. Inset topographic maps show profile points mapped on 20-ft contour lines near the flow-margin at the same scale (1-km UTM grid).

Where the stream had incised significantly (> 10 m), profiles were constructed close to the

inferred pre-incision elevation along the canyon rims by identifying changes in slope and

curvature that are likely the result of the stream incision. Where the two rims are unequal

in elevation the lower rim was used in calculations, and where the rim profiles climb over

pressure ridges, the elevation gain was cut off. assuming that streams exploited gaps in

ridges. These assumptions produce a conservative estimate of incision.

Knickpoints were identified along the profiles by identifying zones of high convexity

in the rim profiles. Concavity was calculated using a concavity index (CI) based on Langbein

and Leopold (1964), which is illustrated in Fig. 3). The profiles were resampled at 5-m

intervals and concavity maps were produced by calculating CI for all stream lengths > 100 m

with at least 20 m of stream relief. Knickpoints were identified where the rim exhibits high

convexity, and the length of the reach was determined by the length over which the

difference in CI between the stream and rim profile was greatest. This provided an

objective means of selecting knickpoints out of complex profile interactions. Some

knickpoints were complicated by interactions with major tributaries entering the main-stem

channel or from complex flow morphology that interfered with the accurate definition of

the original rhyolite flow topography. Reaches were eliminated where the original rim

profiles were poorly constrained. CI for the entire profiles ranges from ~-0.2 to -0.5,

whereas individual stream reaches through knickpoint zones were nearly straight (average

CI = 0.01) and the rim profiles have CI values ranging from about -0.2 to -0.9 in those

reaches.

Of the 18 streams selected, 7 were identified as likely having received significant

meltwater from the late Pleistocene Yellowstone ice cap. This determination was based on

three factors: (1) the position and orientation of the drainage basin relative to the mapped

position of the ice cap terminus and inferred ice flow direction (Licciardi and Pierce, 2018),

(2) stream reaches identified as glacial meltwater channels on surficial geologic maps (e.g.

Richmond, 1973; Waldrop, 1975) and (3) the presence of deposits of meter-scale boulders

in stream channels that the stream appears unfit to transport, which may represent glacial

flood deposits. Most if not all of the basins have been glaciated for some period, but the

position of the ice margin and inferred ice flow direction allows for the differentiation of

basins that likely received considerable meltwater input from those that did not (Fig. 17).

Basins oriented opposite to glacier flow or without drainage area where an advancing or

retreating glacial margin would have persisted were considered less likely to be impacted by

glacial meltwater. Streams identified as glacial meltwater channels on surficial maps of YNP

often contain the deposits of multi-meter sized boulders, and also fit the topographic

characteristics above as likely influenced by meltwater.
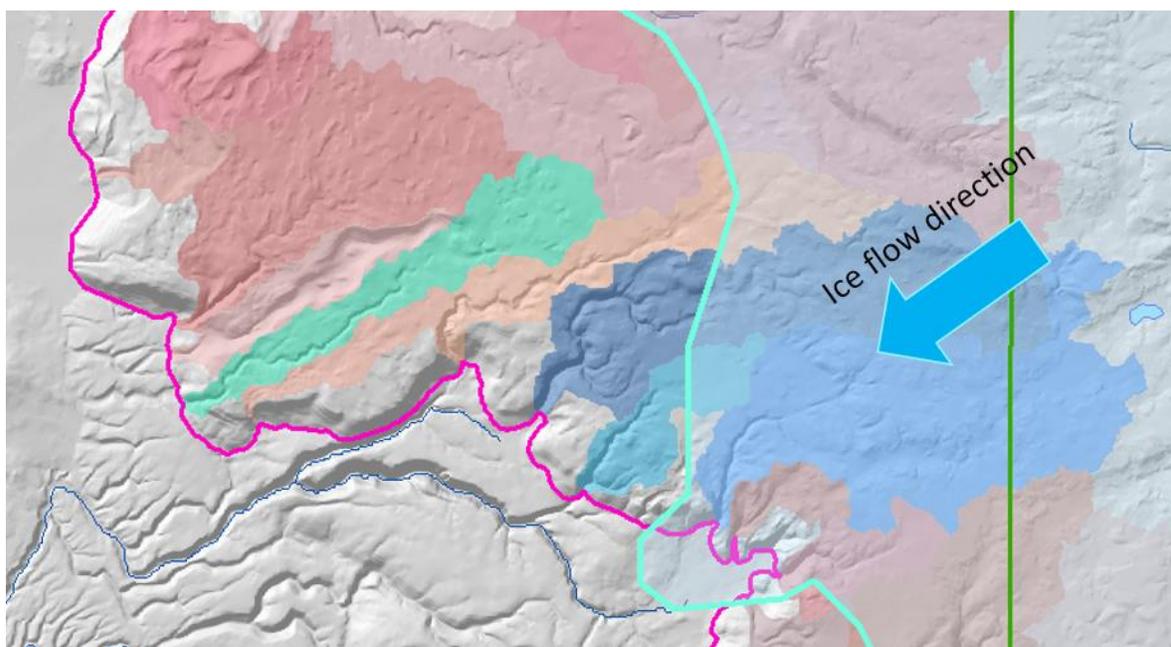
Figure 17. Late Pleistocene (Pinedale-age) Yellowstone ice cap margin (light blue line) with ice flow direction indicated (after Licciardi and Pierce, 2008). The 3 sub-basins of Partridge Creek (blue) are inferred to have received glacial meltwater from the Pinedale ice cap, while Baker Creek (green) did not. Margin of the Buffalo Lake Flow is marked by the pink line and the western border of YNP is marked by the green line; additional drainage basins used in the DEM analysis are shaded orange to red.

For each knickpoint, the difference in CI between the rim and stream profile was calculated, as well as several measures of stream incision including:

1) Maximum incision: the single highest incision value in the knickpoint reach

2) Total incision: the total area between the stream and rim profiles

3) Average incision: total incision divided by the reach length

CI difference and incision were strongly influenced by the contributing drainage area above the reach and the gradient of the reach. Differences in stream power and bed shear stress have long been associated with a stream's ability to incise (Gilbert, 1877; Bagnold, 1973; Howard and Kerby, 1983; Venditti et al., 2019) and are directly related to discharge and slope. Assuming that discharge is proportional to drainage area (Hack, 1957; Strahler, 1964) the erosion rate (E) of a reach is commonly expressed as:

Eq. 11 $E = KA^nS^m$

where K is a coefficient of erosivity and m and n are positive exponents (Howard and Kerby, 1983; Kooi and Beaumont, 1994). Appropriate values of m and n have been debated and are dependent on a variety of fluvial system properties, but typically range from $0.3 < n < 1$ and $0.7 < m < 1$ (Howard et al, 1994; Venditti et al., 2019) based on whether the system is modeled after the stream power equation, bed shear stress equation, or empirical relationships between discharge and slope.

CI and the 3 measures of incision were normalized for potential erosion rate by dividing by $A^{0.5}S^1$ as in Eq. 11. The values for m and n chosen are generally consistent with those reported, provided some of the best fits to the data, and create unitless normalized

incision values. The full range of values for m and n above were tested with the CI and incision data; higher values of m and lower values of n altered r^2 values by up to 0.2, but never altered the directionality of the trend.

All the knickpoint measures showed significant trends with flow age (Fig. 18). Incision and concavity increase with flow age and the trends are strongest when meltwater-influenced streams are not included, although regression line slopes change only slightly between the full data and the subset. Streams likely influenced by glacial meltwater exhibited a much greater range of values, with extreme values most commonly found on the upper plateau.

Since many of the knickpoints are small features on the surface of the flows, the flow-margin knickpoint was selected and measured independently to create a subset of the data. Near the flow margins, streams are confined to very distinct fluvial canyons which allows for the most accurate mapping of the pre-incision surface. Streams also have the greatest drainage area and relief at the margin, which reduces the range of those variables for this subset as compared to the full knickpoint data set. The similarity of the data points allowed for a direct comparison of the length of the flow-margin canyons (Fig. 19), which represents the extent to which significant erosion has propagated into the flow interior. This canyon length metric was normalized as for the other knickpoints, but then adjusted to represent incision propagation expected along a stream in a 10 km^2 drainage basin crossing a flow margin of average gradient. Trends in CI difference and incision were similar to those calculated for the entire set.
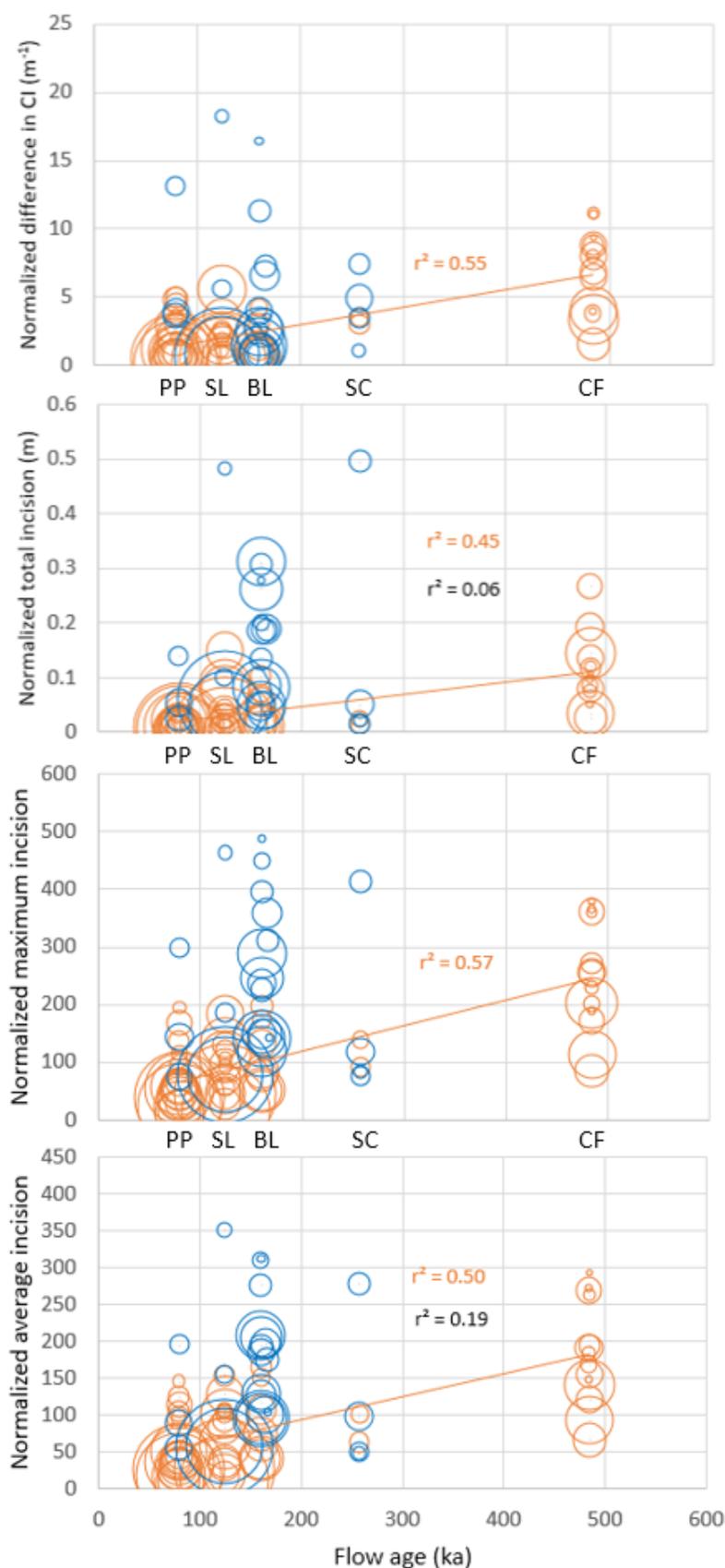
Figure 18. For each knickpoint along the 18 selected streams, difference in concavity index (CI) between the stream and rim profiles and 3 measures of stream incision below the rim are plotted against flow age. Circles for streams likely influenced by glacial meltwater are blue. All other streams are plotted with orange circles with the regression line for these streams; goodness of fit listed in orange (top values). Regression lines for all data are not shown, but r^2 values for those regressions are in black (bottom values); all regressions listed are significant ($p < 0.05$). Circle area is proportional to an index of stream power for that reach ($S*A^{0.5}$).

Selected major flows are labeled between the plots: PP = Pitchstone Plateau, SL = Summit Lake Flow, BL = Buffalo Lake Flow, SC = Spring Creek Flow and CF = Canyon Flow.
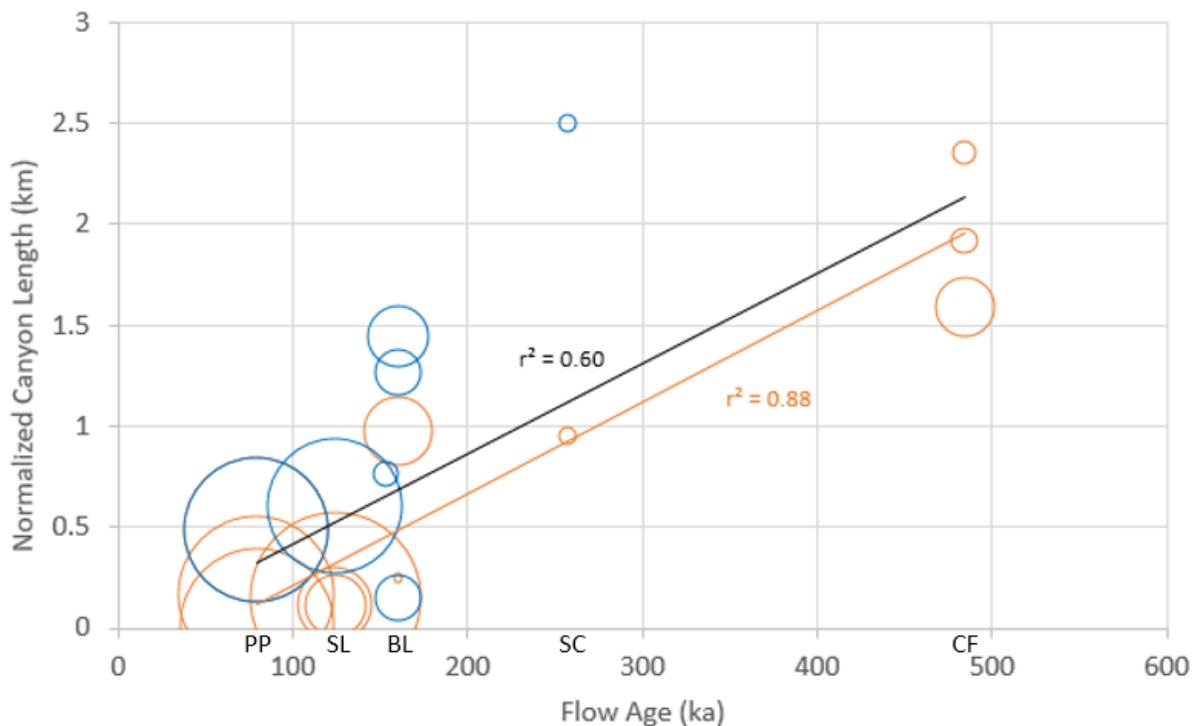
Figure 19. Normalized canyon length at the flow margin. Values normalized to a 10 km^2 drainage basin with average flow margin gradient. Blue circles represent streams interpreted as likely influenced by glacial meltwater, black regression line and r^2 is for the entire data set. Circle area is proportional to an index of stream power for that reach (S*A$^{0.5}$). Some flows are labeled at bottom: PP = Pitchstone Plateau, SL = Summit Lake Flow, BL = Buffalo Lake Flow, SC = Spring Creek Flow and CF = Canyon Flow.

4. Discussion

4.1 Suitability of the Rhyolite Plateau for space-for-time substitution

The space-for-time substitution model requires surfaces of different ages that are otherwise similar in geology and experience similar geomorphic processes. All of the flows have radioisotopic age dates ranging from 79 to 484 with standard deviations of 3-15 ka. The flows are all of similar bulk composition (Christiansen, 2001) and minerology, and all have the same basic morphologic shape as indicated by similarity in hypsometric curves (Fig. 5). Original volcanic constructional features such as pressure ridges, flow lobes and

vents can be identified on each flow. The flows have all experienced some degree of ice cap

glaciation (evidence for glacial erosion is discussed below), and all are mantled by broadly

similar surficial materials. The climate across the area of the flows is fairly uniform,

although the younger flows in the southwestern portion of the study receive more

precipitation, which falls primarily as snow in the winter months

(www.wcc.nrcs.usda.gov/snow). The Canyon Flow appears to be the most different from

the other flows by just about any of these measures. However, many of those differences

can be attributed to its age rather than initial form, for example the somewhat lower

plateau surface and margin elevations on the hypsometric curve are likely the result of

greater incision in the lower reaches of the drainage basin as compared to the younger

flows.

To test whether fluvial processes occur at similar rates across the Rhyolite Plateau,

we consider the fundamental geomorphic principles of stream power and bed shear stress,

which drive incision through convex knickpoints. In drainages without evidence of glacial

meltwater influence, incision into knickpoints has progressed at a nearly linear rate when

the values are normalized by drainage area and slope. Linear regressions through the

knickpoint incision data display reasonably high goodness of fit for spatial data extracted

from diverse drainage basins with a range of basin area, relief, and other local topographic,

climatic and geologic variables. The y-intercepts for the regression lines are all close to

zero, which should be the case for any channel not following an original channel-like

volcanic form, and forcing the lines to pass through the origin reduces r^2 values by < 10%.

The resolution and filling-in of closed depressions creates additional error in the measurements taken from the DEM. Filling the DEM should have little impact on hypsometry or basin shape, but it does influence drainage area calculations by including closed depressions, and it affects the slope-area curve since basins are flattened. Since closed depressions account for ~3-9% of the rhyolite flow surfaces (Burnett, 2020 [Ch. 1]) and are more prevalent on younger flows, drainage area is slightly over-estimated for knickpoints and stream junction calculations. The 6% difference between the youngest and oldest flows represents only a small portion of the variability in these data sets. Basin filling reduced the slope of low-gradient basins between pressure ridges, however this likely has little impact on median slope-area values, since the areas that get filled tend to have low gradients (< 1 %) already. The impact of DEM filling along the stream channel was reduced by training the stream to the NHD streams, which reduces cuts of impinging hillslopes that might otherwise cause artificial filling along the channel. Similarly, by calculating slopes along the stream network using only other nearby cells identified as part of the channel, potential slope errors are reduced further.

4.2 Influence of glaciation on plateau morphology and stream systems

The extent, duration and nature of glacial erosion and deposition have varied across the plateau, and are likely the most significant factors that influence the suitability of the Rhyolite Plateau for space-for-time substitution study stream networks and incision. The duration of Yellowstone ice cap glaciation and the timing of ice advance and retreat on the Rhyolite Plateau specifically is poorly constrained (Licciardi and Pierce, 2018). The ice cap phase of glaciation may only occur during peak glacial periods and likely represents only a

small portion of the Pleistocene. Most of the Rhyolite Plateau may have been glaciated for

only ~3 kyr during the last glacial maximum (Licciardi and Pierce, 2018). While evidence for

glaciation on the rhyolite flows is widespread, evidence for significant erosion of flow

surfaces or thick glacial deposits is not. There is almost no direct topographic expression of

glaciation visible on USGS 7.5' quadrangles. Valleys and canyons on the plateau are V-

shaped, except in inter-lobe areas where the valley sides follow the shape of the flow lobes.

There are some valleys located between flows, like Bechler Canyon, where ice may have

preferentially flowed. These valleys are more U-shaped, and were not used in this study.

Moraines and other constructional glacial features are largely absent except locally at the

limit of Pinedale glaciation. Where present, moraines tend to be low-relief and indistinct in

the study area. Thick glacio-lacustrine deposits are common within the caldera and in some

valleys, but those areas were largely avoided for this study. Striations exist on bedrock

knobs, but are rare and are mostly found on small protuberances that are only centimeters

wide and would have been removed entirely if glacial erosion had been extensive. Faceted

cobbles and boulders, which are common indicators of glacial transport and erosion, were

not found over the course of 4 months of field work. Erratics and boulders of exotic

lithologies are rare. Although till and glacial rubble have been mapped over most of the

flow surfaces, streams that have incised into the surficial deposits rarely expose diamicton

except on hillslopes where colluviation is active. One of the most common surficial

materials on the upper surfaces of the flows, particularly in basins between pressure ridges,

is well-sorted silt of eolian and locally lacustrine origin.   The silt is commonly deposited on

the well-sorted pea gravel that also dominates most low-gradient active stream channels on

the plateau, or deposited on mixed pea gravel to boulder deposits that grade into bedrock and may represent the original surface rubble of the rhyolite flow.

Glaciation does appear to have impacted some stream systems with meltwater temporarily enhancing stream power, incision, and competence. Large boulder deposits found in streams that appear unfit to transport those materials may be the result of ice dam failures, outburst floods from subglacial reservoirs, or extreme warm-season meltwater flooding. These sorts of floods and discharge added from non-flood meltwater would also be expected to have an impact on stream incision as well. The circle areas in Figs. 18 and 19 are scaled to the estimate of modern stream power for a knickpoint reach (A*S). Points with extremely high normalized incision and CI values plot far above the regression lines and mostly have low stream power values (small circles). These knickpoints have experienced more incision than what would be expected given their relatively low contributing area or gradient. Glacial meltwater and outburst floods while the ice terminus lies within the drainage basin may add a significant amount of stream power to reaches that otherwise have relatively low stream power, thereby driving up their normalized incision values. However, for reaches with high modern stream power on the same streams, the addition of glacial meltwater and flooding appears to have little effect on their long-term incision, and these knickpoints sit close to the regression line. There are a few exceptions where knickpoints with moderately high stream power also sit well above the regression line, but not at the top of the plot. These knickpoints are in the three forks of Partridge Creek on the Buffalo Lake flow (labeled BL on Fig. 18 and colored blue on Fig. 17). The Pinedale glacial terminus crosses through the Partridge Creek drainage basins (Licciardi and

Pierce, 2018), and these basins likely experienced greater and longer-lived glacial meltwater influence than other glaciated basins on the plateau, which explains why knickpoints in these basins with moderate stream power are elevated off the regression line and not just those with low stream power estimates. The penultimate (Bull Lake) glacial maximum ice margin is poorly constrained here and is likely similar that of the more recent Pinedale limit, but the older glaciation may have influenced additional basins on the Buffalo Lake flow.

4.3 Evolution of stream concavity

Streams on the Rhyolite Plateau have significantly reduced the convexity of their profiles at several different scales. The development of the typical concave-up stream profile has been attributed to downstream changes in the factors driving and resisting bed erosion, primarily stream power and sediment size respectively (Hack, 1957; Snow and Slingerland, 1987; Sinha and Parker, 1996). All individual knickpoints, including the flow margins, show an increase in concavity (positive CI difference), but the raw CI data indicate that the stream profiles are on average nearly straight in individual reaches. Sediment size, discharge and slope are the three primary factors that could be influencing convexity. By definition, knickpoints contain steeper slopes and higher stream power than neighboring reaches, and this is presumed to be the primary factor in the straightening of the profiles though convex reaches. Median sediment size (D_{50}) does not change systematically along stream reaches and exhibits extreme variability over short distances. Steep knickpoint reaches are commonly boulder-bedded (D_{50} = 200-800 mm) and followed by a transition to pea gravel-dominated stream beds (D_{50} = 10 mm) over a few 10s of meters of channel length. This pattern in bed sediment size repeats as the stream cuts through subsequent

pressure ridge knickpoints. Although not directly analyzed, these changes in sediment

appear to be driven by slope-mediated changes in stream power and sorting of sediment,

and are thus are largely a consequence of variations in concavity and not a driver of it. The

reaches used for individual knickpoints are 100 meters to a few kilometers long, and most

do not have a significant change in discharge along their lengths because major tributary

junctions tend to occur between knickpoints. Therefore, variation in discharge cannot be

used to explain the change in concavity of the individual reaches. However, the raw incision

and CI data (not normalized by drainage area and gradient) have r^2 values that range from

0.01 to 0.2, and low significance (P > 0.05 in most cases). This indicates that stream power,

with drainage area as a proxy for discharge, does play a major role in controlling incision

rates across the full length of the profile, even if the stream hasn't carved a concave profile

through the rhyolite.

The concavity of the full profile is best represented by Region 3 of the slope-area

curve, which includes streams that are generally second-order or higher. The three regions

of the slope-area curve identified in this study correspond reasonably well to the three

regions identified on slope-area curves by Willgoose et al. (1991) and the three regions

identified on cumulative area distribution curves by Perera and Willgoose (1998), but

Region 2 overlaps the debris flow-to-fluvial transition identified by Hooshyar et al. (2017).

As noted in those studies and others utilizing the slope-area curve, Region 3 is strongly

influenced by boundary conditions such as base level control by a master stream or bedrock

structures. For the Rhyolite Plateau, the convex flow margins control that boundary

condition. Streams in Region 3 on the younger flows (≤ 160 ka) are highly convex (positive u

values, Fig. 15) with large standard deviations. The convexity of these streams is controlled

by the original highly convex flow margin (e.g. Falls River on Fig. 16), which is in itself highly

variable. In contrast, u values for Region 3 streams on the Canyon Flow are negative and

indicate straight to slightly concave stream profiles and exhibit a much smaller standard

deviation. This trend indicates that over about half a million years, large streams (A > 1

km^2) are capable of incising through major bedrock convexities and producing slightly

concave profiles. The reduction in variance around the mean u value for the Canyon Flow

indicates a systematic progression towards concave profiles as well. The hypsometric

curves for different flows have similar variance (Fig. 5), indicating that the flows have similar

ranges of profile shapes. The smaller standard deviation in Region 3 u values for the

Canyon flow suggests that incision has occurred faster along streams with greater initial

convexity and slower along streams with less, thereby reducing the variance in the resulting

stream channels.

These observations support the assertion that the Rhyolite Plateau landscapes are

evolving from a state dominated by convex constructional volcanic features toward one

dominated by fluvial erosion. Even the 484 ka Canyon Flow remains in a relatively nascent

stage of development, with significant and continuous incision propagating only a few

kilometers from the margin (Figs. 16 A, and 19). It exhibits u values well above those of

much older fluvial landscapes (-0.4 > u > -0.8), which typically have more concave profiles

(Flint, 1974). Estimating rates of change in the landscape are difficult, in part because u

values are not derived from linear parameters and because u values for the highly convex

profiles of the younger streams are dependent on measurement scale and bin size used to

define the median slope values for use in the power regression. Changing bin size altered

the slope of the regression but did not change the direction or significance. Incision rates

indicated by the knickpoint data (Fig. 18) appear to be linear, and y-intercepts near zero

validate the method used to estimate the pre-incision surface. All of the y-intercept values

are slightly positive (3-12 % of maximum value) which indicates either a slight exaggeration

of the elevation of the original flow surface, or that incision processes have slowed

somewhat over time. The latter case would be expected as the incision process reduces

convexity and local slope, and therefore local stream power over time. In contrast, the

propagation of incision into the flows from the margin (Fig. 19) has a negative y-intercept,

which may indicate that a threshold of incision needs to be met before significant

knickpoint retreat occurs. The regression line that runs through all the streams, including

those with inferred glacial meltwater influence, has a y-intercept close to zero. Using the

full data set may be appropriate in this case since streams have relatively high discharge

and stream power near the margin, so the relative influence of glacial meltwater may not

be as great.

4.4 Evolution of the stream network

Volcanic flows have no initial surface streams or drainage network and have

relatively high infiltration rates because of irregular topography, closed depressions, often

mostly brecciated and rubbly porous surfaces, and abundant open fractures. Development

of drainage networks is promoted by weathering, deposition of fine-grained sediments, and

soil development, which work to reduce infiltration and increase surface runoff (Wells et al.,

1985; Jefferson et al., 2010). Previous space-for-time studies on basaltic flows in arid

climates have found that drainage density increases with flow age for flows younger than 1

million years old, and that significant incision of those surfaces occurred later (Wells et al.,

1985, Dohrenwend et al., 1987; 1989). However, even the youngest rhyolite flow in this

study (Pitchstone Plateau, 79 ka) contains drainage networks that fully extend into the

plateau summit area. I attribute this to differences in initial permeability, climate and

sedimentation rates. Estimates of hydraulic conductivity on the Rhyolite Plateau indicate

that initial permeability of the flows may be lower than that of the basalts studied in arid

climates (Burnett, 2020 [Ch. 1]). The Rhyolite Plateau also sits downwind of the Snake River

Plain and likely experienced relatively rapid deposition of fine-grained loess (Lewis and

Fosberg, 1982; Forman et al., 1993) during times without ice cover, which were

predominant on the plateau in the Quaternary, along with till during maximum glacial times

when the plateau was covered by the Yellowstone ice cap. This dominantly fine-grained

surficial cover promotes runoff during snowmelt and rainfall. With greater precipitation

and runoff, stream networks were established faster in Yellowstone than in more arid

climates.

Drainage density decreases with flow age on the Rhyolite Plateau (Fig. 9) indicating

that the drainage networks are evolving through time. Glock (1931) proposed that after

initial expansion and elaboration of a stream network, incision of mainstem streams would

reduce the number of first-order basins by integrating them into the larger valley and

sideslopes. This integration produces a reduction in both drainage density and stream

frequency as first-order basins are lost. However, incised streams on the plateau create

narrow canyons (generally < 20 m wide at the bottom and < 200 m from rim to rim) that

generally have not widened enough to integrate smaller drainages. The decrease in

drainage density on the Rhyolite Plateau can be mostly attributed to a decrease in first-

order stream length (Fig. 9C). However, there is no significant decrease in stream

frequency, which indicates that the first-order streams are getting shorter, but not being

integrated into larger valleys. This pattern reflects an increase in network efficiency with

first-order streams finding shorter, more direct flow paths across the volcanic landscape.

Incision of higher-order streams may also increase local gradient and promote shortcutting

of first-order streams across relatively flat basins. On upper plateau surfaces of the

youngest flows (79-124 ka), some basins between pressure ridges contain wandering

streams that follow circuitous routes through the basins to gaps in the ridges (Fig. 20).

Figure 20. Two first-order streams on the Pitchstone Plateau surveyed by GPS. Both streams start in a broad basin and cross through steeper, forested pressure ridges. Channels contain gray pea gravel made mostly of obsidian; tan silt deposits form the tan-to-brown non-channelized areas. The 2 streams may be connected during snowmelt when snow dams block one outlet or the other.

During the dry summer season, flow direction in these ephemeral channels is not obvious.

Such streams were not observed on older flows as the basins appear to be more

consistently graded towards the gaps in pressure ridges that streams flow through.

Stream junction angles have little indication of evolving over time (Fig. 12) on the

Rhyolite Plateau. Junction angles generally follow patterns observed elsewhere (Horton,

1932, 1945; Howard, 1971; Rodriguez-Iturbe et al., 1992; Hooshyar et al., 2017). Streams

with higher drainage area and discharge tend to dominate the junction geometry by

maintaining a straighter path through the junction (Figs. 11-13). Small, steep tributaries

that intersect larger streams intersect at higher angles as predicted by geometric

constraints (Howard, 1971) and observed in a wide range of fluvial landscapes (Hooshyar et

al., 2017). Most notably, the median junction angles predominantly fall between the angles

predicted by the modified Horton model for junction angles using the upper and lower

estimates of u from Region 2 of the slope-area curve (Fig. 12, purple lines), and well below

the range predicted for older landscapes (Fig. 12, black dashed lines). These predicted

values are also similar to predicted values for minimum power loss (Howard, 1971). Since

the median junction angles for all flows predominantly lie within this predicted range, and

there is no significant trend between the flows based on their relative ages, stream

junctions must either initially form at efficient and geometrically stable angles or evolve

quickly (< 79 ka) to reach that state.

The modified Horton equation can also be used calculate u values based on junction angle

data, and these values mostly fit within the standard deviation of the Region 2 data (Fig.

15). The strong concurrence of u values from these completely independent calculations

indicates that junction angles and the Region 2 portion of the slope-area curve accurately represent the same portion of the drainage basins. This is to be expected since Region 2 includes first-order streams and the hillslope-fluvial transition point, and since first-order streams comprise the majority of stream segments and are involved in the majority of stream junctions. The concurrence of u values also validates the methods used to calculate junction angles and slope-area exponents and the use of the 10-m DEM for slope calculations. The similarity in these u values highlights the strong contrast between Region 2 and 3 u values. Since Region 2 u values do not change significantly with flow age, it appears that while first-order streams are shortening somewhat through time, the adjacent topography is not evolving. These low-order systems have relatively little drainage area and mostly form on the relatively low-relief upper plateau surfaces, thus stream power and the potential for geomorphic change on the upper plateaus are very limited. This condition may change as incision propagates into the plateau from the margin. The Region 3 u value on the Canyon Flow is approaching that of the Region 2 value. Continued incision and increasing concavity in Region 3 may begin lowering the u value of Region 2 towards the more typical values of -0.4 > u > -0.8 observed in other fluvial landscapes.

Although the fit between predicted and observed junction angles is highly significant (Fig. 15), some portions of the median β curve lie outside the range of predicted junction angles. This is true in cases where one tributary has at least 4 times as much drainage area as the other (drainage area ratios > 0.8 and < 0.2). In these regions, observed angles are higher than predicted, indicating that large streams are not as straight as predicted and total junction angles are higher than predicted for tributaries with widely different drainage

area. Both of these effects may be products of the rhyolite bedrock structure. The pressure

ridges produce a rectangular drainage network with junctions commonly occurring where a

stream turns to cross a pressure ridge (Fig. 2). The rectangular drainage pattern is also

consistent with α values near 90°, which is common for tributaries on the Rhyolite Plateau

with relatively unequal slope (Fig. 10C) and drainage area (Fig. 13), but are higher than

those found in other fluvial networks (Hooshyar et al., 2017). The pressure ridge

morphology appears to have greater influence at junctions between unequal tributaries,

whereas the minimum power expenditure and geometric criteria play a larger role in

controlling junction angles between relatively equal tributaries.

The only significant difference in junction angles identified between flows of

different ages is that the Canyon Flow has higher α values. This difference is best expressed

in Fig. 13, where stream junctions on the Canyon Flow become nearly rectangular (80° < α <

90°) at a discharge ratio for the smaller streams (R_2) ≤ 0.3, whereas other flows reach the

same α values at R_2 ≤ 0.12 on average. This suggests that rather than evolving towards the

junction angles predicted by geometric and minimum power criteria, the network may

become more rectangular through time as a result of the stream incising into bedrock and

becoming entrenched under significant control by the pressure ridge system and associated

fractures.

The basins defined by the stream network show only subtle evidence of evolving

through time. Shape factor (s) and W/L increase and compactness (C) decrease with

increasing flow age, indicating that the basins become slightly rounder with a more uniform

perimeter over time. These adjustments are progressive (as indicated by high r^2 of flow-

averaged values), but flow age only accounts for a very small proportion of the total variance between basins and is relatively unimportant in defining the overall morphology of the drainage basin. The high variance is likely a result of stream networks being controlled by the pressure ridge network and the overall flow shape. The small changes in C are consistent with the interpretation that limited alteration of the headwaters topography and basin divides has occurred. W/L and s are invariant across stream order indicating that the basins are self-similar and don't elongate with increasing basin size as predicted by Hack's (1957) law. Bennett and Liu (2016) observed self-similar basins in a soft-sediment experiment shorty after drainage network developed, so self-similarity may be a characteristic of relatively young drainage networks, or on the Rhyolite Plateau, it could be driven by the flow structure which limits major reorganization of the network.

5. Conclusions

In the young volcanic landscapes of the Rhyolite Plateau, stream networks and profile shapes are dominantly controlled by constructional volcanic features such as pressure ridges and the broadly convex morphology of the massive flows. Nonetheless, streams have significantly altered the landscape by incising into convex reaches and by increasing the concavity along their longitudinal profiles. For streams on the younger flows (≤ 160 ka), this incision tends to be localized within small knickpoints along the profile. On the much older Canyon Flow (484 ka), however, major streams with basin area greater than 1 km^2 have cut through the large convex flow margins, and that incision has propagated a few kilometers into the flow interior. Slope-area relationship exponents (u) are higher than those of most fluvial landscapes, which is consistent with an early stage of evolution and a

landscape strongly influenced by bedrock or base-level controls. The concurrence of u

values from two independent data sets validates the methods used to calculate slope and

stream junction angles and confirms that these measures represent similar portions of the

landscape. The u values of larger streams (Region 3) on the plateau decrease with flow age,

indicating that the system is evolving towards a fluvially dominated landscape through time

and from the flow margins towards the plateau center. Decrease in drainage density has

occurred in the headwater regions of the basins, however, which can be accounted for by

first-order streams finding more efficient flow paths over time. Modification of the

topography by glaciers is limited, but in basins located along the Pinedale ice margin and

where channel deposits are inferred to be deposited by glacial meltwater floods, stream

reaches with limited modern stream power show elevated incision and a reduction in

profile convexity.

Stream networks and basin morphologies show relatively little change with flow age

and follow patterns that are for the most part like typical fluvial drainage systems. Stream

junction angles generally align well with predictions based on geometric constraints and the

minimum power criterion as defined by Howard (1971). Stream junctions are therefore

relatively efficient, particularly for junctions between streams of similar magnitude. This

alignment exists even on the youngest flow, indicating that efficient junction angles are

either characteristic of initial drainage networks, or develop rapidly during the integration

of the network across the flow surface (< 79 ka). However, stream junction angles are also

influenced by the pressure ridge system and driven towards a rectangular ($80° < \alpha < 90°$)

pattern. This is particularly true for junctions involving streams with extremely different

drainage area or slope, which is where higher junction angles (~ 76°) are commonly found in other stream networks (Hooshyar et al., 2017). The Canyon Flow has a more rectangular drainage network than the younger flows, which may be a result of the network becoming entrenched in the pressure ridge network as incision into bedrock progresses.

These results conform to many of the basic principles of geomorphology and landscape evolution, including the importance of stream power in incision rates, and the headward advance of incision into an undissected landscape. But these results also emphasize the control that local geology plays on the evolution of stream networks and drainage basins. I propose that the interplay of rhyolite flow morphology, eolian deposition, glaciation and stream development would be extremely difficult to accurately represent in a forward model, but that their individual effects can be differentiated using the space-for-time model. Additional work is needed to fully describe the patterns in sedimentary deposits along streams, slopes and closed basins on the plateau, including those inferred as glacial meltwater deposits. Attribution of those materials to specific depositional processes will help to constrain the impact of glacial, eolian and lacustrine processes on the plateau and their implications for stream development. Additionally, it may be possible to find older rhyolite flows in Idaho along the Yellowstone hotspot track that could be analyzed to extend the age record, and test the hypothesis that incision along Region 3 drives down the slope-area exponent in that region, and eventually in Region 2 as incision advances headward. Finally, development of a high-resolution DEM through airborne LIDAR collection would allow for a more detailed investigation of slope-area relationship and knickpoint incision across the entire Rhyolite Plateau.

6. References

Abrahams, A. D. (1972). The significance of maximum extension of drainage networks for the frequency distribution of interior link lengths. *The Journal of Geology*, *80*(6), 730-736.

Bagnold, R. A. (1973). The nature of saltation and of 'bed-load' transport in water. *Proceedings of the Royal Society of London. A. Mathematical and Physical Sciences*, *332*(1591), 473-504.

Bárdossy, A., & Schmidt, F. (2002). GIS approach to scale issues of perimeter-based shape indices for drainage basins. *Hydrological Sciences Journal*, *47*(6), 931-942.

Bennett, S. J., & Liu, R. (2016). Basin self-similarity, Hack's law, and the evolution of experimental rill networks. *Geology*, *44*(1), 35-38.

Braun, J. (2018). A review of numerical modeling studies of passive margin escarpments leading to a new analytical expression for the rate of escarpment migration velocity. *Gondwana Research*, *53*, 209-224.

Brierley, G. J., & Fryirs, K. A. (2013). *Geomorphology and river management: applications of the river styles framework*. John Wiley & Sons.

Brocklehurst, S. H., & Whipple, K. X. (2004). Hypsometry of glaciated landscapes. *Earth Surface Processes and Landforms: The Journal of the British Geomorphological Research Group*, *29*(7), 907-926.

Brush, L. M. (1961). *Drainage basins, channels, and flow characteristics of selected streams in central Pennsylvania* (Vol. 282). US Government Printing Office.

Burnett, B. N., (2020). Fluvial Geomorphic and Hydrologic Evolution and Climate Change Resilience in Young Volcanic Landscapes: Rhyolite Plateau and Lamar Valley, Yellowstone National Park. Doctoral Dissertation, University of New Mexico.

Castelltort, S., & Yamato, P. (2013). The influence of surface slope on the shape of river basins: Comparison between nature and numerical landscape simulations. *Geomorphology*, *192*, 71-79.

Christiansen, R. L. (2001). *The Quaternary and Pliocene Yellowstone Plateau volcanic field of Wyoming, Idaho, and Montana* (No. 729-G).

Christiansen, R. L., Lowenstern, J. B., Smith, R. B., Heasler, H., Morgan, L. A., Nathenson, M., Masten, L. G., Muffler, L. J. P., & Robinson, J. E. (2007). *Preliminary assessment of volcanic and hydrothermal hazards in Yellowstone National Park and vicinity*. U. S. Geological Survey.

Cohen, S., Willgoose, G., & Hancock, G. (2008). A methodology for calculating the spatial distribution of the area-slope equation and the hypsometric integral within a catchment. *Journal of Geophysical Research: Earth Surface*, *113*(F3).

Dohrenwend, J. C., Abrahams, A. D., & Turrin, B. D. (1987). Drainage development on basaltic lava flows, Cima volcanic field, southeast California, and Lunar Crater volcanic field, south-central Nevada. *Geological Society of America Bulletin*, *99*(3), 405-413.

Dohrenwend, J. C., Abrahams, A. D., Turrin, B. D. (1989) Drainage development on basaltic lava flows, Cima volcanic field, southeast California, and Lunar Crater volcanic field, south-central Nevada: Reply. Geological Society of America Bulletin 101.7: 982-986.

Flint, J. J. (1974). Stream gradient as a function of order, magnitude, and discharge. *Water Resources Research*, *10*(5), 969-973.

Forman, S. L., Smith, R. P., Hackett, W. R., Tullis, J. A., & McDaniel, P. A. (1993). Timing of late Quaternary glaciations in the western United States based on the age of loess on the eastern Snake River Plain, Idaho. *Quaternary Research*, *40*(1), 30-37.

Giacometti, A., Maritan, A., & Banavar, J. R. (1995). Continuum model for river networks. *Physical review letters*, *75*(3), 577.

Gilbert, G. K. (1877). *Geology of the Henry mountains* (pp. i-160). Government Printing Office.

Gilbert, G. K. (1909). The convexity of hilltops. *The Journal of Geology*, *17*(4), 344-350.

Glock, W. S. (1931). The development of drainage systems: A synoptic view. *Geographical Review*, *21*(3), 475-482.

Gomez, B., & Mullen, V. T. (1992). An experimental study of sapped drainage network development. *Earth Surface Processes and Landforms*, *17*(5), 465-476.

Gravelius, H. (1914) Grundrifi der gesamten Gewcisserkunde. Band I: Flufikunde (Compendium of Hydrology, vol. I. Rivers, in German). Goschen, Berlin, Germany.

Hack, J. T. (1957). *Studies of longitudinal stream profiles in Virginia and Maryland* (Vol. 294). US Government Printing Office.

Hancock, G. R., & Willgoose, G. R. (2004). An experimental and computer simulation study of erosion on a mine tailings dam wall. *Earth Surface Processes and Landforms*, *29*(4), 457-475.

Hooshyar, M., Singh, A., & Wang, D. (2017). Hydrologic controls on junction angle of river networks. *Water Resources Research*, *53*(5), 4073-4083.

Horton, R. E. (1932). Drainage-basin characteristics. *Transactions, American Geophysical Union, 13*(1), 350-361.

Horton, R. E. (1945). Erosional development of streams and their drainage basins; hydrophysical approach to quantitative morphology. *Geological society of America bulletin*, *56*(3), 275-370.

Howard, A. D. (1971). Optimal angles of stream junction: Geometric, stability to capture, and minimum power criteria. *Water Resources Research*, *7*(4), 863-873.

Howard, A. D., Dietrich, W. E., & Seidl, M. A. (1994). Modeling fluvial erosion on regional to continental scales. *Journal of Geophysical Research: Solid Earth*, *99*(B7), 13971-13986.

Howard, A. D., & Kerby, G. (1983). Channel changes in badlands. *Geological Society of America Bulletin*, *94*(6), 739-752.

Jefferson, A., Grant, G. E., Lewis, S. L., & Lancaster, S. T. (2010). Coevolution of hydrology and topography on a basalt landscape in the Oregon Cascade Range, USA. *Earth Surface Processes and Landforms: The Journal of the British Geomorphological Research Group*, *35*(7), 803-816.

Keller, E. A., Zepeda, R. L., Rockwell, T. K., Ku, T. L., & Dinklage, W. S. (1998). Active tectonics at Wheeler ridge, southern San Joaquin valley, California. *Geological Society of America Bulletin*, *110*(3), 298-310.

Knighton, D. (2014). *Fluvial forms and processes: a new perspective*. Routledge.

Kooi, H., & Beaumont, C. (1994). Escarpment evolution on high-elevation rifted margins: Insights derived from a surface processes model that combines diffusion, advection, and reaction. *Journal of Geophysical Research: Solid Earth*, *99*(B6), 12191-12209.

Langbein, W. B., & Leopold, L. B. (1964). Quasi-equilibrium states in channel morphology. *American Journal of Science*, *262*(6), 782-794.

Larue, J. P. (2008). Effects of tectonics and lithology on long profiles of 16 rivers of the southern Central Massif border between the Aude and the Orb (France). *Geomorphology*, *93*(3-4), 343-367.

Leheny, R. L. (1995). Simple model for river network evolution. *Physical Review E*, *52*(5), 5610.

Leheny, R. L., & Nagel, S. R. (1993). Model for the evolution of river networks. *Physical review letters*, *71*(9), 1470.

Leopold, L. B., & Langbein, W. B. (1962). *The concept of entropy in landscape evolution* (Vol. 500). US Government Printing Office.

Lewis, G. C., & Fosberg, M. A. (1982). Distribution and character of loess and loess soils in southeastern Idaho. *Cenozoic Geology of Idaho: Idaho Bureau of Mines and Geology Bulletin*, *26*, 705-716.

Licciardi, J. M., & Pierce, K. L. (2018). History and dynamics of the Greater Yellowstone Glacial System during the last two glaciations. *Quaternary Science Reviews*, *200*, 1-33.

Lohse, K. A., & Dietrich, W. E. (2005). Contrasting effects of soil development on hydrological properties and flow paths. *Water Resources Research*, *41*(12).

Luo, W., & Stepinski, T. (2008). Identification of geologic contrasts from landscape dissection pattern: An application to the Cascade Range, Oregon, USA. *Geomorphology*, *99*(1-4), 90-98.

Matthews, N. E., Vazquez, J. A., & Calvert, A. T. (2015). Age of the Lava Creek supereruption and magma chamber assembly at Yellowstone based on 40 A r/39 A r and U-P b dating of sanidine and zircon crystals. *Geochemistry, Geophysics, Geosystems*, *16*(8), 2508-2528.

Minasny, B., & McBratney, A. B. (2001). A rudimentary mechanistic model for soil formation and landscape development: II. A two-dimensional model incorporating chemical weathering. *Geoderma*, *103*(1-2), 161-179.

Montgomery, D. R., & Dietrich, W. E. (1992). Channel initiation and the problem of landscape scale. *Science*, *255*(5046), 826-830.

Morgan, R. P. C. (1976). The role of climate in the denudation system: a case study from West Malaysia. Geomorphology and *Climate, Wiley, UK*, 317-343.

Morisawa, M. (1964). Development of drainage systems on an upraised lake floor. *American Journal of Science*, *262*(3), 340-354.

Ohmori, H. (1991). Change in the mathematical function type describing the longitudinal profile of a river through an evolutionary process. *The Journal of Geology*, *99*(1), 97-110.

Pallard, B., Castellarin, A., & Montanari, A. (2009). A look at the links between drainage density and flood statistics. *Hydrology and Earth System Sciences*, *13*(7), 1019.

Pazzaglia, F. J. (2003). Landscape evolution models. *Developments in Quaternary Sciences*, *1*, 247-274.

Pazzaglia, F. J., Gardner, T. W., & Merritts, D. J. (1998). Bedrock fluvial incision and longitudinal profile development over geologic time scales determined by fluvial terraces. *Geophysical Monograph-American Geophysical Union*, *107*, 207-236.

Pelletier, J. D. (2003). Drainage basin evolution in the Rainfall Erosion Facility: dependence on initial conditions. *Geomorphology*, *53*(1-2), 183-196.

Perera, H., & Willgoose, G. (1998). A physical explanation of the cumulative area distribution curve. *Water Resources Research*, *34*(5), 1335-1343.

Phillips, J. D., & Lutz, J. D. (2008). Profile convexities in bedrock and alluvial streams. *Geomorphology*, *102*(3-4), 554-566.

Pierce, K. L. (2003). Pleistocene glaciations of the Rocky Mountains. *Developments in Quaternary Sciences*, *1*, 63-76.

Radoane, M., Rãdoane, N., & Dumitriu, D. (2003). Geomorphological evolution of longitudinal river profiles in the Carpathians. *Geomorphology*, *50*(4), 293-306.

Richmond, G. M. (1973). *Surficial geologic map of the Grassy Lake Reservoir quadrangle, Yellowstone National Park and adjoining area, Wyoming,* USGS Miscellaneous Geologic Investigations Map I-644.

Rigon, R., Rodriguez-Iturbe, I., Maritan, A., Giacometti, A., Tarboton, D. G., & Rinaldo, A. (1996). On Hack's law. *Water Resources Research*, *32*(11), 3367-3374.

Ritter, J. B., & Gardner, T. W. (1993). Hydrologic evolution of drainage basins disturbed by surface mining, central Pennsylvania. *Geological Society of America Bulletin*, *105*(1), 101-115.

Rodríguez-Iturbe, I., Escobar, L. A. (1982). The dependence of drainage density on climate and geomorphology. *Hydrological Sciences Journal*, *27*(2), 129-137.

Rodríguez-Iturbe, I., Rinaldo, A., Rigon, R., Bras, R. L., Marani, A., & Ijjász-Vásquez, E. (1992). Energy dissipation, runoff production, and the three-dimensional structure of river basins. *Water Resources Research*, *28*(4), 1095-1103.

Roy, A. G. (1983). Optimal angular geometry models of river branching. *Geographical Analysis*, *15*(2), 87-96.

Schneider, A., Gerke, H. H., Maurer, T., & Nenov, R. (2013). Initial hydro-geomorphic development and rill network evolution in an artificial catchment. *Earth Surface Processes and Landforms*, *38*(13), 1496-1512.

Shelef, E. (2018). Channel Profile and Plan-View Controls on the Aspect Ratio of River Basins. *Geophysical Research Letters*, *45*(21), 11-712.

Shepherd, R. G. (1985). Regression analysis of river profiles. *The Journal of Geology*, *93*(3), 377-384.

Sinha, S. K., & Parker, G. (1996). Causes of concavity in longitudinal profiles of rivers. *Water Resources Research*, *32*(5), 1417-1428.

Snow, R. S., & Slingerland, R. L. (1987). Mathematical modeling of graded river profiles. *The journal of geology*, *95*(1), 15-33.

Snyder, N. P., Whipple, K. X., Tucker, G. E., & Merritts, D. J. (2000). Landscape response to tectonic forcing: Digital elevation model analysis of stream profiles in the Mendocino triple junction region, northern California. *Geological Society of America Bulletin*, *112*(8), 1250-1263.

Strahler, A. N. (1952). Hypsometric (area-altitude) analysis of erosional topography. *Geological Society of America Bulletin*, *63*(11), 1117-1142.

Strahler, A. N. (1957). Quantitative analysis of watershed geomorphology. *Eos, Transactions American Geophysical Union*, *38*(6), 913-920.

Strahler, A. N. (1964). Part II. Quantitative geomorphology of drainage basins and channel networks. *Handbook of Applied Hydrology: McGraw-Hill, New York*, 4-39.

Tucker, G. E., & Whipple, K. X. (2002). Topographic outcomes predicted by stream erosion models: Sensitivity analysis and intermodel comparison. *Journal of Geophysical Research: Solid Earth*, *107*(B9), ETG-1.

Venditti, J. G., Li, T., Deal, E., Dingle, E., & Church, M. (2019). Struggles with stream power: Connecting theory across scales. Geomorphology, 106817.

Waldrop, H. A. (1975). *Surficial Geologic Map of the Old Faithful Quadrangle, Yellowstone National Park, Wyoming.* USGS Miscellaneous Geologic Investigations Map I-649.

Wells, S. G., Dohrenwend, J. C., McFadden, L. D., Turrin, B. D., & Mahrer, K. D. (1985). Late Cenozoic landscape evolution on lava flow surfaces of the Cima volcanic field, Mojave Desert, California. *Geological Society of America Bulletin*, *96*(12), 1518-1529.

Wheeler, D. A. (1979). The overall shape of longitudinal profiles of streams. *Geographical approaches to fluvial processes*, 241-260.

Willgoose, G., Bras, R. L., & Rodriguez-Iturbe, I. (1991). A physical explanation of an observed link area-slope relationship. *Water Resources Research*, *27*(7), 1697-1702.

Wilson, D. D. (1985). Erosional and depositional trends in rivers of the Canterbury Plains, New Zealand. *Journal of Hydrology (New Zealand)*, 32-44.

Chapter 3

Profile Adjustments of the Lamar River and its Tributaries Following Catastrophic Volcanism: Lithologic, Volcanic and Tectonic Controls on Incision and Stream Capture, Yellowstone National Park

1. Abstract

Magmatism associated with the Yellowstone hot spot has created three major caldera-forming supereruptions. In the last eruption at 0.63 Ma, voluminous sheets of ash-flow tuff blanketed the greater Yellowstone region, filling in valleys and covering mesas and ridges, and postcaldera lava flows have also filled valleys. As the valleys erode back towards their former levels, remnants of the flows are left on the valley walls that can be used to reconstruct the incision history of the valley. I used remnants of the 0.63 Ma Lava Creek Tuff and the 0.26 Ma Osprey Basalt to calculate incision rates in the Lamar River drainage basin. An additional geomorphic surface was identified within the valleys that was likely formed ca. 1-2 Ma, but requires further age constraint to use quantitatively. I interpret that some valleys that head along the caldera rim lost significant drainage area as a result of the eruption and collapse of the caldera. For valleys that did not experience major loss of drainage areas, the disruption resulting from the emplacement of 100-200 m of welded ash-flow tuff is mitigated relatively quickly. Streams and glaciers in these basins reoccupied their former valleys, and in the 0.63 My since emplacement of the Lava Creek Tuff, have all incised through the tuff and well below their former elevations in their middle to upper reaches. A knickpoint caused by erosion-resistant crystalline rock has prevented base level lowering and limited incision in the lower reaches of the river.

Thick ash-flow tuffs fill valleys bordering the caldera rim, but the collapse of the caldera downdropped some of their headwaters into the caldera, resulting in stream capture and a loss of headwaters drainage area for valleys that flow into the Lamar River from the caldera rim. Streams in these valleys are underfit and skirt around the edges of the thick tuff units. The former valleys, in some cased filled with tuff, are left as some of the highest topographic features in the basins.

Net incision rates (excluding the thickness of emplaced volcanics and fault movement) within the Lamar River system range from 0.01 – 0.15 mm/yr and are relatively low compared to other records from the area (Pierce and Morgan, 1992, 2009). *Total* incision rates, calculated using the full thickness of Quaternary volcanics accumulated at individual points, are ~0.12 – 0.55 mm/yr, similar to if slightly higher than other nearby river systems. Total incision is highly dependent on the thickness of emplaced material, with higher rates occurring where greater emplaced thickness creates a steeper slope and a greater potential for erosion. In this way, streams and glaciers are able to adjust rapidly and produce concave long profiles similar in shape to the original profiles. However, valleys that have lost significant headwaters regions lack the stream power and mountain glaciers required to fully readjust their profiles to the emplacement of the volcanics, and after 0.63 My still have irregular longitudinal profiles dominated by bedrock knickpoints.

2. Introduction

Yellowstone National Park and the surrounding areas have experienced three volcanic cataclysms over the Quaternary period, when caldera-forming supereruptions mantled parts of the landscape with thick ash-flow tuff up to hundreds of meters thick

(Christiansen, 2001). Before and after the supereruptions, rhyolite and basalt were extruded from vents near the caldera rim. Rhyolite flows created domes and plateaus partially filling the caldera, whereas basaltic flows spilled over the rim of the caldera, following valley bottoms to lower elevations. The volcanic units disrupt fluvial and glacial systems by partially filling valleys and introducing additional variation in bedrock erodibility. As rivers and glacial ice streams incise through valley-filling units, remnants of the flows are left that provide clues as to the elevation of the infilled valley floor. I use these remnants to reconstruct the valley floors of the Lamar River and four of its tributaries (Fig. 1, Table 1). The profiles of the former valleys are used to calculate incision magnitudes and rates along the profile length and interpret the impact that variations in volcanic infilling and bedrock erodibility have on incision. Valley incision is one of the most important processes in landscape change, but while river response to modern volcanism has received substantial attention (e.g. Whipple et al., 2000; Gran and Montgomery, 2005), studies of long-term incision influenced by major volcanic deposition are limited. Incision rate information for the greater Yellowstone region comes from river terraces outside of or on the edge of Yellowstone National Park, mostly with limited or no influence from emplacement of volcanics (Dethier, 2001; Hancock et al., 1999; Pierce and Morgan, 1992, 2009; Reheis et al., 1991). This study greatly expands the study of valley incision within the park and that of long-term drainage evolution related to volcanic disturbance.
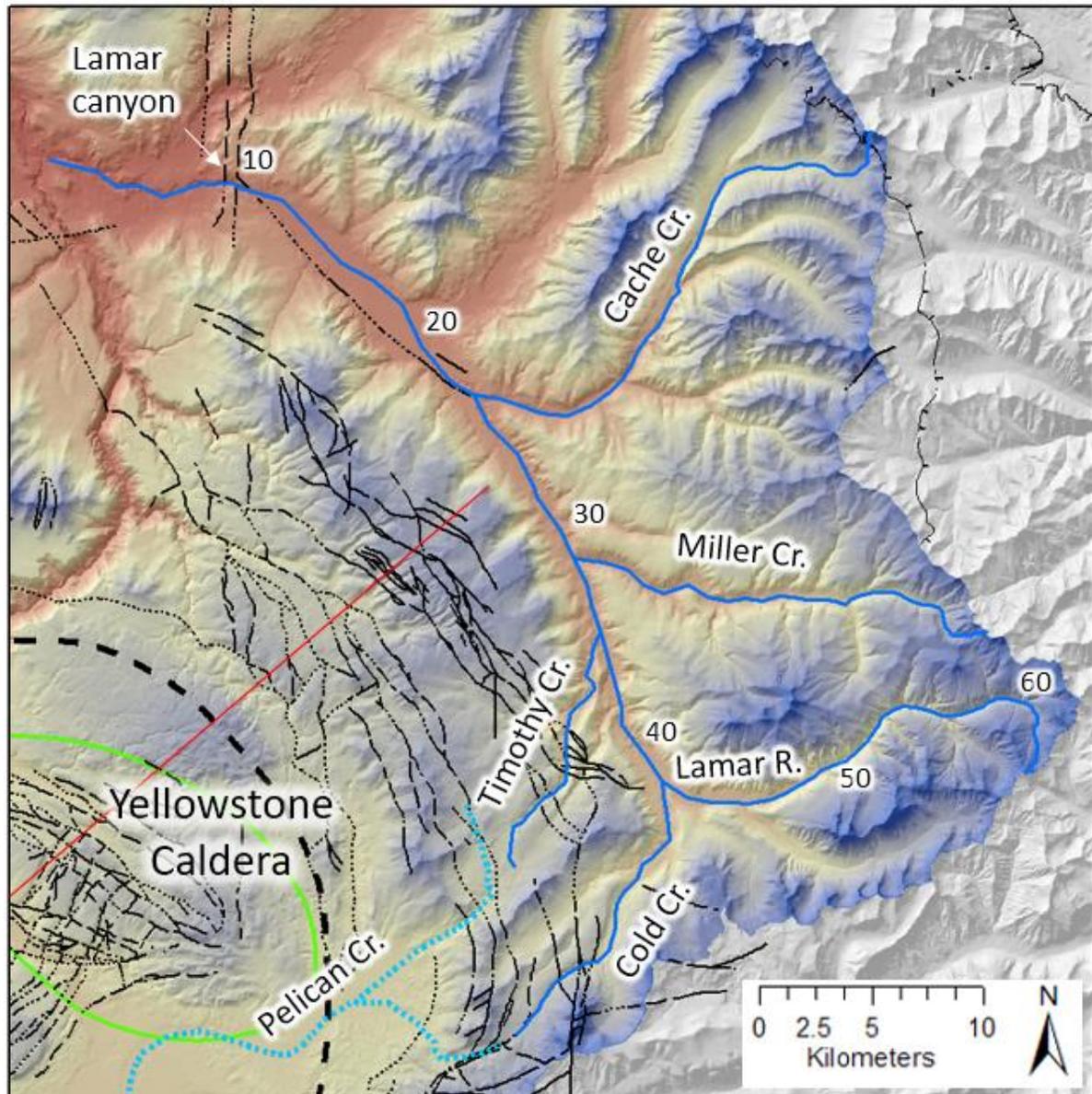
Figure 1. Northeastern corner of Yellowstone National Park (elevation colored) showing the tributaries of the Lamar River used in this study (dark blue lines). Distance along the mainstem Lamar River is labeled in 10 km increments. Tributaries of Pelican Creek (light blue dashed lines) drain into the Yellowstone caldera. Faults are marked in black, and the bold, dashed fault is the inferred inner caldera ring fracture. The Sour Creek resurgent dome (green circle) is shown with the line approximating the axis of the caldera, which runs between the resurgent domes and crosses Mirror Plateau north of Timothy Creek (red line).

Table 1. Summary of Lamar River tributaries used in this study.

	Confluence distance from Yellowstone River (km)	Drainage area (km^2)	Drainage area of Lamar R. at confluence (km^2)	Headwaters location
Lamar River		1266		away from caldera
Cache Cr.	23.3	210	509	away from caldera
Miller Cr.	31.9	100	334	away from caldera
Timothy Cr.	35.3	54	261	caldera rim
Cold Cr.	42.6	78	139	caldera rim

The primary research questions in this study are: (1) How does the thickness of volcanic units emplaced in established valleys impact local incision rates? (2) How does proximity to the caldera and ring fractures impact valley incision? (3) Do variations in rock type and bedrock resistance to erosion impact incision rates and longitudinal profile shape in the Lamar Valley?

The Lamar River flows from peaks of > 3000 m elevation in the Absaroka and Beartooth Ranges down to the Yellowstone River confluence at 1800 m. These ranges are part of the Yellowstone crescent of high terrain (YCHT), described as a bow wave-shaped pattern of uplift extending ahead of the Yellowstone hot spot to the northeast and wrapping around to both the south and the west. Uplift and incision rates in the most tectonically active portions of the YCHT range from 0.1-0.4 mm/yr (Pierce and Morgan, 1992, 2009). The Lamar River wraps around the northeast rim of the caldera, and drainages on the southwest side of the main valley have headwaters along the caldera rim, whereas those on the northeast side drain peaks that are 10s of kilometers from the caldera. The drainage network is well integrated, dendritic and contained in deep mountain valleys, in contrast to those in the caldera and on the Rhyolite Plateau, which are relatively immature,

having largely developed since the formation of the caldera and emplacement of younger flows (Burnett, 2020 [Ch. 2]). The pre-Quaternary bedrock into which the river and its tributaries are incised is primarily composed of Eocene volcaniclastic sedimentary rocks and intermediate-to-mafic volcanic flows of the Langford, Lamar River and Wapiti Formations and the Trout Creek Trachyandesite. Two Quaternary volcanic units in the Lamar River drainage basin are widely dispersed and can be used for profile and valley form reconstruction. The older unit is the Lava Creek Tuff (abbreviated Qyl), a voluminous (1000 km^3) welded ash-flow tuff extruded during the most recent caldera eruption at 0.63 Ma (Christiansen, 2001; Matthews et al., 2015; Jicha et al., 2016; Mark et al., 2017). Member B of the Lava Creek Tuff is interpreted to have filled the Lamar Valley up to 100-200 m in thickness and blanketed the low- to moderate-relief slopes below the high peaks separating drainages (Christiansen, 2001). Many remnants of the Lava Creek Tuff sit on a bench that is typically 100 to 200 m above river level. The younger unit is the Osprey Basalt (Lamar Valley flow, abbreviated Qo), which originated in a vent near the caldera rim along the Buffalo Fork of Timothy Creek (hereafter referred to as Timothy Creek). The basaltic lava flowed down Timothy Creek and into the Lamar River valley at 0.26 Ma (Abedini et al., 2007). Near the mouth of Timothy Creek, several distinct, stacked flows can be identified reaching thicknesses of up to 60-70 m, but in the lower reaches of Lamar Valley it is about 20 m thick. The most down-valley occurrences of these volcanic units studied herein are immediately above Lamar Canyon, a 3 km reach where the river is incised up to 200 m into Precambrian granitic gneiss and drops 100 m in elevation before flowing 8 km to the Yellowstone River confluence.

A wide range of surficial processes have modified the Lamar River drainage basin, where upper valleys have been heavily modified by Quaternary glaciation. Cirques, U-shaped valleys and moraines from valley glaciers are found in drainages that reach elevations of 3000 m, where glaciers likely existed during a substantial if unquantified portion of the Pleistocene. During peak glacial intervals, individual mountain glaciers coalesced into a large ice cap encompassing the entire Yellowstone caldera, volcanic plateau and adjacent mountain ranges and valleys (Pierce, 1979). The development of the ice cap is complicated and includes multiple phases as its own growth influenced local precipitation patterns (Licciardi and Pierce, 2008, 2018). The ice cap divide is interpreted to cross the Lamar Valley, running from the Beartooth Range in the northeast to the Yellowstone plateau in the southwest. At this time, ice may have flowed to the southeast over the basin's topographic divides. During the latest Pleistocene (0.0155 – 0.012 Ma), ice damming occurred when glaciers flowing south from the Beartooth Range blocked the Lamar Valley, and lacustrine deposits are present in the Lamar Valley (Pierce, 1974, 1979; Meyer et al., 1995). The modern valley floor is dominated by fluvial processes, but the river commonly interacts with glacial, lacustrine, and landslide deposits and bedrock. The river meanders where the valley is broad (>150 m wide) and has locally cut Holocene terraces into late-glacial outwash (Meyer et al., 1995). In other places, the river is restricted to narrow (50-100 m) valley floors where it has incised into bedrock or lacustrine deposits or where landslide, alluvial fan, or glacial deposits constrict the channel.

A quantitative assessment of the magnitude or relative importance of glacial and fluvial erosion at all parts of the basin was not done. Based on cross-section shapes of the

valleys, longitudinal profiles and cirque development, valley glaciers appear to be the dominant geomorphic agent in drainages with headwaters above 3000 m, but the down-valley extent of the valley glacier signal varies with the area and elevation range of the headwaters. As the Yellowstone ice cap forms, ice likely flows in different directions at different times, based on the changing location of the ice cap drainage divide. During peak glaciation, an ice divide of very low gradient is inferred to cross the middle of the Lamar River basin (Licciardi and Pierce, 2018), a condition that I infer would lead to limited basal sliding and erosion. Ultimately, the geomorphic importance of this large-scale glaciation is difficult to discern. The morphology of the middle and lower Lamar Valley does not appear to be dominantly either glacial or fluvial. The valley is widened, as is common in glacial valleys, but the valley floor is typically a flat floodplain and (or) fluvial terrace, or contains a small narrow canyon incised into the Osprey Basalt and lacustrine deposits. Longitudinal profiles for most streams are predominantly concave-up, with most of the convexities associated with the stream cutting through bedrock knickpoints or thick surficial deposits. Hanging valleys and glacially carved bedrock steps are largely restricted to headwater basins. The basins in this study are named for the streams they contain, and the use of the stream name to identify the basin does not imply that only the stream played a role in its formation or incision. I assume that glacial and fluvial processes have both played a significant role in shaping all of the major basins.

3. Methods

The extents of the two Quaternary volcanic units in the Lamar drainage basin were interpreted from USGS geologic maps (e.g. Prostka et al., 1975a, 1975b; Christiansen, 2001)

and GIS sources (catalog.data.gov). The maps were used to approximate the location and

elevation of six geomorphic or volcanic surfaces (Fig. 2), listed from youngest to oldest:

1. The modern river valley

2. The top of the Osprey Basalt flow (0.26 Ma)

3. The valley floor at the time of Osprey Basalt emplacement

4. The surface of the Lava Creek Tuff (0.63 Ma)

5. The valley floor at the time of Lava Creek Tuff emplacement

6. A set of benches on the valley side ~100-200 m above modern river (>> 0.63 Ma)

The modern valley profile was defined by measuring straight-line distances between

points where the river crossed contour lined on 7.5' USGS quadrangles. By excluding

meanders, this method creates a longitudinal profile comparable to the other valley floor

measurements. Distance along the valley was measured from the confluence of the Lamar

River and Yellowstone River.

Ground-truthing of the data was conducted by surveying many of the key localities

along the Lamar River, Cache Creek and Timothy Creek using GPS, map and compass, and a

tape measure and pocket transit. The Osprey Basalt is locally exposed along the river

channel and its thickness and elevation above the river were measured in the field. The

Lava Creek Tuff is mostly exposed on valley walls and the base of the unit is almost

universally covered with colluvium, talus, till, alluvium or lacustrine deposits. Many of the

contacts were verified by float mapping of colluvium, which was greatly aided by abundant

tree-throw. Air photos from Google Earth and ESRI.com were used to identify the extent of

bedrock ledges, cliffs and other exposures that could be traced laterally to confirm or adjust

some contacts. Most air-photo traceable exposures were sedimentary or volcanic strata in

the Eocene bedrock or cliffy edges of the Osprey Basalt flow.
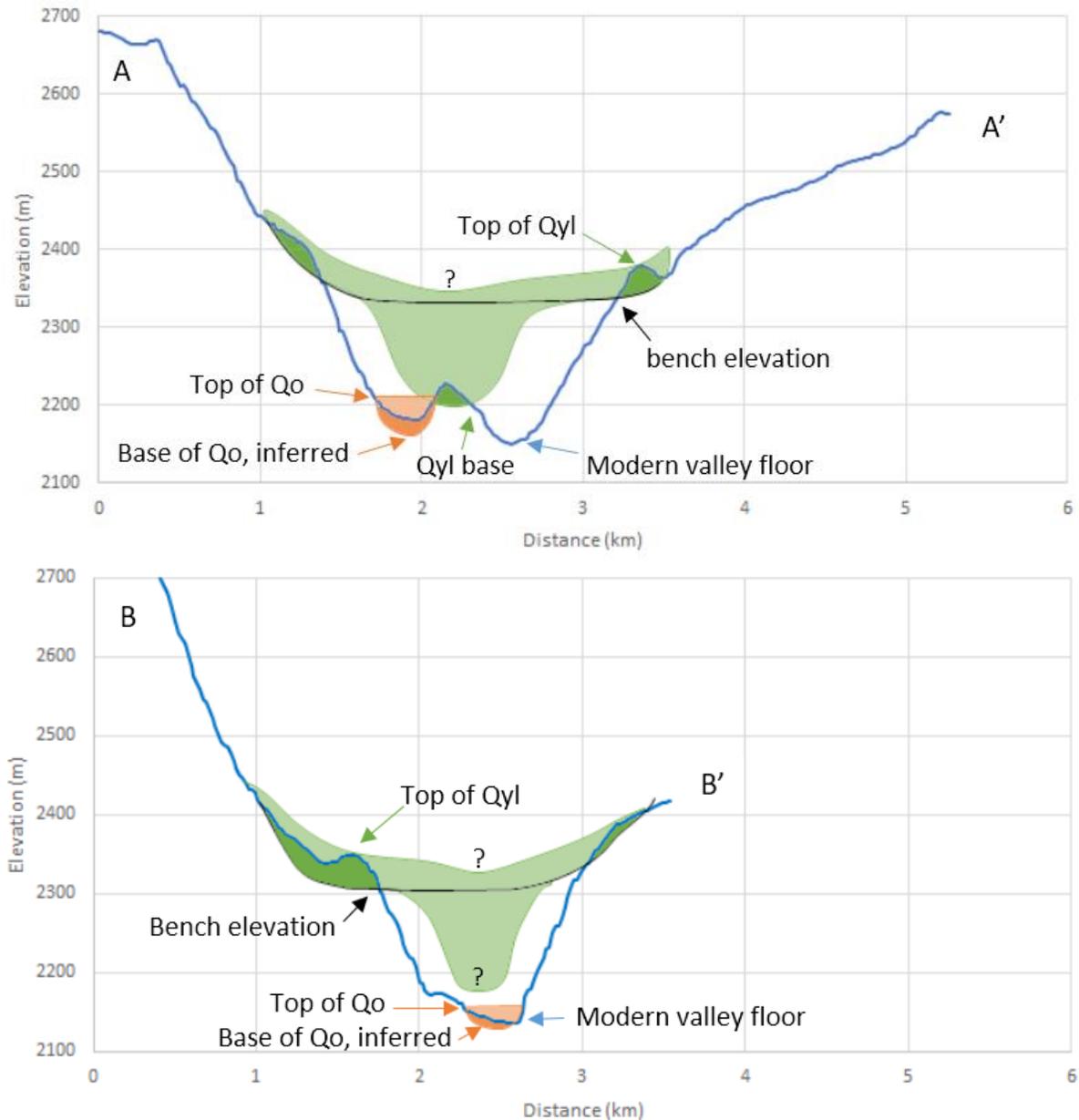
Figure 2. Cross-sections (located on Fig. 3) showing the 6 surfaces identified from geologic maps and in the field. Modern topography (blue line) with inferred extents of Lava Creek Tuff (Qyl, green) and Osprey Basalt (Qo, orange). Darker shades are remnants present today; lighter shades indicate inferred eroded areas of the two units. Inferred position of the high bench indicated by the black line. A: Cross-section just above the confluence of Timothy Creek (left, west valley) and Lamar Valley (right, east valley). Osprey Basalt is not shown in Lamar Valley because it is completely buried by lacustrine sediment or absent here. B: Lamar Valley cross-section about 2 km downstream (north) of A.
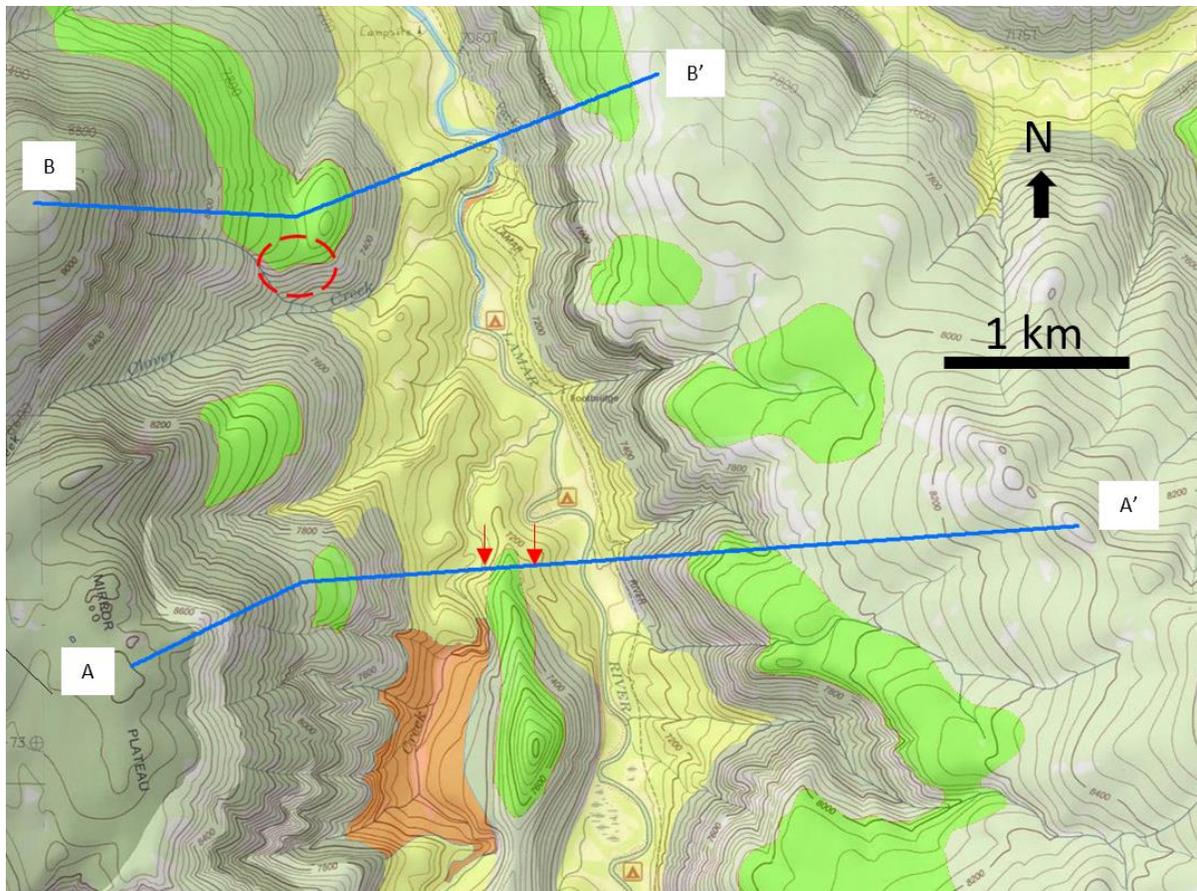
Figure 3. Geologic map (catalog.data.gov) overlay on USGS topographic quadrangles (40 ft contours). Position of cross-sections A and B (Fig. 2) are shown in blue. Geologic units mapped are Quaternary sediments (yellow), Osprey Basalt (orange), Lava Creek Tuff (green), and Eocene formations (various shades of gray). Timothy Creek (west) and Lamar River (east) meet near the center of the map and flow north. Red circle indicates one of the most definite locations of the high bench underlying the Lava Creek Tuff. Red arrows indicate modification to the USGS-mapped Lava Creek Tuff contact based on mapping in this study.

The geologic map and field data were combined in GIS, and elevations for surfaces 4 through 6 were measured where clearly exposed or were estimated from cross-valley profiles. Gullies cut into the Lava Creek remnants on the valley sides provided information as to the gradient of the underlying surface. Where Lava Creek Tuff was emplaced on low gradient surfaces (< 5 %), the surface was identified as belonging to either the pre-Lava Creek valley floor (Fig. 2A, Qyl base) or the high bench (Fig. 2). Along-valley profiles were

created by compiling the data and interpolating between points. A qualitative confidence level for each point was used to weight its importance in the final interpretation of the surfaces. The elevation of the modern river was subtracted from the profiles to provide a measure of incision along the profile and at different points in time.

In addition to identifying profiles, the mapped extents of the Quaternary volcanic units and faults were used to identify patterns in drainage network adjustment including reoccupation of former valleys, glacial avulsion and stream capture, and the development of inverted topography. Together these observations were used to identify the importance of volcanic, tectonic, and lithologic controls on the stream network and its incision.

4. Results

Field mapping confirmed that the published geologic maps were accurate enough to estimate contacts in the desired positions to within a few meters, roughly matching the accuracy of a GPS or topographic map (40 ft contours) in most places. Contacts were adjusted at a few locations, typically at contacts with surficial sediments (Fig 2, red arrows) or where the Osprey Basalt was mapped too far up the valley side. Profiles of the 6 surfaces are drawn from the confluence of the Lamar and Yellowstone Rivers, and for each profile, a plot showing difference in elevation between the modern river and each surface is presented (Fig. 4-9).
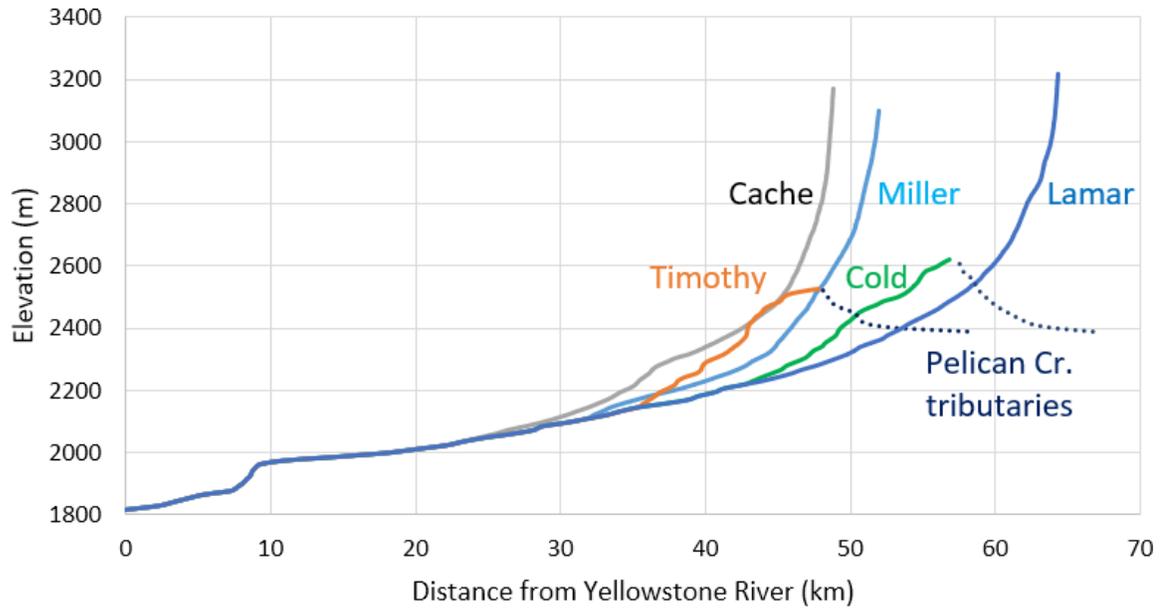
Figure 4. Longitudinal profiles of the five tributaries. Cache Creek, Miller Creek and Lamar River are plotted along their largest stream to the divide. Timothy Creek and Cold Creek are plotted to the divide at the head of their valleys and then tributaries of Pelican Creek are tracked down into the Yellowstone caldera.
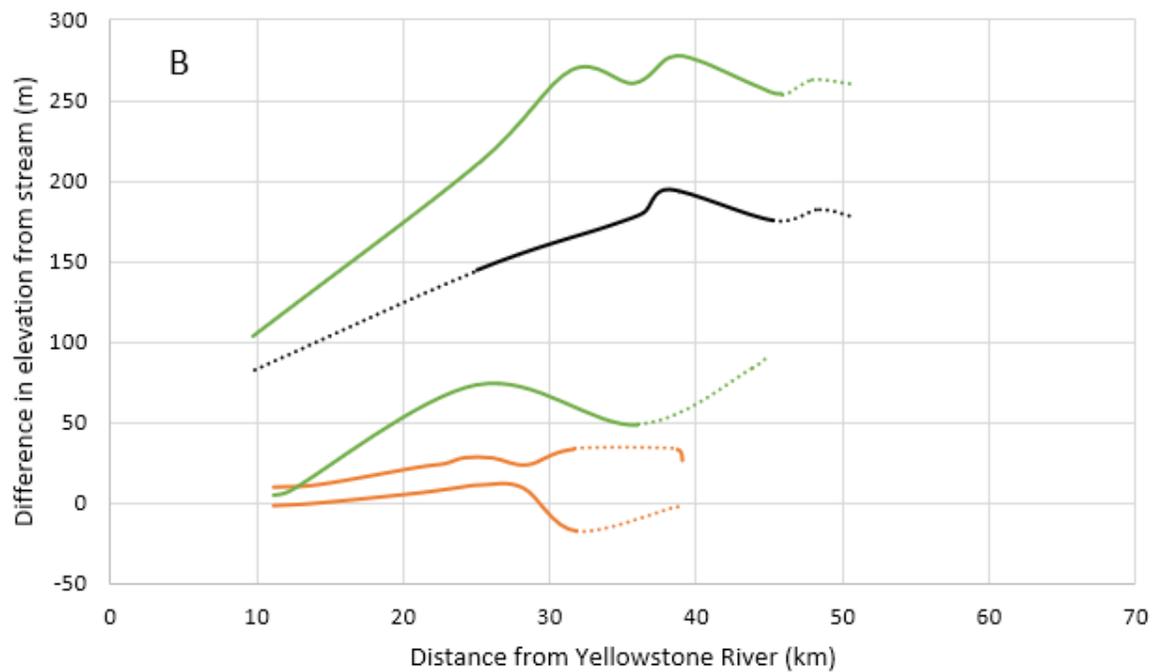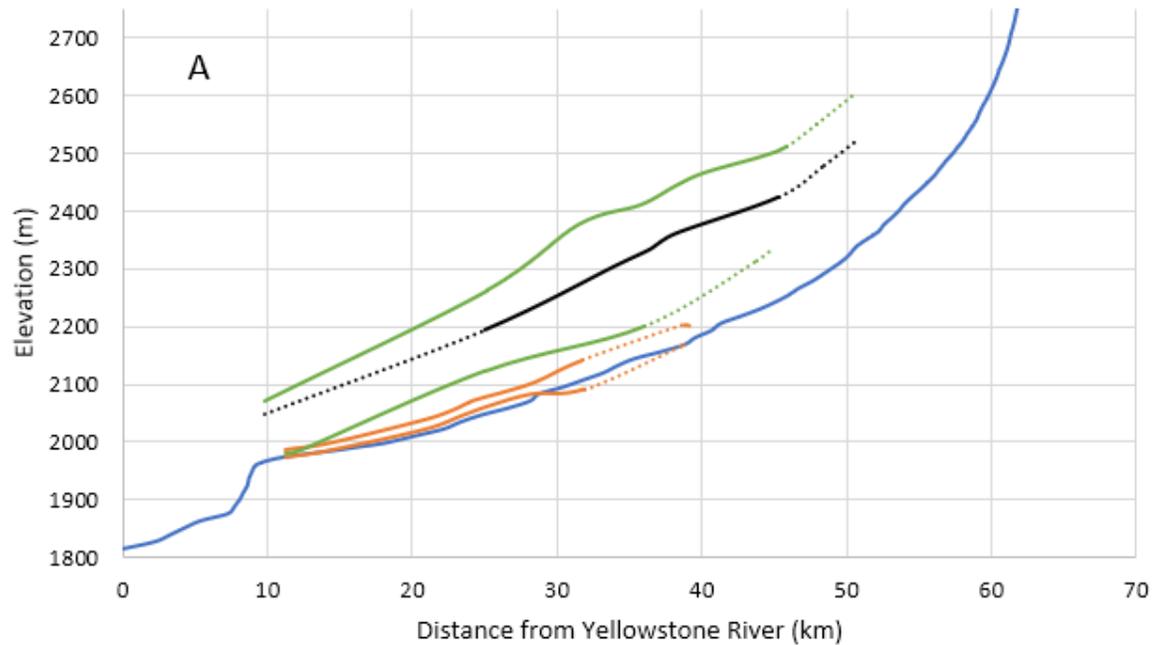
Figure 5. A: Longitudinal profiles for Lamar River (blue), top and bottom of Osprey Basalt (orange), top and bottom of Lava Creek Tuff (green), and high bench (black).
B: Difference in profile elevation and modern river elevation indicating the relative degree of incision since each surface was an active valley floor. Colors same as A.
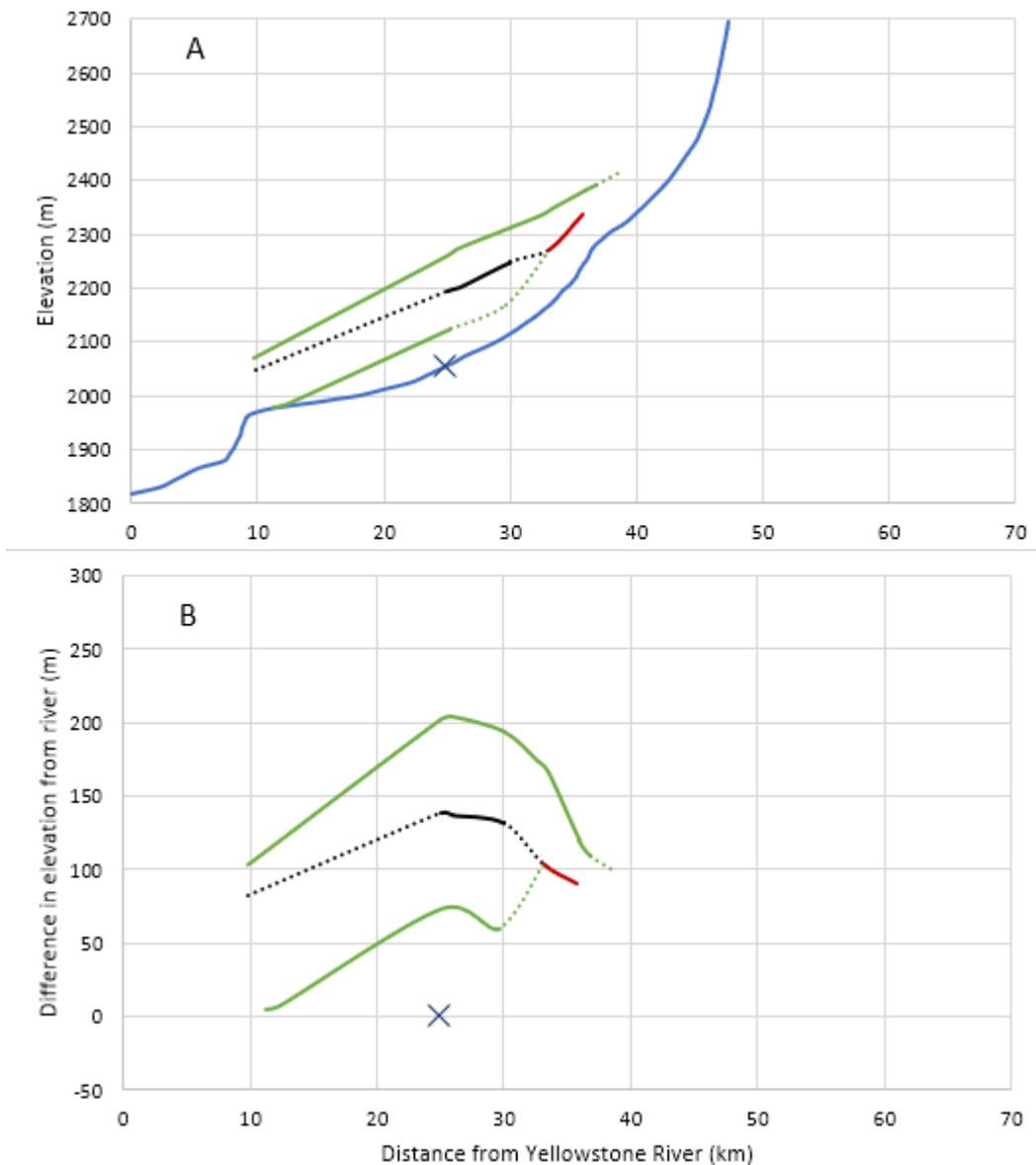
Figure 6. A: Longitudinal profiles for Cache Creek (blue), top and bottom of Lava Creek Tuff (green), and high bench (black), red line is either the lower Lava Creek Tuff or the high bench. Blue X indicates confluence with Lamar River; profiles below that point are the same as the Lamar River.

B: Difference in profile elevation and modern river elevation, indicating the relative degree of incision since each surface was an active valley floor. Colors same as A.
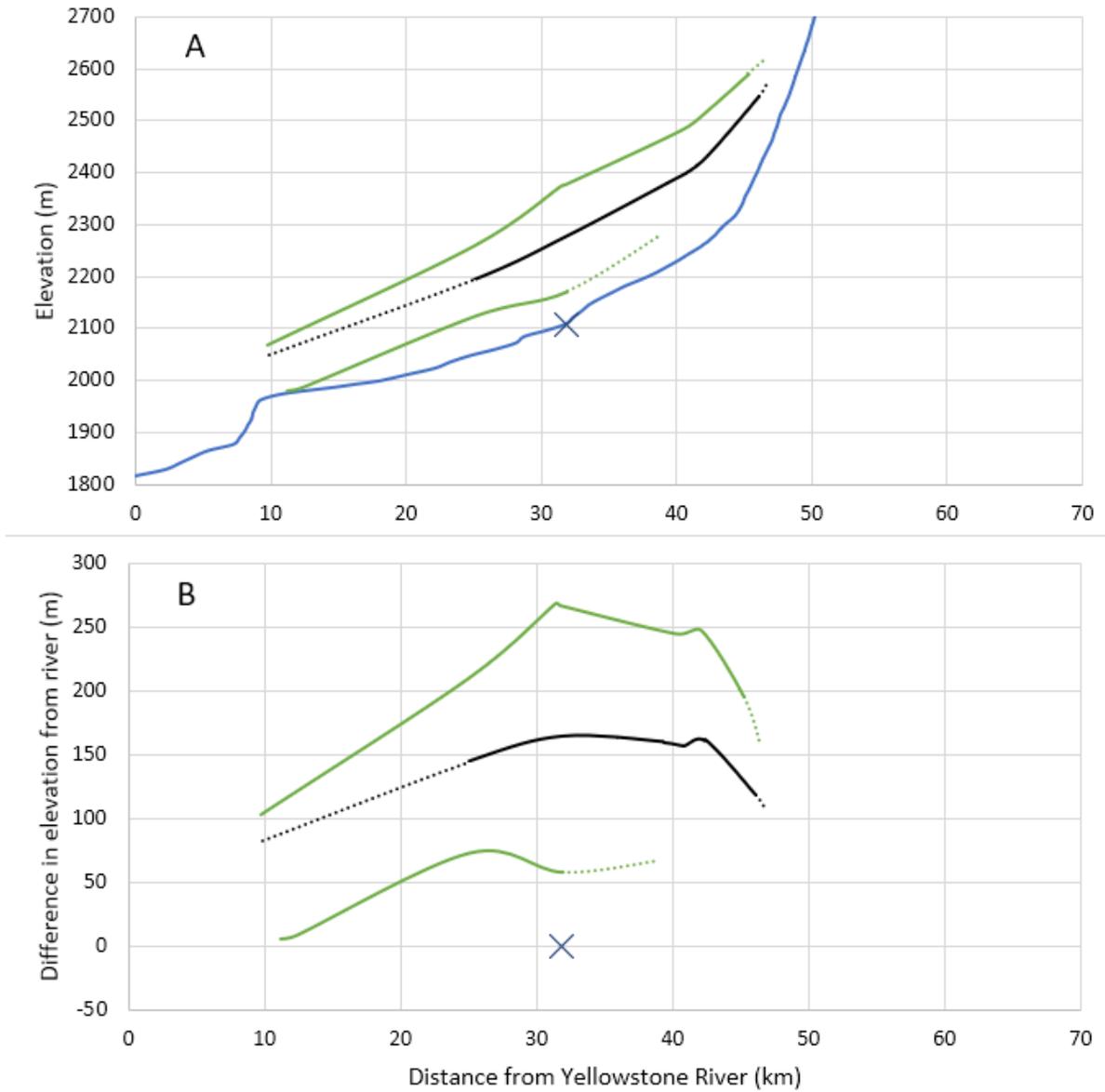
Figure 7. A: Longitudinal profiles for Miller Creek (blue), top and bottom of Lava Creek Tuff (green), and high bench (black). Blue X indicates confluence with Lamar River; profiles below that point are the same as the Lamar River.

B: Difference in profile elevation and modern river elevation, indicating the relative degree of incision since each surface was an active valley floor. Colors same as A.
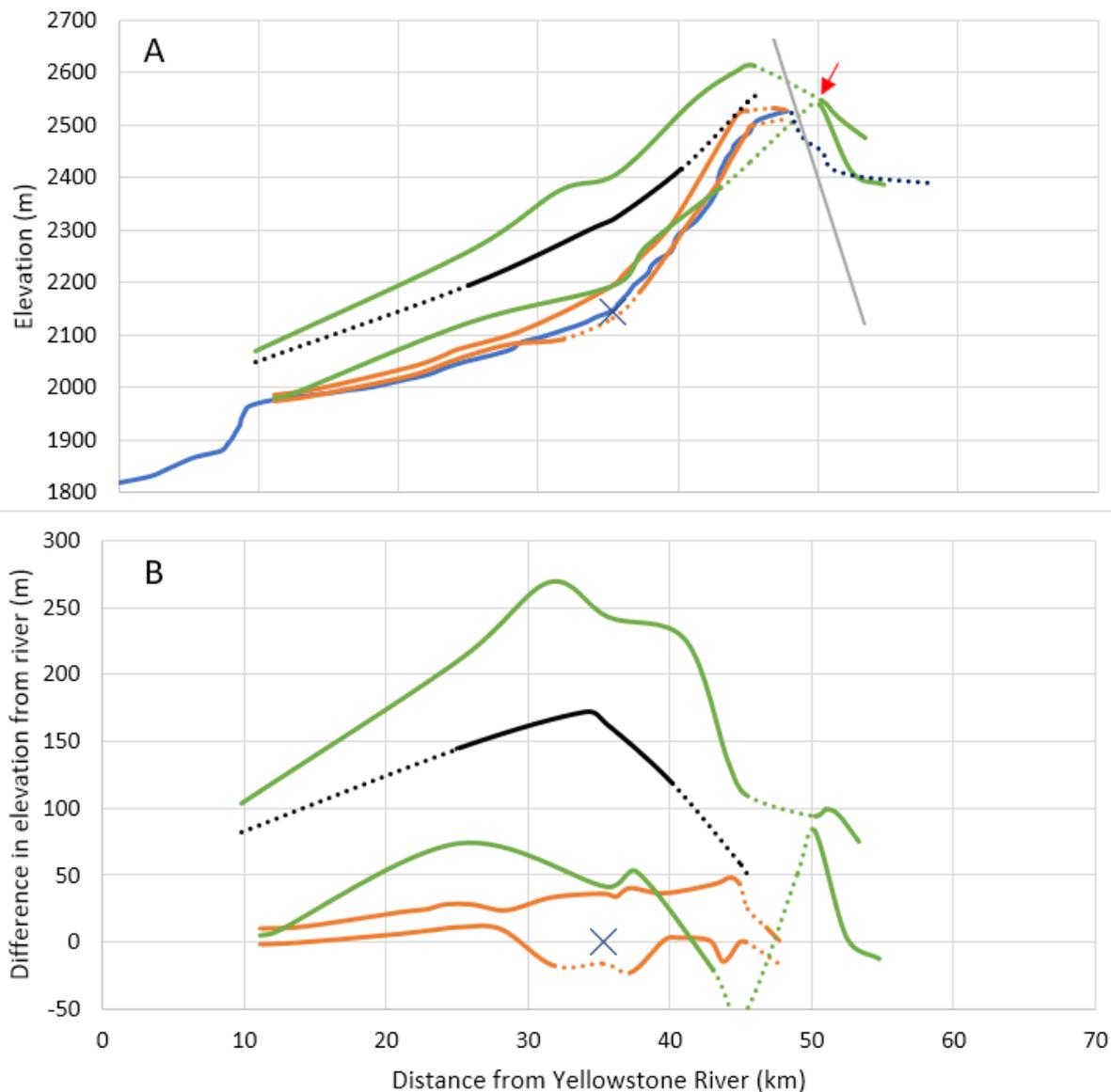
Figure 8. A: Longitudinal profiles for Timothy Creek (blue), top and bottom of Osprey Basalt (orange), top and bottom of Lava Creek Tuff (green), and high bench (black). Blue X indicates confluence with Lamar River; profiles below that point are the same as per the Lamar River. Gray line is a fault. Dark blue dotted line is a tributary of Pelican Creek. Red arrow indicates the location of a gap in the inferred former drainage divide that facilitated stream capture of the headwaters of Timothy Creek to Pelican Creek after the caldera collapsed.
B: Difference in profile elevation and modern river elevation, indicating the relative degree of incision since each surface was an active valley floor. Colors same as A.
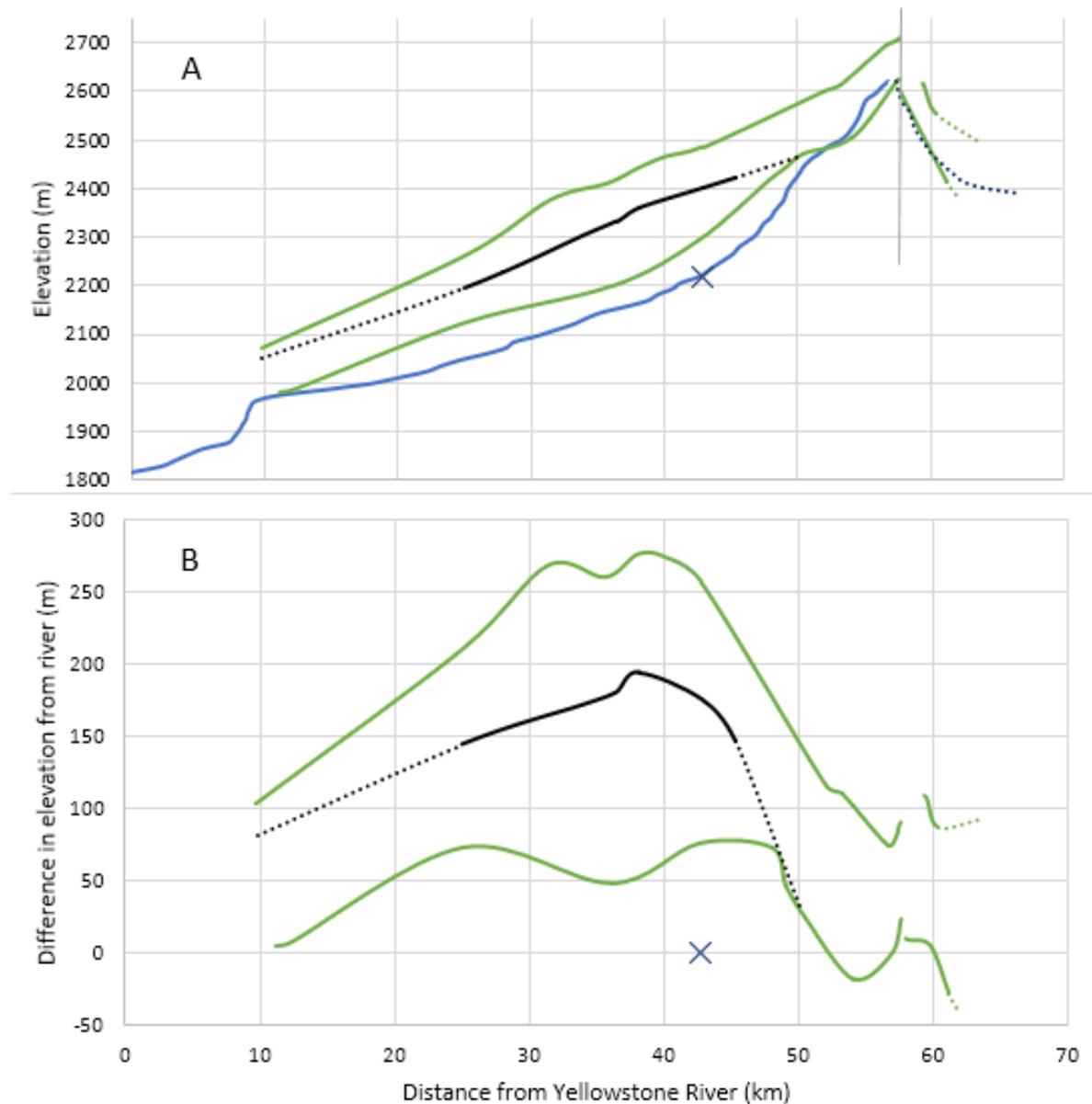
Figure 9. A: Longitudinal profiles for Cold Creek (blue), top and bottom of Lava Creek Tuff (green), high bench (black). Blue X indicates confluence with Lamar River; profiles below that point are the same as per the Lamar River. Gray line is a fault. Dark blue dotted line is a tributary of Pelican Creek.

B: Difference in profile elevation and modern river elevation, indicating the relative degree of incision since each surface was an active valley floor. Colors same as A.

The longitudinal river profiles of the rivers that drain high peaks away from the caldera (Lamar R., Cache and Miller Creeks) are strongly concave-up with only a few convex knickpoints, the largest of which is in Cache Creek near a major stream junction (Fig. 6, ~36 km). The profiles of Timothy Creek and Cold Creek (Figs. 8, 9) each contain several major knickpoints and are overall fairly straight (not dominantly concave or convex), but would be concave-up if drawn to high peaks off to the sides of the valley instead of over the saddle at the head of each valley.

The Lava Creek Tuff was thickest 30 to 40 km above the Yellowstone River confluence, which is where the main valley is closest to the caldera. Cache Creek, farthest from the caldera, had the thinnest Lava Creek Tuff. All of the Lamar River tributaries that are away from the caldera have eroded through the total thickness of Lava Creek Tuff along their headwaters reaches and have reduced outcrops of the unit to isolated remnants high on the valley sides. This lack of preservation limits the accuracy with which the pre-Lava Creek Tuff valley floor can be identified. On the caldera side of the basin, ~100 m of Lava Creek Tuff was emplaced near the caldera rim, and 100+ m thick units remain in some valleys and on broad ridges.

The Osprey Basalt is thickest in Timothy Creek and Lamar Valley near the junction with Timothy Creek and thins down valley. Timothy Creek and the Lamar River cut completely through the Osprey Basalt in some places, but in others they have not. There is an outcrop of basalt up-valley from the confluence of Timothy Creek and the Lamar River, which is higher in elevation than the Osprey Basalt mapped at the junction. The origin of

this basalt is unclear and thick lacustrine deposits in this area make direct correlation in the field impossible.

The bases of both Quaternary volcanic units grade to the modern river level just above Lamar Canyon. There has been practically no net incision, with the river flowing directly on Osprey Basalt, and with Lava Creek Tuff exposed down to within a few meters of the river level. Higher in the drainage basin, net incision calculated from the time just before the Lava Creek eruption (base of Qyl) to present ranges between 0.08 mm/yr to 0.15 mm/yr. Net incision from the base of the Osprey Basalt flow is even lower. In many reaches, the Lamar River and Timothy Creek have not cut all the way through the basalt, and the greatest net incision rate for both streams through the base of the Osprey Basalt is < 0.02 mm/yr. Timothy and Cold Creeks have very low net incision in their headwaters and have not incised through the Quaternary volcanics along their entire lengths, as the headwater reaches of the other valleys have.

Total incision includes the thickness of all units incised through, and is by convention always greater than net incision. Total incision has been greatest in the 30-40 km reach where the Lamar River and Miller Creek have incised through ~250 m of Yellowstone volcanic material and another 50 m of Eocene bedrock. If this estimate is correct, it corresponds to incision rates ~0.5 mm/yr. There are two major sources of uncertainty associated with the assignment of the top of the Lava Creek Tuff: (1) The value assigned was typically the elevation of the top of the unit resting on the high bench, but the tuff may not have filled the inner valley to this elevation and compaction of the tuff during welding would have been greatest near the center of the filled valley (fig. 2, question mark on upper

Qyl surface) where the tuff was thickest (Griggs, 1922; Curtis, 1969). An effort was made to account for the slope of the tuff on top of the bench, but there is considerable error in this estimate, likely in the range of a few tens of meters. (2) The degree of welding of the tuff at the top of the unit is unknown and it may be inappropriate to compare the erosion of the upper tuff to incision of bedrock. Even if only using half the thickness of tuff, incision rates would be > 0.3 mm/yr, toward the high end of values reported on other nearby rivers (Dethier, 2001; Hancock et al., 1999; Pierce and Morgan, 1992, 2009; Reheis et al., 1991). Incision through the Osprey Basalt has occurred at a slower pace, up to 0.15 mm/yr for much of the Lamar River and Timothy Creek length, which is more similar to other river incision rates around the YCHT.

5. Discussion

The high bench is present in all of the tributaries and most commonly manifests as a series of Lava Creek Tuff remnants lining the valley sides. It cuts across stratigraphy of the Eocene bedrock and is not lithologically controlled. This surface is present on both sides of most tributaries and in places clearly resembles a flat valley floor. Its morphology is similar to that of a terrace, but insufficient data was found to confirm the process that produced it. However, given its high position on the valley walls it represents a surface much older than the Lava Creek Tuff. Being considerably broader than the modern valley and the valley that existed just before the Lava Creek Tuff was emplaced, it seems likely that it was produced under significantly different climatic, tectonic or base-level conditions. It typically sits 2 to 3 times higher than the Lava Creek valley bottom, which would suggest an age of 1 to 2 million years old using linear extrapolation. This places the surface age before the mid-

Pleistocene transition (Pisias and Moore, 1981; Clark et al., 2006; Hönisch et al., 2009) and

possibly as old as the start of the Quaternary. In the adjacent Jones Creek drainage, south

of the upper Lamar River basin, a similar bench is preserved more clearly and the 2.1 Ma

Huckleberry Ridge Tuff (Lanphere, 2002) is mapped on it (Prostka et al., 1975a). Lava Creek

Tuff is not found extensively in Jones Creek, so the preservation of this older unit is possible,

however some isolated outcrops of Lava Creek Tuff have been mis-identified as Huckleberry

Ridge in the past (Wilson et al., 2018). The Jones Creek bench is up to 600 m above the

valley floor. This difference may simply be a result in different base level controls, or it

might indicate that these are not coeval geomorphic surfaces. If these surfaces represent

similar processes and environments, then the Lamar Valley bench could predate the

Quaternary period and represent an unglaciated landscape. That could account for a

difference in form from the modern valley and it might be similar to other low-relief pre-

Quaternary surfaces observed in the Absaroka Mountains, e.g. Hurricane Mesa just east of

the Lamar River basin, but those are typically upland surfaces or summit plateaus (Pierce

and Morgan, 2009). More likely, the surface age is 1 – 2 Ma and represents a valley floor

formed before the mid-Pleistocene transition, when glacial-interglacial cycles had a shorter

period and peak global ice volumes were smaller (Pisias and Moore, 1981, Hönisch et al.,

2009). Assuming that the magnitude of glaciation in the Lamar drainage basin can be

broadly correlated to global CO_2, temperature and ice volume, then the extent of glaciation

in the valleys would have been smaller during the first half of the Quaternary and possibly

restricted to areas above where the high bench is preserved. In this case, the high bench

may represent a glacial outwash terrace that has been incised into as glacial cycles increased in magnitude and the deeper modern valley was carved.

Each tributary of the Lamar River studied here has had a unique response to the infilling of its valley floor, disruption of its stream network due to volcanic and tectonic factors, and variations in bedrock erodibility. Above the Lamar Canyon knickpoint, the main stem of the Lamar River has incised no more than a few meters below the base of the Lava Creek Tuff at < 0.01 mm/yr. The total incision rate is < 0.2 mm/yr, even with the assumption that the valley was filled as high as the remnants on the valley sides (Fig. 5). This relatively low incision can be attributed to two main factors: (1) Below this point the river runs through a highly resistant bedrock knickpoint composed of relatively little jointed Archean granitic gneiss, which acts as a local base level control, limiting further incision. The river gradient increases by an order of magnitude as is cuts through the canyon, which indicates the relative resistance to erosion between the gneiss and the younger rocks. (2) The Lamar fault runs along the southwest edge of the valley and crosses the river in Lamar Canyon. Total offset of Eocene and older rocks has been interpreted as 400 m (Brown, 1961), but the Lava Creek Tuff appears to only be offset by < 30 m, based on the relative position of a pair of benches that the fault cuts through. There are however several benches on the slope and the relationship cannot be directly verified due to sedimentary cover between them. Where the fault cuts the Precambrian gneiss, there is a slope on the up-thrown block that may be a fault scarp with ~30 m relief. Across the river, there continues to be apparent topographic offset, but of only 10-15 m.   Adding 30 m of total

incision raises the total incision value only modestly, indicating that the erodibility of the gneiss is likely the strongest control on the persistence of the river at that level.

The Lamar River has only cut through the entire Osprey Basalt at 15-30 km above the Yellowstone River confluence (Figs. 5B, 10), where the flow is thin and well upstream of the base level control of the Lamar Canyon gneiss. This section of the profile exhibits the greatest net incision, which could be explained by relatively less volcanic emplacement, but both the lower Osprey and lower Lava Creek profiles appear slightly bowed upward as well (Fig. 5). This section is in line with the axis that runs between the two resurgent domes in the caldera (Fig. 1) that has been associated with cyclic Holocene and modern uplift and subsidence (Locke and Meyer, 1994; Pierce et al., 2007; Dzurisin et al., 2012). The section is also adjacent to the Mirror Plateau, shown to have anomalously low seismic velocity (Farrell et al., 2014), which could indicate relatively buoyant crust. These two factors may help promote uplift, incision, and isostatic rise of the old profiles, however the length scale (~10 km) is fairly short for crustal deformation.

Between 30 and 40 km from the confluence with the Yellowstone River, the thickness of the Lava Creek Tuff and Osprey Basalt increases. This section is where total incision is greatest, and the predicted slope of the top of the Lava Creek Tuff is also steeper (Fig. 5). This condition likely created a negative feedback where the greater accumulation of the tuff led to higher valley gradients, driving faster erosion rates and a more rapid reduction in the elevation of the volcanic material than in neighboring areas.
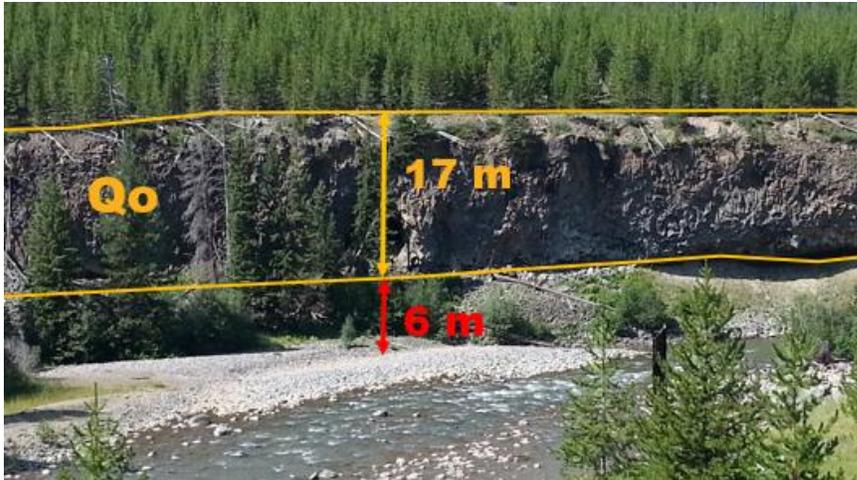
Figure 10. Location where the Lamar River has incised through the Osprey Basalt, located ~21 km upstream from the confluence with the Yellowstone River.

Streams and glaciers on the east side of the Lamar drainage basin have for the most part reoccupied their same valleys after the emplacement of the Lava Creek Tuff. This likely occurred because the upper valleys received relatively less material and drainage would have been funneled back into the same main channel areas. Due to this reoccupation of the former valley, there are very few remnants that can be considered to overlie the valley floor that existed just before Lava Creek Tuff emplacement, adding uncertainty to estimates of its position. In Cache Creek, lack of preservation leads to uncertainty as to whether the well-defined shelf (Fig. 6, red line) represents the base of the Lava Creek-age valley, or if it represents a continuation of the high bench. There is a knickpoint just upstream from this location and just above a junction with a major tributary. The knickpoint appears to be associated with a resistant bedrock ledge in the Eocene sedimentary. Interpolating the base of the Lava Creek valley up to the bench (red line) in Fig. 6 creates a profile with a knickpoint similar to the modern profile and would indicate a headward migration of that knickpoint. The sideslopes of the Cache Creek valley are relatively steep and it is likely that the high shelf has been eroded away here. Alternatively, the knickpoint could be produced by enhanced incision by glaciers from the tributary and would not have migrated from

downstream, but the main stem tributary has 3.5 times the drainage area of the side tributary, so this seems unlikely.

Timothy and Cold Creeks were directly impacted by the caldera collapse and have a resulting geomorphic history that is drastically different than the basins draining mountains away from the rim. I interpret that both drainages had part of their headwaters faulted down into and toward the caldera as a result of the Lava Creek eruption and collapse. The morphology of the ridges and basins below Pelican Cone (circled on Fig. 11) appears to be aligned with the Timothy Creek drainage to the northeast. A series of caldera rim-parallel fractures separates the Pelican Cone ridge (purple line) from the modern drainage divide (red line). I propose that during or after the emplacement of the Lava Creek Tuff member B, Pelican Cone was down-dropped towards the west. As a result of faulting and variations in tuff emplacement thickness, a low gap in the Pelican Cone ridge (Figs. 8, 11, red arrow) became the lowest point in the headwaters region and a narrow canyon has been incised at that place. Today, Raven Creek drains the east side of Pelican Cone through this gap to Pelican Creek in the west.

Just north of Timothy Creek is a broad valley with no stream that may have been the precaldera Timothy Creek valley. The morphology of the upper Timothy Creek valley doesn't fit well with any standard model of fluvial or valley glacier erosion. Based on topography and air photos, the upper basin (labeled "Buffalo" on Fig. 10) most closely resembles an alluvial plain on a flat lava flow. The relationship between that flow and the long steep slopes mapped as Osprey Basalt is unclear, however. The area is remote and difficult to access, and was not observed in the field.
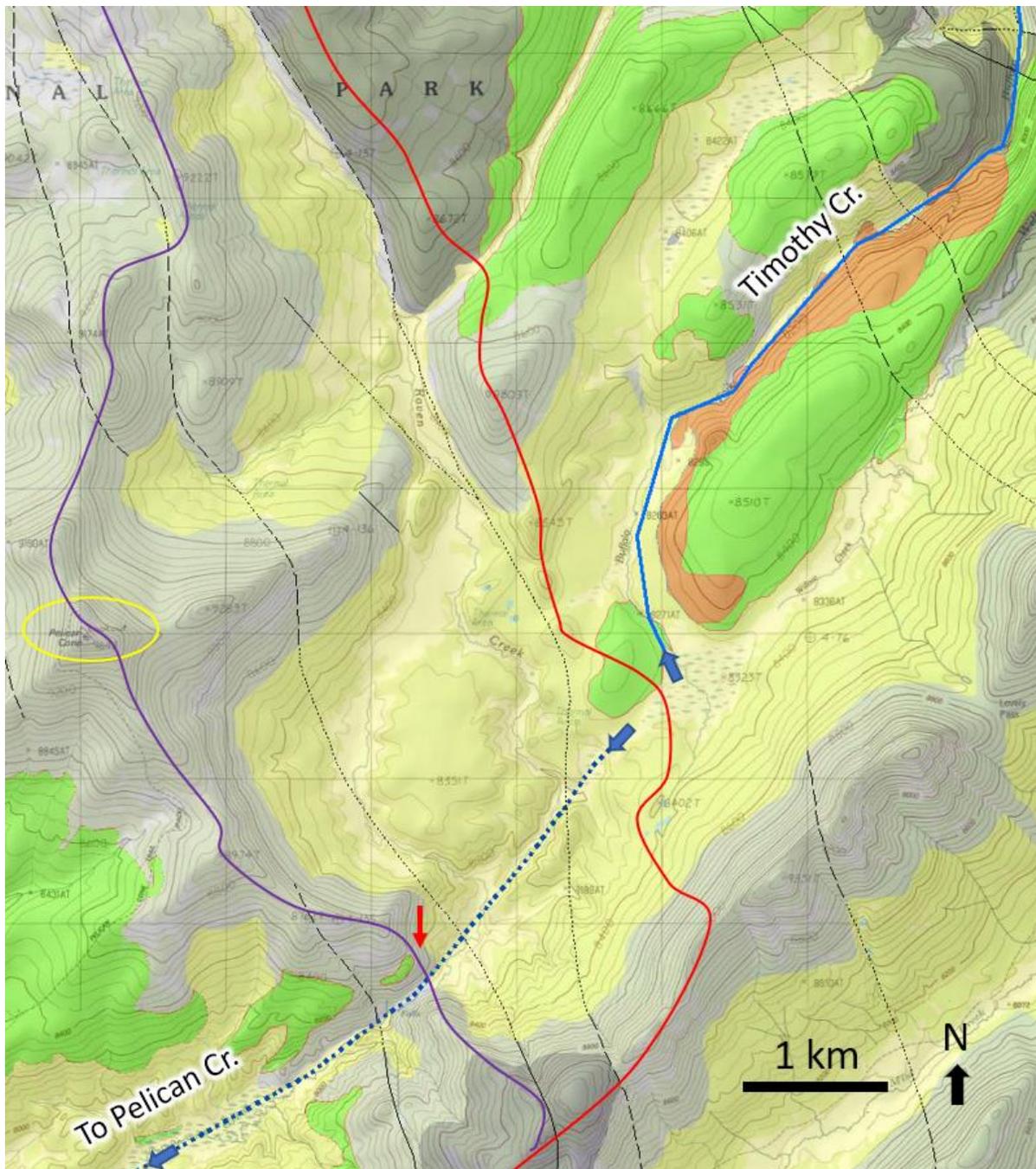
Figure 11. Geologic map overlay (catalog.data.gov) on USGS topographic quadrangles (40 ft contours). Geologic units mapped are: Quaternary sediments (yellow), Osprey Basalt (orange), Lava Creek Tuff (green), Eocene formations (various shades of gray). Timothy Creek (solid blue) flows to the north, Raven Creek (dotted dark blue line) flows southwest to Pelican Creek in the caldera; blue arrows show flow direction in creeks. Red line is modern drainage divide, purple line is the Pelican Cone ridge, which I infer to be the former drainage divide for Timothy Creek. Red arrow is the inferred stream capture point. North is at the top of the page and 1-km UTM gridlines are shown for scale.

Like Timothy Creek, Cold Creek is inferred to have lost some of its headwaters to caldera faulting and stream capture. The Lava Creek Tuff has filled the former Cold Creek valley (Fig. 12). Where Cold Creek approaches the modern drainage divide (Fig. 12, red line), the Lava Creek Tuff continues up the hillside on the other side of the divide, likely following the path of a valley now captured by Pelican Creek to the northwest. The loss of headwaters has left Cold Creek unable to cut through the Lava Creek Tuff, and instead, Cold Creek and a tributary of Mist Creek to the north are incising around the tuff. This has left the center of the old valley as a high ridge of Lava Creek Tuff, an example of inverted topography. Similarly, valley glaciers that formed in the small cirques at the modern valley head appear to have carved a glacial trough across the former valley instead of along it. Farther to the east, a tributary of Cold Creek with higher headwaters has more effectively incised through the Lava Creek Tuff (Fig. 12). Long, broad ridges of Lava Creek Tuff in the Timothy Creek area may also be inverted topography. As a result of limited drainage area, Timothy and Cold Creek have not cut through the Quaternary volcanics and have not reestablished a classic concave-up long profile associated with streams in or approaching equilibrium (Langbein and Leopold, 1964).
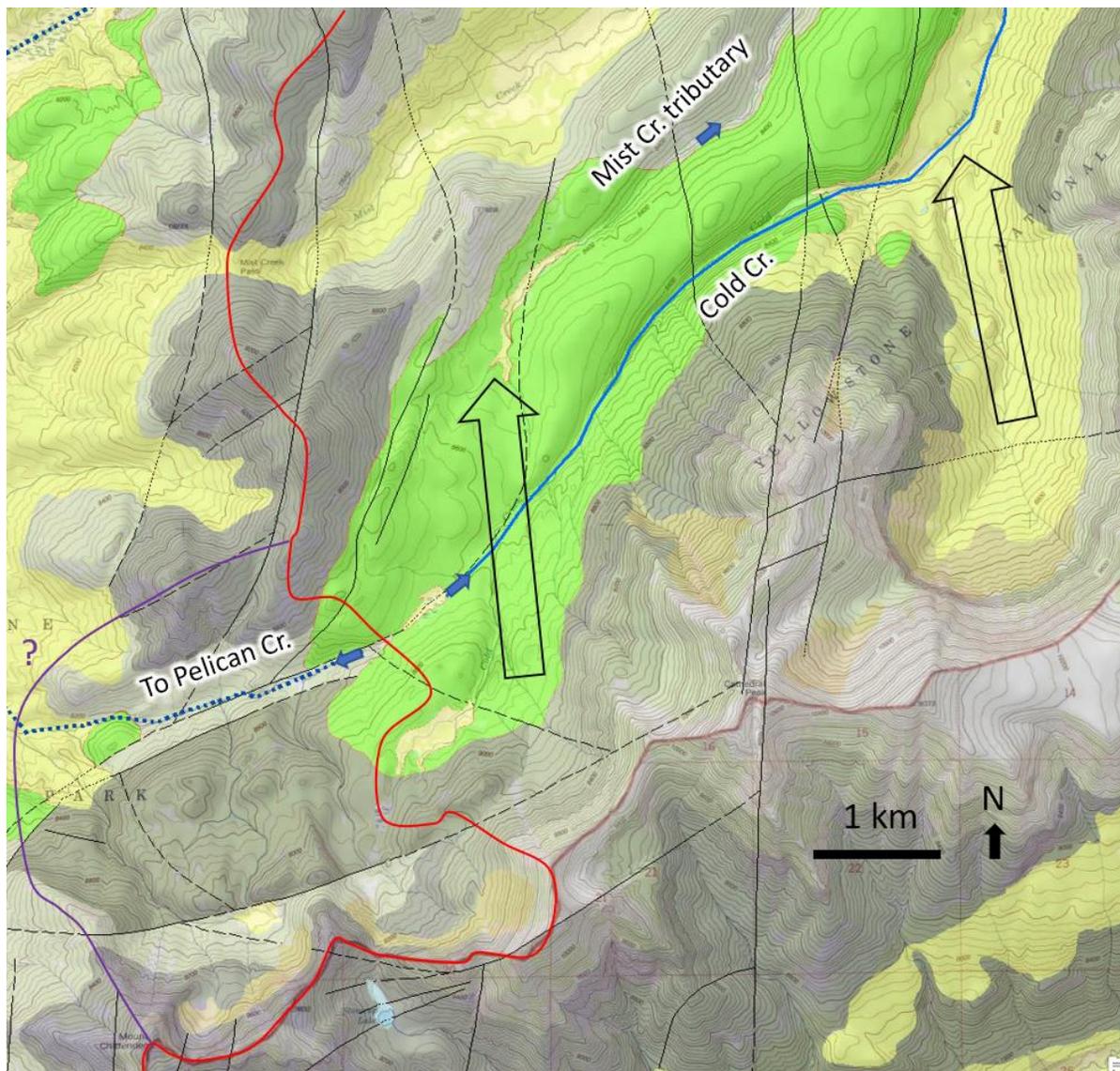
Figure 12. Geologic map (catalog.data.gov) overlay on USGS topographic quadrangles (40 ft contours). Geologic units mapped are: Quaternary sediments (yellow), Osprey Basalt (orange), Lava Creek Tuff (green), Eocene formations (various shades of gray). Cold Creek (solid blue) flows to the northeast, and a tributary of Pelican Creek (dotted dark blue line) drains into the caldera; blue arrows indicate flow direction in streams. Red line is modern drainage divide, purple line is the inferred pre-caldera drainage divide; full extent of the former Cold Creek drainage basin is unknown. Black outlined arrows indicate inferred valley glacier trenches.

6. Conclusions

Bedrock lithology appears to play the greatest role in controlling the longitudinal profiles of the Lamar River and its tributaries, with caldera-related faulting and stream capture playing a major role in a few streams. Thickness of the emplaced Lava Creek Tuff appears to play a relatively minor role in influencing net incision in large drainages, since total incision rates increase where thicker units were emplaced. I infer that incision is enhanced below where the thickest degree of infilling occurred due to steeper valley gradients. This creates a feedback that drives the system back towards its original condition and supports the concept of quasi-equilibrium conditions on rivers, even under heavy disturbance from volcanic and glacial processes. The strength of this conclusion depends on the error for the elevation of the top of the Lava Creek Tuff in the middle of the valley, which is one of the least constrained values in this study. Additional field work is needed to identify the sedimentary character of the high bench and to determine its age and formation process. This information would provide valuable insight into surficial processes and incision rates during a time period for which most of the local physical record has been eroded.

The lowest incision rates are at the top of the Lamar Canyon where relatively thin Lava Creek and Osprey units remain little incised. The slow net incision (< 0.01 mm/yr) is a result of the ~3 km knickpoint through highly resistant granitic gneiss. The Lamar fault may be reducing incision rates by forcing the river to cut through an additional 30 m of uplifted rock since the emplacement of the Lava Creek Tuff, but even this keeps total incision rates to a maximum value of 0.19 mm/yr.

Net incision is greatest where the river passes near the shallow low seismic velocity zone under the Mirror Plateau, which also corresponds to the axis of the Yellowstone caldera resurgent domes that have been shown to inflate and deflate over timescales ranging from a few decades to millennia (Locke and Meyer, 1994; Pierce et al., 2007; Dzurisin et al., 2012). However, direct evidence for long-term uplift outside the caldera is limited, and the high net incision at 20-30 km above the Yellowstone River confluence (Fig. 5) may simply be a result of the Quaternary units being relatively thin in that reach.

Streams and glaciers in basins that maintained essentially constant contributing areas have reoccupied their valleys and adjusted to the emplacement of the tuff relatively quickly. They have incised through the tuff and into the older Eocene volcaniclastic and sedimentary rock. Where the headwaters of basins were captured by the caldera, the resulting streams are underfit, and are diverted to narrow side canyons, abandoning former valley floors. Down-dropping of headwater regions also reduced accumulation area for valley glaciers, and glacial erosion at the heads of Timothy and Cold Creeks is less pronounced than in adjacent valleys like the eastern tributary of Cold Creek (Fig. 12). In some cases, the former valleys are left as high mesas or ridges capped by thick ash-flow tuff units. These drastic differences in response to disturbance between adjacent basins illustrate the importance of detailed drainage basin studies like this one.

7. References

Abedini, A., Meng, F., & Raleigh, D. P. (2007). A single-point mutation converts the highly amyloidogenic human islet amyloid polypeptide into a potent fibrillization inhibitor. *Journal of the American Chemical Society*, *129*(37), 11300-11301.

Brown, C. W. (1961). Cenozoic stratigraphy and structural geology, northeast Yellowstone National Park, Wyoming and Montana. *Geological Society of America Bulletin*, *72*(8), 1173-1193.

Christiansen, R. L. (2001). *The Quaternary and Pliocene Yellowstone Plateau volcanic field of Wyoming, Idaho, and Montana* (No. 729-G).

Clark, P. U., Archer, D., Pollard, D., Blum, J. D., Rial, J. A., Brovkin, V., ... & Roy, M. (2006). The middle Pleistocene transition: characteristics, mechanisms, and implications for long-term changes in atmospheric pCO2. *Quaternary Science Reviews*, *25*(23-24), 3150-3184.

Curtis, G. H. (1968). The stratigraphy of the ejecta from the 1912 eruption of Mount Katmai and Novarupta, Alaska. *Studies in Volcanology: Geological Society of America Memoir*, *116*, 153-210.

Dethier, D. P. (2001). Pleistocene incision rates in the western United States calibrated using Lava Creek B tephra. *Geology*, *29*(9), 783-786.

Dzurisin, D., Wicks, C. W., & Poland, M. P. (2012). *History of surface displacements at the Yellowstone Caldera, Wyoming, from leveling surveys and InSAR observations, 1923-2008* (No. 1788). US Geological Survey.

Farrell, J., Smith, R. B., Husen, S., & Diehl, T. (2014). Tomography from 26 years of seismicity revealing that the spatial extent of the Yellowstone crustal magma reservoir extends well beyond the Yellowstone caldera. *Geophysical Research Letters*, *41*(9), 3068-3073.

Gran, K. B., & Montgomery, D. R. (2005). Spatial and temporal patterns in fluvial recovery following volcanic eruptions: Channel response to basin-wide sediment loading at Mount Pinatubo, Philippines. GSA Bulletin, 117(1-2), 195-211.

Griggs, R. F. (1922). *The valley of ten thousand smokes*. National geographic society.

Hancock, G. S., Anderson, R. S., Chadwick, O. A., & Finkel, R. C. (1999). Dating fluvial terraces with [10]Be and [26]Al profiles: Application to the Wind River, Wyoming. Geomorphology, 27(1-2), 41-60.

Hönisch, B., Hemming, N. G., Archer, D., Siddall, M., & McManus, J. F. (2009). Atmospheric carbon dioxide concentration across the mid-Pleistocene transition. *Science*, *324*(5934), 1551-1554.

Langbein, W. B., & Leopold, L. B. (1964). Quasi-equilibrium states in channel morphology. *American Journal of Science*, *262*(6), 782-794.

Lanphere, M. A., Champion, D. E., Christiansen, R. L., Izett, G. A., & Obradovich, J. D. (2002). Revised ages for tuffs of the Yellowstone Plateau volcanic field: Assignment of the Huckleberry Ridge Tuff to a new geomagnetic polarity event. *Geological Society of America Bulletin*, *114*(5), 559-568.

Licciardi, J. M., & Pierce, K. L. (2018). History and dynamics of the Greater Yellowstone Glacial System during the last two glaciations. *Quaternary Science Reviews*, *200*, 1-33.

Locke, W. W., & Meyer, G. A. (1994). A 12,000-year record of vertical deformation across the Yellowstone caldera margin: The shorelines of Yellowstone Lake. *Journal of Geophysical Research: Solid Earth*, *99*(B10), 20079-20094.

Love, J. D. (1961). Reconnaissance study of Quaternary faults in and south of Yellowstone National Park, Wyoming. *Geological Society of America Bulletin*, *72*(12), 1749-1764.

Meyer, G. A., Wells, S. G., & Timothy Jull, A. J. (1995). Fire and alluvial chronology in Yellowstone National Park: climatic and intrinsic controls on Holocene geomorphic processes. *Geological Society of America Bulletin*, *107*(10), 1211-1230.

Pisias, N. G., & Moore Jr, T. C. (1981). The evolution of Pleistocene climate: a time series approach. *Earth and Planetary Science Letters*, *52*(2), 450-458.

Pierce, K. L. (1974). Surficial geologic map of the Abiathar Peak quadrangle and parts of adjacent quadrangles. *Yellowstone National Park, Wyoming and Montana: US Geological Survey Miscellaneous Geological Investigations Map I-646, scale*, *1*(62), 500.

Pierce, K. L. (1979). History and dynamics of glaciation in the northern Yellowstone National Park area: US Geol. *Survey Prof. Paper*.

Pierce, K. L., & Morgan, L. A. (1992). The track of the Yellowstone hot spot: Volcanism, faulting, and uplift. *Regional geology of eastern Idaho and western Wyoming: Geological Society of America Memoir*, *179*(322), 1-53.

Pierce, K.L., Cannon, K.P., Meyer, G.A., Trebesch, M.J. and Watts, R.D., (2007). Postglacial inflation-deflation cycles, tilting, and faulting in the Yellowstone Caldera based on Yellowstone Lake shorelines. U.S. Geological Survey Professional Paper 1717, 1-41.

Pierce, K. L., & Morgan, L. A. (2009). Is the track of the Yellowstone hotspot driven by a deep mantle plume? Review of volcanism, faulting, and uplift in light of new data. *Journal of Volcanology and Geothermal Research*, *188*(1-3), 1-25.

Porter, S. C. (1983). Late Wisconsin mountain glaciation in the western United States. *Late-Quaternary Environments of the United States, Vol. 1: The Late Pleistocene*, 71-111.Reheis, M. C.,

Prostka, H. J., Smedes, H. W., & Christiansen, R. L. (1975a). *Geologic map of the Pelican Cone quadrangle, Yellowstone National Park and vicinity, Wyoming*. US Geological Survey, *Geological Quadrangle Map GQ-1243*.

Prostka, H. J., Blank Jr, H. R., Christiansen, R. L., & Ruppel, E. T. (1975b). Geologic map of the Tower Junction quadrangle. *Yellowstone National Park, Wyoming: US Geological Survey, Geological Quadrangle Map GQ-1247*.

Reheis, M. C., Palmquist, R. C., Agard, S. S., Jaworowski, C., Mears Jr, B., Madole, R. F., Osborn, G. D. (1991). Quaternary history of some southern and central Rocky Mountain basins. *Quaternary nonglacial geology: Conterminous US: Boulder, Colorado, Geological Society of America, Geology of North America*, *2*, 407-440.

Whipple, K. X., Snyder, N. P., & Dollenmayer, K. (2000). Rates and processes of bedrock incision by the Upper Ukak River since the 1912 Novarupta ash flow in the Valley of Ten Thousand Smokes, Alaska. Geology, 28(9), 835-838.

Wilson, C. J., Stelten, M. E., & Lowenstern, J. B. (2018). Contrasting perspectives on the Lava Creek Tuff eruption, Yellowstone, from new U–Pb and 40 Ar/39 Ar age determinations. *Bulletin of Volcanology*, *80*(6), 53.